A STUDY ON CORROSION EVALUATION OF STEEL REINFORCEMENT IN CONCRETE DURING INITIATION AND PROPAGATION STAGE DUE TO CHLORIDE ATTACK

ダリア, パタ

https://doi.org/10.15017/2534439

出版情報：Kyushu University, 2019, 博士（工学）, 課程博士
バージョン：
権利関係：

A STUDY ON CORROSION EVALUATION OF STEEL REINFORCEMENT IN CONCRETE DURING INITIATION AND PROPAGATION STAGE DUE TO CHLORIDE ATTACK

塩害の潜伏期および進展期における埋設鉄筋の腐食評価に関する研究

DAHLIA PATAH

STUDY ON CORROSION EVALUATION OF STEEL REINFORCEMENT IN CONCRETE DURING INITIATION AND PROPAGATION STAGE DUE TO CHLORIDE ATTACK

A DISSERTATION

Submitted to
Kyushu University
in partial fulfillment of the requirements
for the degree of
Doctor of Engineering

by

DAHLIA PATAH

DEPARTMENT OF CIVIL AND STRUCTURAL ENGINEERING
GRADUATE SCHOOL OF ENGINEERING
KYUSHU UNIVERSITY
September 2019

ACKNOWLEDGMENT

Up and above anything else, praises are due to Almighty Allah alone, the omnipotent, and the omnipresent.

It is a matter of great pleasure and honor for me to express my heartiest gratitude and appreciation to respected and learned research supervisor Prof. Hidenori HAMADA, under whose kind supervision and sympathetic attitude, the present research was completed. His guidance enabled me to treat this work objectively and comprehensively. Thank you for your kindness and for accepting me three years ago to experience your extensive knowledge in Concrete Engineering.

I would also like to address my thanks to Assoc. Prof. Yasutaka SAGAWA for his worth guidance and valuable advice during my research and writing of this dissertation. Thank you for taking laboratory members and me to the site visit and sit together during JCI preparation. It may look small but your humble attitude despite your excellent knowledge in Concrete Engineering really impressed me.

I am sincerely grateful to all esteemed members of the Doctoral Committee, Prof. Koji TAKEWAKA, Associate Professor Shigenobu KAINUMA and Associate Professor Yasutaka SAGAWA for their precious suggestions and insightful comments with regard to improve this research work. Thank you also for letting my defense be a memorable moment.

Special thanks are expressed to Mr. Daisuke YAMAMOTO for his tremendous attention, assistance and guidance. Also, my gratitude goes to present and past members of Concrete Engineering Laboratory for their brotherhood, support and cooperation during my study.

Sincere appreciation goes to MEXT (Ministry of Education, Culture, Sports, Science and Technology, Japan) for awarding highly prestigious “Monbukagakusho Scholarship” to support this study in Kyushu University. My gratitude also extends to Sulawesi Barat University, Indonesia for their kind attention, support and assistance through my three years of research in Japan.

No acknowledgment would ever adequately express my obligation to my beloved husband, my lovely daughters, my parents, parent-in-law, my brother/sisters, and brother/sister-in-law who have always wished to see me flying high up at the skies of success. Without their prayers, sacrifices and encouragements the present work have been a merry dream.

Dahlia Patah
Kyushu University
September, 2019

DEDICATION

To my beloved family

Amry Dasar
Hikari Azzahramugni Amry
Hiromi Atthahirahmugni Amry

for the prayers, support, encouragement, sacrifices and patience

ABSTRACT

Deterioration of RC structures due to harsh environmental conditions lead to performance degradation of RC structures, and premature deterioration before completing expected service life is a primary concern for engineers and researchers, maintainers, and infrastructure owners. Considering marine exposure conditions and use either sea sand/seawater for heavy construction in many countries, chloride-induced corrosion is one of major causes of deterioration of RC structures. In the literature, reliable chloride threshold for both new structures design and condition assessment of existing structures is important as the remaining service life is often considered as the time required to reach the chloride threshold value at a depth of steel bar. Several critical disasters due to steel corrosion have been reported, including the collapse of building and bridge. The total estimated direct cost for repairing or preventing corrosion is reported to be expensive. For these reasons needs to be increasing consideration of optimum durability design. Different mineral admixtures are often added in concrete to improve the durability, rheology of fresh concrete, and mechanical properties of hardened concrete. Optimal design important advances in the knowledge base relevant to the durability evaluation of RC structure in marine environments, including the role of mineral admixture for durability, the methods of measuring, and design for long-lasting of RC structures in marine environments. Therefore, this study aims 1) to propose a reliable detection method to determine the chloride threshold value to corrosion initiation of steel bars in various mineral admixtures such as fly ash, silica fume, metakaolin, and BFS; 2) to determine the performance of OPC mortar with difference chloride contaminated from moderate to high corrosion rate under certain period of exposure; 3) to determine the better performance of concrete mixed with seawater after 36-years exposure; 4) to propose a reliable assessment method to predict corrosion activity in RC structure; and 5) to determine some consideration regarding durability of seawater in RC structures. Further, this study expected to contribute for necessary information and may guide engineers in the development of longer-lasting RC structures, because it provides a demonstration of the long-term behavior of a commonly used construction material, permitting the prediction of the behaviors of existing structures and the more informed design and study of structures to be built.

This dissertation consists mainly of seven chapters.

Chapter 1 describes the background of this study, research objective, research contribution and dissertation outline.

Chapter 2 describes the brief background to chloride-induced reinforcement corrosion, literature review of previous studies about utilization of mineral admixture for resistance against chloride-induced corrosion and report on seawater-mixed concrete in performance and corrosion issue. The results of previous researches on an investigation of seawater in concrete

mixture are reviewed. Some factors affecting the durability of seawater mixed concrete are also viewed. The issues to be addressed in this study were discussed.

Chapter 3 describes the OPC mortar contaminated chloride was tested during the propagation period of corrosion from moderate to high corrosion rate. The main objective of this study is to identify and determine corrosion behavior and the extent of corrosion of OPC mortar during the early period of the propagation stage by using several corrosion measurement methods. From the present test results, the factors influence of corrosion behavior of OPC mortar with difference chloride contaminated from moderate to high corrosion rate is proposed. The sensitivity of the corrosion potential against chloride content tends to be decreased after a certain period of exposure. The value is 13~15% of corrosion area can be defined as high corrosion degree and categorized into propagation stage. Therefore, from moderate to high corrosion rate, after 8-years exposure of OPC mortar has increased the probability from pitting to generate corrosion.

Chapter 4 describes the chloride threshold value to corrosion initiation by using mineral admixtures such as fly ash, silica fume, metakaolin, and BFS. Corrosion potential and corrosion current density were conducted to examine the threshold chloride concentration. The amount of chloride was determined according to the added amount of chlorides, type of mineral admixtures and W/B ratios. The specimens were stored in the laboratory atmosphere condition room and after one year, specimens were exposed in accelerated carbonation chamber until the sign of corrosion initiating. From the present test results, the factors influencing threshold chloride concentration are investigated, and the reliable ranges of threshold chloride concentration causing active corrosion of steel bar are proposed. In performance-based design determined by chloride attack and carbonation, it is possible to use seawater and if mortar mixed with BFS and fly ash with maximum W/B ratio of 0.5. Therefore, establish the threshold total and free chloride content using mineral admixtures for the initiation of corrosion steel bars in concrete structures become the main contributions of this study.

Chapter 5 introduces several investigations on concrete mixed with seawater and tap water. Ten number of RC beams have been evaluated. The specimens were exposed to a tidal pool utilizing seawater directly from the sea. The major test variables include mixing water, various of cover depth, water to cement ratios, various bending load and exposure condition. The study aims to evaluate the effect of seawater mixing and exposure condition (tidal and splash) on deterioration and steel corrosion of RC beam under service load after 36-years of exposure. Visual observation, some electrochemical and physical evaluation were evaluated. From the present test results, the use of seawater as mixing water improved concrete strength, concrete resistance, oxygen permeability resistance and maintained very dense microstructure. And, the results of 36-years exposure test of concrete mixed with seawater with concrete cover 50 mm demonstrated the high possibility of using seawater as an alternative and sustainable material of reinforced concrete, especially in marine tidal environment. The results will be beneficial to provide notable information regarding the long-term performance of concrete

mixed with tap water and seawater under marine environment. The information expected to assist future optimum design of seawater mixed.

Chapter 6 presents the importance of reinforcement corrosion monitoring and describes the different methods for evaluating the corrosion state of RC structures. The main objective of this study was to compare the corrosion level of long-term exposure of RC beam using several corrosion measurement methods and discuss an overview of utilization of seawater in concrete structures. The data of corrosion level were taken from Chapter 5 then analysis and categorized into deterioration and degradation stage level. This study proposes a reliable assessment method to predict corrosion activity of steel corrosion caused severe damage of RC structure. Additionally, a potential correlation of actual corrosion and corrosion measurement was explored. From the present test results, proposal equation for estimation deterioration and performance reduction of RC structure after long-term exposure were included. Some consideration regarding durability of seawater mixing in RC structure, particularly in marine environment was summarized. In addition, the corrosion current density was observed as important parameter to detect corrosion initiation of steel bar at short-term exposure. Moreover, the oxygen permeability evaluation was suggested as the most critical factor in order to detect deterioration of RC structure after long-term exposure.

Chapter 7 conveys summary, conclusion, and recommendation for research works in the future.

TABLE OF CONTENTS

ACKNOWLEDGMENT i
ABSTRACT iii
TABLE OF CONTENTS vi
LIST OF TABLES x
LIST OF FIGURES xii
LIST OF PHOTOS xv

CHAPTER 1 GENERAL INTRODUCTION 1
1.1 Research background 1
1.2 Research objective and limitation 3
1.3 Dissertation outline 4
References 4

CHAPTER 2 STATE OF THE ART ON CORROSION OF STEEL BAR 6
2.1 Introduction 6
2.2 Fundamentals of steel corrosion in concrete 6
2.2.1 Corrosion stage 6
2.2.2 Steel corrosion in concrete 8
2.3 Assessment of reinforcement corrosion in concrete 10
2.3.1 Corrosion potential 10
2.3.2 Corrosion rate 12
2.3.3 Anodic-cathodic polarization 13
2.3.4 Electrical resistivity 15
2.4 Corrosion initiation 16
2.4.1 Chloride-induced corrosion 16
2.4.2 Carbonation-induced corrosion 18
2.5 Chloride Threshold 19
2.5.1 Chloride threshold value (CTV) 19
2.5.2 Effect of mineral admixtures and water to binder ratio on CTV 21
2.5.3 Free and bound chlorides 22

2.6 Seawater mixing 23
2.7 Issues addressed in this study 24
References 25

CHAPTER 3 CORROSION MONITORING OF STEEL BAR IN OPC MORTAR FROM MODERATE TO HIGH CORROSION RATE 29

3.1 Introduction 29
3.2 Experimental method 30
3.2.1 Materials and mix proportions 30
3.2.2 Specimens 31
3.2.3 Proportions of mixture 31
3.3 Experimental method 32
3.3.1 Corrosion potential 32
3.3.2 Corrosion current density 33
3.3.3 Grade passivity and oxygen permeability 33
3.3.4 Electrical resistivity 35
3.3.5 Corroded area 35
3.4 Results 35
3.4.1 Corrosion potential 35
3.4.2 Corrosion current density 37
3.4.3 Grade passivity 39
3.4.4 Oxygen permeability 40
3.4.5 Electrical resistance 41
3.4.6 Physical evaluation of corrosion 42
3.5 Discussion 44
3.6 Conclusions 45
References 46

CHAPTER 4 THE EFFECTIVENESS OF MINERAL ADMIXTURE ON CORROSION RESISTANCE OF STEEL BAR IN MORTAR 47

4.1 Introduction 47
4.2 Test Program 49

4.2.1 Material 49
4.2.2 Specimens 50
4.2.3 Proportions of Mixture 51
4.3 Experimental Methods 52
4.3.1 Compressive strength and porosity 52
4.3.2 Corrosion potential and corrosion current density 52
4.3.3 Electrical resistivity and permeability 54
4.3.4 Oxygen Permeability 54
4.3.5 Physical analysis and visual inspection 54
4.3.6 Carbonation 54
4.3.7 Chloride analysis 55
4.4 Result and discussion 55
4.4.1 Result of previous study 55
4.4.2 Compressive strength and porosity 56
4.4.3 Corrosion potential, corrosion current density 57
4.4.4 Electrical resistance 60
4.4.5 Oxygen permeability 61
4.4.6 Carbonation 62
4.4.7 Total chloride content values 63
4.4.8 Visual observation 65
4.5 Discussion 66
4.5.1 Proposed on chloride threshold 66
4.5.2 Determination on of chloride threshold value (CTV) 68
4.5.3 Influence of mineral admixtures on chloride threshold value 72
4.5.4 Possibility of mineral admixture mixed with seawater 74
4.6 Conclusions 74
References 75

CHAPTER 5 PERFORMANCE OF SEAWATER-MIXED CONCRETE IN NATURAL CORROSION ENVIRONMENTS 79
5.1 Introduction 79
5.2 Test Program 80
5.2.1 Exposure conditions 80
5.2.2 Experimental methods 82

5.3 Result and discussion 84
5.3.1 Visual observation-crack maps 84
5.3.2 Electrochemical measurements 89
5.3.3 Carbonation depth and chloride ingress 94
5.3.4 Quality of concrete 96
5.3.5 Surface corroded area 99
5.3.6 Cross-sectional loss 100
5.3.7 Tensile Test 104
5.4 Conclusions 112
References 112

CHAPTER 6 AN ASSESSMENT FOR CORROSION ACTIVITY OF RC STRUCTURES IN NATURAL CORROSION ENVIRONMENTS 115
6.1 Introduction 115
6.2 Test Program 116
6.3 Experimental method and establishing corrosion level 117
6.4 Result and discussion 122
6.4.1 Corrosion level 122
6.4.2 Multiple regression analysis 124
6.5 Some considerations utilization of seawater mixed concrete with OPC and mineral admixture 127
6.6 Conclusions 130
References 130

CHAPTER 7 CONCLUSIONS AND FUTURE WORKS 132
7.1 Summary 132
7.2 Overview of contributions and conclusions 133
7.3 Future works 135

LIST OF TABLES

Table No		Page
Table 2.1	Definition of deterioration stages due to chloride attack	8
Table 2.2	Criteria for diagnosis of deterioration degree	8
Table 2.3	Cu/CuSO4 and Ag/AgCl potentials and associated risk of corrosion	11
Table 2.4	Qualitative guide for the assessment of corrosion rates	13
Table 2.5	Grade of passivity film associated anodic polarization curve	15
Table 2.6	Relationship between resistivity and corrosion risk	16
Table 3.1	Physical and chemical compositions of cement	30
Table 3.2	Chemical compositions of steel bar	30
Table 3.3	Design of chloride content	32
Table 3.4	Mixture proportions of mortar	32
Table 3.5	Anodic current density at 200V and 600mV and passivity grade	40
Table 4.1	Literature reviews	48
Table 4.2	Physical and chemical compositions of cement	49
Table 4.3	Classifications of fly ash, silica fume, and blast furnace slag cement	50
Table 4.4	Chemical compositions of steel bar	50
Table 4.5	Mixture proportions of mortar	51
Table 4.6	Design of chloride content	52
Table 4.7	Corrosion potential (E_{corr}) and corrosion current (I_{corr}) at depassivation time	59
Table 4.8	Carbonation depth after 42-weeks accelerated in CO_2 chamber	62
Table 4.9	The corroded area	66
Table 4.10	Chloride threshold value for total chloride	71
Table 4.11	Chloride threshold value for water-soluble chloride	71
Table 5.1	Summary of RC beam specimens	80
Table 5.2	Criteria for the diagnosis of deterioration degree	85
Table 5.3	Current density of polarization curve	93
Table 5.4	Total chloride, water-soluble chloride and bond chloride concentration	95

Table 5.5	Summary of quality of concrete	97
Table 5.6	Mechanical properties of steel bar (JIS G 3112)	104
Table 5.7	Properties of reinforcement according to Euro code 2	108
Table 5.8	Summary of tensile test results	108
Table 6.1	Summary of RC beam specimens	116
Table 6.2	Selected assessment method	118
Table 6.3	Summary result of electrochemical analysis	118
Table 6.4	Summary result of mechanical properties	119
Table 6.5	Interpretation of corrosion level of electrochemical methods	121
Table 6.6	Level of mechanical properties	122
Table 6.7	Deterioration degree of all RC beams	123
Table 6.8	Performance reduction of RC beams	124
Table 6.9	Equation for deterioration degree and performance reduction	125
Table 6.10	Multiple correlation coefficient with the corroded area as a criterion variable	126
Table 6.11	Multiple correlation coefficient with elongation as criterion variable	126
Table 6.12	Limiting values for composition and properties of concrete subject to general structures for 50 years design life in tidal, splash & spray zones	127
Table 6.13	Summary of composition and properties of RC-beam and mortar contain mineral admixture	128
Table 6.14	Proposal utilization of seawater mixing for design life in tidal and atmosphere exposure	129

LIST OF FIGURES

Figure No		Page
Fig. 1.1	Conceptual deterioration model showing the stages during the service life of RC structure	2
Fig. 1.2	Structure of the dissertation outline	5
Fig. 2.2	A schematic illustration of the corrosion process in concrete	9
Fig. 2.3	Relative volume of iron corrosion products	9
Fig. 2.4	Schematic of corrosion potential measurement	11
Fig. 2.5	The schematic diagram of the electrical circuit of the cportable corrosion meter and polarization technique	13
Fig. 2.6	Evaluation of polarization curve	15
Fig. 2.7	Principle of Wenner probe measurement of concrete resistivity	16
Fig. 2.8	Corrosion of reinforcement in concrete exposed to chloride ions	17
Fig. 2.9	Cross-section of concrete showing the carbonated and carbonated zones	19
Fig. 2.10	Definitions for chloride thresholds	20
Fig. 2.11	Contribution of various mechanisms influencing durability	23
Fig. 2.12	Investigated items related to seawater mixed concrete	24
Fig. 3.1	Appearance and details of specimen	31
Fig. 3.2	The schematic of the exposure condition	31
Fig. 3.3	Measurement of corrosion potential	33
Fig. 3.4	Measurement of micro-cell corrosion	33
Fig. 3.5	The schematic diagram of the electrical circuit of polarization technique	34
Fig. 3.6	Corrosion potential at the age of 6-years and 8-years	35
Fig. 3.7	Time dependence change of Ecorr	36
Fig. 3.8	Relationship between Ecorr and chloride content	37
Fig. 3.9	Time dependence change of corrosion current density	38
Fig. 3.10	Anodic polarization curves	39
Fig. 3.11	Oxygen permeability through concrete cover	41
Fig. 3.12	Concrete resistance	41

Fig. 3.13	Appearance of split-open mortar at the age of 6-years and 8-years	42
Fig. 3.14	Appearance of steel corroded at 6-years and 8-years	43
Fig. 3.15	The corroded area	44
Fig. 3.16	Relationship between electrochemical and physical analysis	45
Fig. 4.1	Details of specimen	50
Fig. 4.2	The schematic diagram of curing and exposure time of the specimen	51
Fig. 4.3	Measurement setup for corrosion potential	53
Fig. 4.4	The schematic diagram of the electrical circuit of the polarization technique	53
Fig. 4.5	Time dependences changes of Ecorr and Icorr for OPC mortar	55
Fig. 4.6	Polarization resistance as a function of chloride content	56
Fig. 4.7	Compressive strength and total pore volume	56
Fig. 4.8	Total pore volume	57
Fig. 4.9	Cumulative pore volume as a function of pore diameter of specimen	57
Fig. 4.10	Time dependences changes of E_{corr} and I_{corr} for FB	58
Fig. 4.11	Time dependences changes of E_{corr} and I_{corr} for SA	58
Fig. 4.12	Time dependences changes of E_{corr} and I_{corr} for BBMKP	59
Fig. 4.13	Time dependences changes of E_{corr} and I_{corr} for BB	59
Fig. 4.14	Electrical resistivity as a function of W/B ratio of mineral admixture	60
Fig. 4.15	Permeability and oxygen supply in mortar	61
Fig. 4.16	Carbonation depth	63
Fig. 4.17	Immobilized and water-soluble chloride for each mineral admixture	64
Fig. 4.18	Appearance of steel corroded	65
Fig. 4.19	Relationship between E_{corr} and I_{corr}	67
Fig. 4.20	Corrosion current density as a function of chloride content to determining the CTV of total chloride	69
Fig. 4.21	Corrosion current density as a function of chloride content to determining the CTV of water-soluble chloride	70
Fig. 4.22	Minimum chloride threshold value for total chloride	71
Fig. 4.23	Minimum chloride threshold value for water-soluble chloride	71
Fig. 5.1	Layout details of the RC beam	81
Fig. 5.2	Exposure condition	81
Fig. 5.3	Uniaxial tensile tests of steel bars	84

Fig. 5.4	Overview of the three sides of crack maps of 55-L1-TW-T, 55-L3-TW-T, and 65-L1-TW-T	86
Fig. 5.5	Overview of the three sides of crack maps of 65-L1-SW-T, 45-L1-SW-T, 55-L2-SW-T,55-L3-SW-	87
Fig. 5.6	Overview of the three sides of crack maps of 65-L1-SW-S, 55-L1-SW-S, and 45-L1-SW-S	88
Fig. 5.7	Appearance of RC beam 55-L3-TW-T and 55-L3-SW-T	89
Fig. 5.8	Half-cell potential	90
Fig. 5.9	Grade of passivity	92
Fig. 5.10	Oxygen permeability	94
Fig. 5.11	Cumulative pore volume and incremental pore volume	98
Fig. 5.12	View of surface corroded surface steel bar after removing corrosion products	99
Fig. 5.13	Corroded area of steel bars	100
Fig. 5.14	Loss of cross-section of mixing water: tap water and seawater	101
Fig. 5.15	Loss of cross-section of exposure condition: tidal and splash zone	102
Fig. 5.16	Loss of cross-section of bending load	103
Fig. 5.17	Classification of failure point	104
Fig. 5.18	Failure point of the corrosion pit bar, non-corrosion pit bar, and control bar	105
Fig. 5.19	Failure point of non-corrosion pit bar and corrosion pit bar	106
Fig. 5.20	Stress-strain curves of the tensile tests	106
Fig. 5.21	Relationship between fy, and fu with cross-sectional loss	109
Fig. 5.22	Failure point of the non-corroded bar and corroded bar	110
Fig. 6.1	Layout details of the RC beam	117
Fig. 6.2	Exposure condition	117
Fig. 6.3	Criteria of deterioration and performance reduction of RC structure	120

LIST OF PHOTOS

Photo No		Page
Photo 2.1	Deterioration in a RC structure	10
Photo 2.2	Chloride-induced corrosion in a marine environment	17

CHAPTER 1. GENERAL INTRODUCTION

1.1 Research background

Reinforced concrete (RC) is one of the most common materials used in the construction industry worldwide. The raw materials required for its construction are widely available and the built structures are in general durable. Reinforced concrete is used for the construction of transportation infrastructures such as bridges, tunnels, and harbor structures. It is also used for offshore platforms and a wide range of public and private buildings. Reinforcement corrosion has been widely reported and it is one of the main durability problems. Reinforcement corrosion in concrete is generally considered the most common mode of premature distress and deterioration of structural concrete. This has resulted in a clear need from both industry and field of research that the model was developed to determine the onset of corrosion and to predict the remaining service life of corroded RC structures. The service life of RC structures is, according to the classic model by Tuutti [1.1], divided into two stages, i.e., the initiation stage which involves the penetration of the damaging substance through the concrete cover, and the propagation stage involving active corrosion after steel depassivation (See Fig. 1.1a). While JSCE standard [1.2] proposed a conceptual service life model of RC structures which consist of four stages. i.e., initiation, propagation, acceleration, and deterioration (See Fig. 1.1b). Tuutti [1.1] model proposed that when deterioration enters the propagation stage then judge as to the end of service life, while JSCE standard [1.2] considered that service life until the end of deterioration stage became the main difference by two of proposed service life of RC structures. Therefore, it should be understanding that Tuutti [1.1] model, all of the countermeasures (i.e., maintenance) should be executed during initiation stage, while JSCE standard [1.2] allowable during after initiation stage. The expected service life will include the time needed to corrode steel, which makes the structure unsuitable for further service.

In various applications, reinforced concrete is subjected to a range of exposure conditions, including marine, industrial, or other severe environments. Instead of avoiding the chloride from seawater, the engineer challenged to inverse this situation from disadvantage became an advantage. Demand for using seawater in concrete production seems imperative,

either limited fresh water reserves or fresh water is costly to transport. In the concrete industry, several billion tons of freshwater are used annually in the mixing, curing, and cleaning around the world [1.3]. In the viewpoint of saving freshwater, the possibilities of using seawater-mixed concrete should be investigated comprehensively. JSCE committee reported seawater as mixing water should be avoided to be used in RC structures because of the risk of early corrosion of reinforcement induced by chloride in seawater compounds [1.4]. However, in the case of an unavoidable situation, seawater as mixing water is recommended only for plain concrete [1.4-1.5]. While, if the use of seawater as mixing water in concrete is reliable, it would be very convenient and economical not only in saving freshwater but also in the construction, especially in coastal works and isolated island.

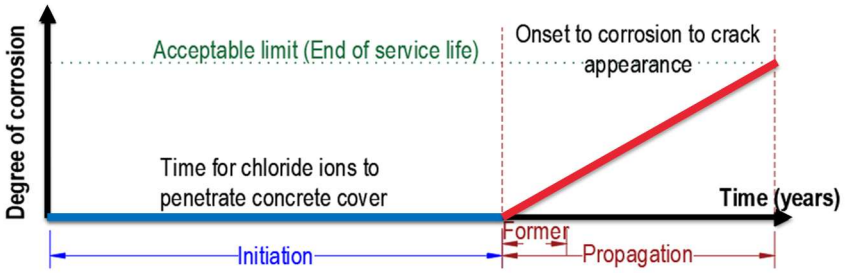

a. Service life model proposed by Tuutti [1.1]

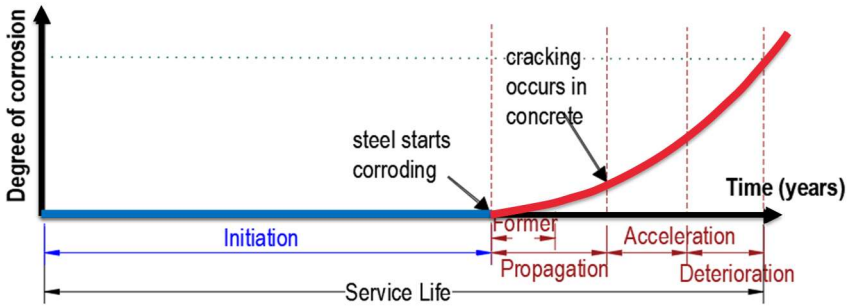

b. Service life model proposed by JSCE Standard [1.2]

Fig. 1.1—Conceptual deterioration model showing the stages during the service life of RC structure

The appropriate concrete design should be a concern for the utilization of mineral admixture. Utilization of mineral admixtures such as fly ash, silica fume, metakaolin, and slag in concrete, has been proposed as one of the effective methods to reduce the corrosion-induced damage in RC structures [1.6-1.7]. In addition, it is evident that the replacement of Ordinary Portland Cement (OPC) with industrial by-products like fly ash, silica fume, and slag is highly beneficial from the standpoint of cost, economy, energy efficiency and overall ecological and environmental benefits. The utilization of mineral admixture as replacement cement in RC

structures like bridges and high rise buildings requires the durability aspect of the concrete to be recommended. Specifically, in the region such as Japan and Indonesia surrounded by sea, the corrosion resistance of embedded steel subjected to salt attack in RC structures becomes a major concern. Furthermore, corrosion monitoring of seawater mixing after long-term exposure of RC structures is also highly important to minimize the economic losses due to corrosion of steel reinforcement. The detailed analysis of RC structure, in the light of laboratory testing, is necessary to determine the cause and mechanism of corrosion, so that those factors should be eliminated to prevent further corrosion damage in real RC structures.

1.2 Research objective and limitation

The purpose of this study is to evaluate the performance of mineral admixture to enhance the durability of RC structures. In addition, deterioration evaluation of the long-term performance of RC structures by suitable and reliable corrosion monitoring in order to achieve summary durability design. Further, this study contributes and provides necessary information on the utilization of mineral admixture and the possibility of seawater to be used as a construction material. Therefore, the main objectives of this study are:

1. To determine the performance of OPC mortar with difference chloride contaminated from moderate to high corrosion rate, under a certain period of exposure (8-years),
2. To propose a reliable detection method to determine the CTV to corrosion initiation of steel bar in various mineral admixtures such as fly ash, silica fume, metakaolin, and blast furnace slag,
3. To evaluate the better performance of seawater mixed concrete after 36-years exposure,
4. To propose a reliable assessment method to predict corrosion activity in RC structure,
5. To determine some considerations regarding the durability of seawater mixing in RC structure.

Hopefully, by conducting this research, it can provide a precious contribution to the design and construction of durable buildings and facilities to the concrete industry in harsh environments, especially Asian countries.

In this study, it should be understood that the limitation is set up for corrosion of reinforcement concrete where the focus on due to chloride attack and carbonation. In addition, the factor that influences on the chloride threshold of corrosion initiation in concrete such as the type of cement (chloride binding capacity) and the W/B ratio are taken into main consideration. The effect of other influences is neglected and not taken into consideration in this study.

1.3 Dissertation outline

The structures of the dissertation outline are shown in Figure 1.2, which divided into seven chapters, as explained below:

Chapter 1 is an introduction intended to present the background of the project as well as the objectives and limitations.

Chapter 2 gives an overview of the theoretical background to chloride-induced reinforcement corrosion, literature review of previous studies about utilization of mineral admixture for resistance against chloride-induced corrosion and report on seawater-mixed concrete in performance and corrosion issue. The results of previous researches on an investigation of seawater in concrete mixture are reviewed. Some factors affecting the durability of seawater mixed concrete are also reviewed. The issues to be addressed in this study were discussed.

Chapter 3 gives the corrosion characteristics of the steel bar in chloride contaminated mortar from moderate to high corrosion rate. The results, interpretation and major conclusions obtained from the experimental work are presented.

Chapter 4 provides the results and discussion about CTV to corrosion initiation by using mineral admixtures such as fly ash, silica fume, BBMKP, and BFS. Also, a reliable detection method for corrosion initiation of steel bar in mineral admixture mortar was introduced. The results of various mineral admixture and water to binder ratio on CTV were also discussed.

Chapter 5 discusses the corrosion behavior of steel reinforcement in the RC beam under continuous loading during 36-years old. The influencing parameters such as mixing water, concrete cover, exposure conditions and bending loads. This chapter provides some consideration regarding the utilization of seawater in RC structures.

Chapter 6 provides a reliable technique for detecting and measuring the corrosion activity of steel bar in RC structures under sustained loading after long-term exposure using several methods of measuring corrosion. This chapter proposed equation, corrosion measurement methods and the main factors that influence the assessment of deterioration progress and performance reduction after long-term exposure in RC structure. In addition, some consideration regarding the durability of seawater mixing in RC structure, particularly in the marine environment was proposed.

Chapter 7 conveys a summary, conclusion, and recommendation for research work in the future.

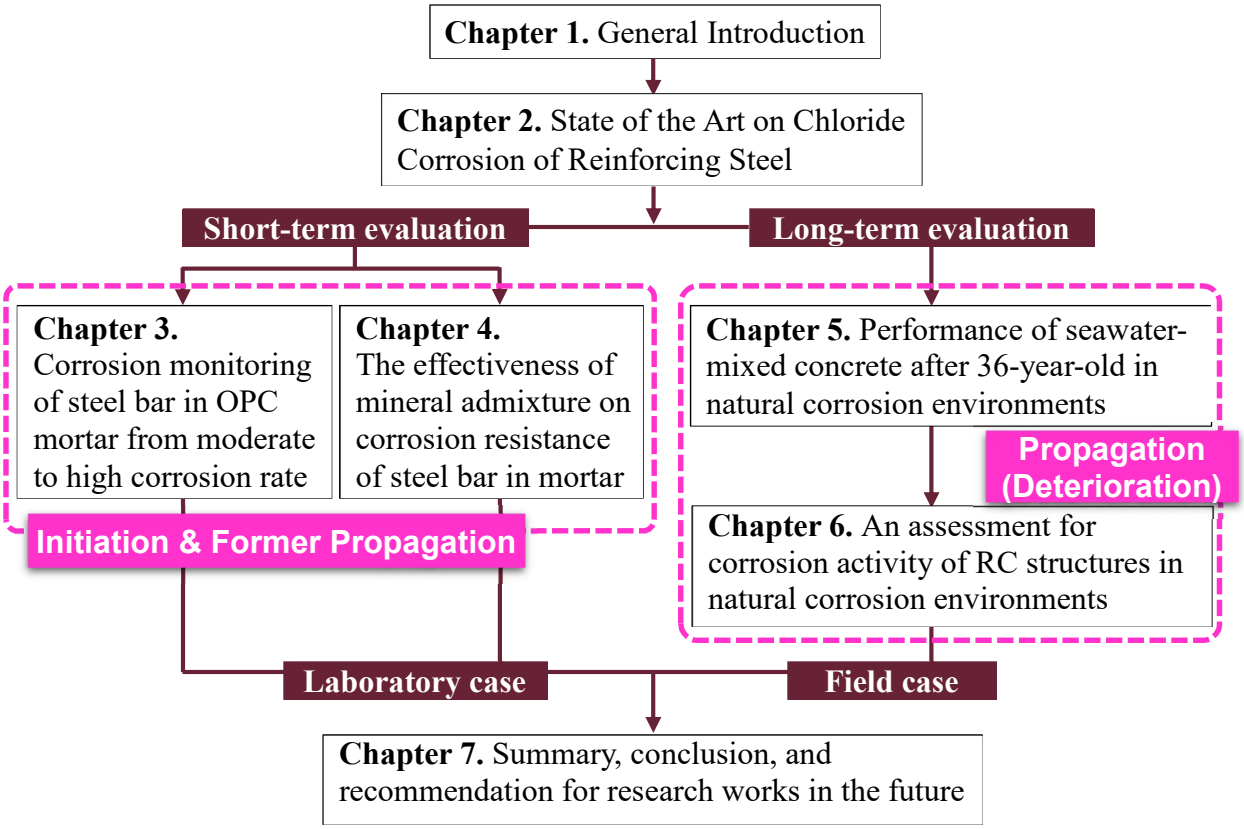

Fig. 1.2—Structure of the dissertation outline

References

[1.1] Tuutti, Kyösti. Corrosion of steel in concrete. Cement-och betonginst., 1982.

[1.2] JSCE, Standard Specification for Concrete Structures (Part: Maintenance), Japan Society of Civil Engineers, Japan, 2007.

[1.3] Nishida, Takahiro, et al. "Some considerations for applicability of seawater as mixing water in concrete." Journal of Materials in Civil engineering 27.7 (2013): B4014004.

[1.4] JGC16. "Standard Specification for Concrete Structures (Materials and Construction)." Japan Society of Civil Engineers, 2007.

[1.5] Neville, Adam. "Seawater in the mixture." Concrete international 23.1 (2001): 48-51.

[1.6] Mehta PK, "Durability- critical issues for the future". Concrete International 19(7) (1997): 27-33.

[1.7] Cabrera, J. G., and P. Ghoddoussi. "Influence of fly ash on the resistivity and rate of corrosion of reinforced concrete." Special Publication 145 (1994): 229-244.

CHAPTER 2 STATE OF THE ART ON CORROSION OF STEEL BAR

2.1 Introduction

The corrosion of reinforced concrete is the most dominant causal factor for the premature deterioration of concrete structures. Chloride-induced corrosion became the main contributor for this deterioration, particularly structures in the marine environment. However, instead of avoiding the chloride from seawater, the engineer challenged to inverse this situation from disadvantage became an advantage. Demand for using seawater in concrete production seems imperative, either limited tap water reserves or tap water is costly to transport. However, it is widely accepted amongst engineers that seawater is not recommended for use in concrete, particularly concrete embedded reinforcing bar as it may lead to corrosion [2.1]. It is believed, if the appropriate concrete design is performed, then seawater has possible in concrete production. The appropriate concrete design should be a concern for the utilization of mineral admixture. The utilization of mineral admixture is one of countermeasure against either chloride-induced corrosion or carbonation. The mineral admixture is believed to improved chloride threshold and resistance against CO_2 for depassivation of reinforcement in concrete. However, the threshold still unclear and still need further research. In this chapter, several kinds of literature regarding corrosion and deterioration of RC structures using seawater as mixing concrete are reviewed. The proper mineral admixture to increased resistance against chloride attack and carbonation are elucidated. The durability issues related to chloride attack and carbonation of mortar are described, briefly.

2.2 Fundamentals of steel corrosion in concrete

2.2.1 Corrosion stage

Chloride attack and carbonation of the concrete strongly linked to corrosion of reinforced concrete. The steel to become thermodynamically unstable (i.e., depassivated) and therefore liable to corrode caused by both of these. It results in degradation of the

concrete structure and may threaten its structural performance once the steel starts to corrode actively. There are four stages as shown in Table 2.1 was involved in the deterioration of RC structures due to steel corrosion. In addition, the relationship between the performance degradation of the structural member and deterioration due to chloride attack is shown in Fig. 2.1.

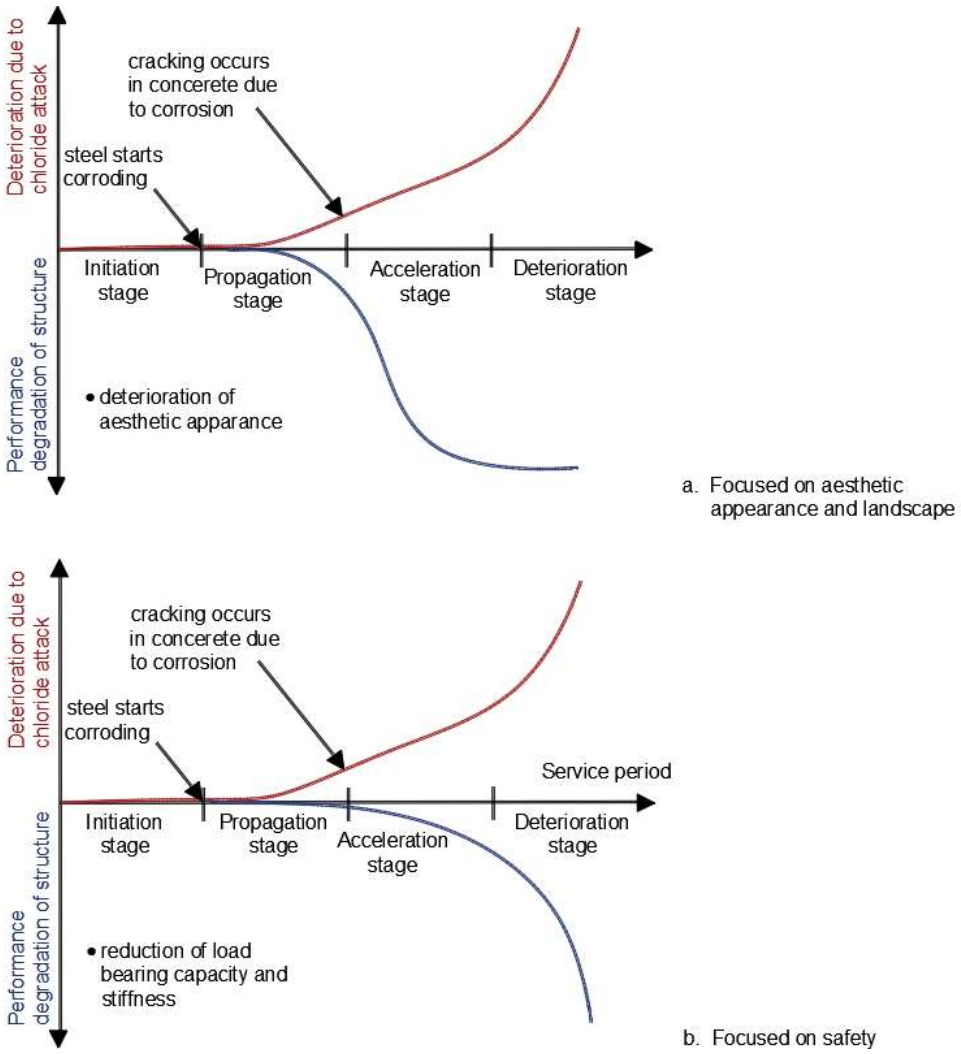

Fig. 2.1— Progress of deterioration due to chloride attack [2.2]

The deterioration progress from chloride attack involves the initiation, propagation, acceleration, and deterioration stages. In each stage, the deterioration has different influences on the beam structure. The degree of deterioration progress with performance degradation also varies according to the performance attribute under investigation. Table 2.2 presents the criteria for the diagnosis of deterioration degree [2.2].

Table 2.1—Definition of deterioration stages due to chloride attack [2.2]

Stage of deterioration	Defenition	Stage determined by
Initiation	Until the chloride ion concentration on the surface of the steel reaches the marginal concentration for the occurrence of corrosion (standard value is 1.2 kg/m^3)	Diffusion of chloride ions Initially contained chloride ion concentration
Propagation	From the initiation of steel corrosion until cracking due to corrosion.	Rate of steel corrosion
Acceleration	Stage in which steel corrodes at a high rate due to cracking due to corrosion.	Rate of corrosion of steel with cracks
Deterioration	Stage in which load-bearing capacity is reduced considerably due to the increase of corrosion amount.	

Table 2.2—Criteria for diagnosis of deterioration degree [2.2]

Evaluation Items	Deterioration Degree					
	0	1	2	3	4	5
Corrosion of steel bar	None	Rust spots found on concrete surface	Partial rust stains found on concrete surface	Significant rust staining	Significant floating rust	Dramatic increase in amount of floating rust
Cracking	None	Partial cracks found on concrete surface	Some cracks	Many cracks, including some of several mm or more in width	Many cracks of several mm in width	-
Spalling covering concrete	None	None	Partial floating concrete found	Partial spalling found	Significant spalling	Drastic spalling

2.2.2 Steel corrosion in concrete

Process in which iron is solubilized at the anode and oxygen is reduced at the cathode, with electrons flowing in the steel between anode and cathode is corrosion process in concrete. The electrolyte is the alkaline pore solution while the steel bar serves as the metallic path between the anode and cathode in reinforced concrete. The anodes and cathodes are formed on the steel surface are shown in Fig. 2.2. The anodic reaction leads to the formation of iron cations as shown in Eq. 2.1.

Anodic: $Fe \rightarrow Fe^{2+} + 2e^{-}$ (2.1)

This reaction is balanced by the cathodic reduction of oxygen, which produces hydroxyl anions according to Eq. 2.2.

Cathodic: $½O_2 + H_2O + 2e- \rightarrow 2OH^{-}$ (2.2)

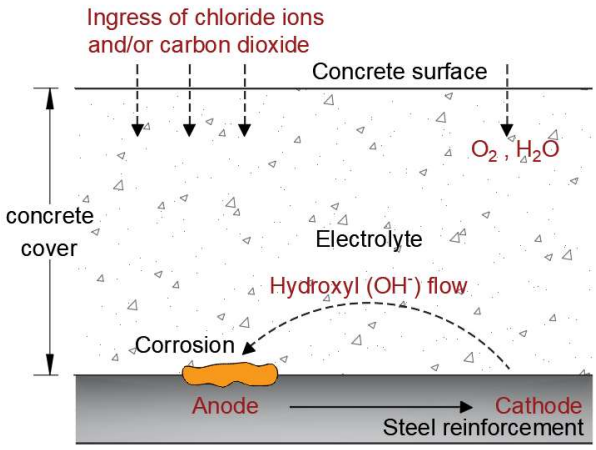

Fig. 2.2—A schematic illustration of the corrosion process in concrete

The stability of the passive film on the steel was built from the combination of the reaction products between anodic and cathodic. Oxygen availability and the pH value in the interface of steel/concrete became the main factor of the stability of this passive film [2.3]. Steel embedded in concrete is naturally protected against corrosion by the high alkalinity of the cement pore solution (pH > 12.5) and by the barrier effect of the concrete cover, which limits the oxygen and moisture required for active corrosion. The high pH suppresses steel corrosion by permitting the formation of a very thin (1-10 nm thick) passivating ferric oxide film (γ-Fe_2O_3) on the steel surface [2.4]. Either a reduction in alkalinity (typically in carbonated concrete) or by chloride ingress (in marine concrete) can be disrupted or de-passivated the passive layer on the steel. Depassivation renders the steel thermodynamically liable to corrode; whether it does so depend primarily on the availability of moisture and oxygen at the cathode.

Iron (Fe) that has been converted to Fe^{2+} can then form corrosion products of hydroxides, oxides, and oxide-hydroxides, depending on conditions of temperature, atmospheric pressure, potential and pH. These corrosion products occupy larger volumes than the original iron, as shown in Fig. 2.3. It is this volume expansion that causes cracking and spalling in the concrete cover.

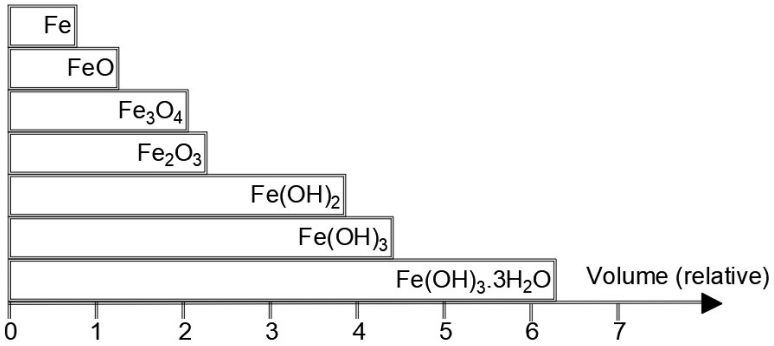

Fig. 2.3—Relative volume of iron corrosion products [2.5]

Photo 2.1 shows a clear example of the effect of corrosion on concrete structure deterioration. It shows cracks, spalling and loss of bond between steel and concrete due to corrosions. This reinforced concrete structure is a part of structures in Gunkanjima Island, Nagasaki, Japan.

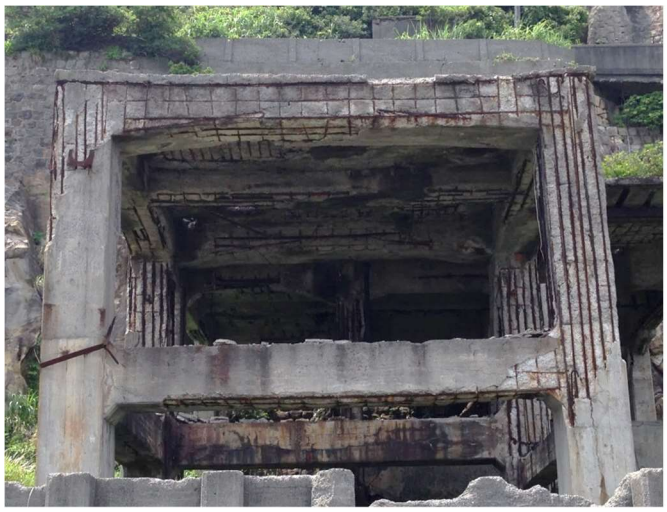

Photo—2.1 Deterioration in a RC structure

2.3 Assessment of reinforcement corrosion in concrete

2.3.1 Corrosion potential

Corrosion potential (E_{corr}) is currently one of the most widely used methods for determining the probability of steel reinforcement corrosion in concrete. Corrosion of reinforcement is associated with anodic and cathodic areas along with the reinforcement with consequent differences in electropotential of the steel. Rebar potentials are usually measured using a reference electrode connected to a handheld voltmeter, with an external attachment to the reinforcing steel (shown in Fig. 2.4). Corrosion potential measurements

cannot evaluate the kinetics of the corrosion reaction and should only be used as an indication of the corrosion risk of the steel. ASTM guidelines for interpreting rebar potentials measured with either a copper/copper sulfate ($Cu/CuSO_4$) or silver/silver chloride (Ag/AgCl) half-cell (ASTM-C876-15) are shown in Table 2.3 [2.6]. Because this reference electrode is a silver-silver chloride electrode (SCE) and the ASTM standard is based on copper-copper sulfate (CSE), the conversion from SCE to CSE is conducted by the following equation.

$$U_{Cu} = (U_{ag} - 120 - 1.1(T - 25))/1000 \quad (2.3)$$

Where U_{Cu} and U_{Ag} are the half-cell potential of CSE and SCE reference electrodes, respectively. T is ambient temperature (25°C).

Since actively corroding steel has a much more negative potential than passive steel in concrete it is also possible to detect depassivation based on potential readings. In this case, a certain shift in corrosion potential indicates depassivation. This shift is usually very pronounced and many researchers used this as a criterion in order to identify the time of depassivation. However, it should be noted that a shift in potential can have several reasons and does not always mean significant activity.

Table 2.3—$Cu/CuSO_4$ and Ag/AgCl potentials and associated risk of corrosion [2.6]

Rebar potential (mV)		Qualitative risk of corrosion
$Cu/CuSO_4$ electrode	Ag/AgCl electrode	Likely corrosion condition
> – 200	> –106	Low (10% risk of corrosion)
– 200 to – 350	– 106 to – 256	Intermediate corrosion risk
< – 350	< – 256	High (> 90% risk of corrosion)
< – 500	< – 406	Severe corrosion

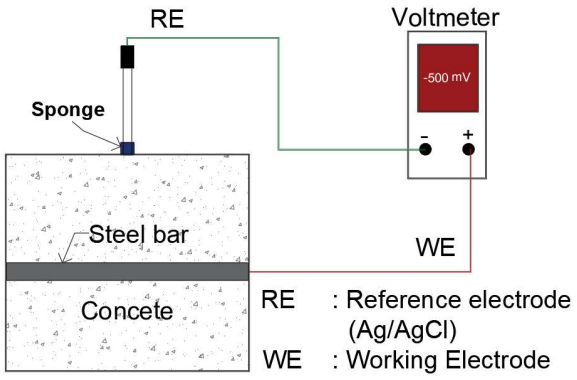

Fig. 2.4—Schematic of corrosion potential measurement

2.3.2 Corrosion rate

Corrosion rate, also known as corrosion current density (i_{corr}), is a measure of the rate of electron transfer between the anode and cathode. Corrosion rate measurements are the only reliable means of assessing corrosion activity in RC structure which can be measured using a rebar corrosion meter machine and linear polarisation resistance (LPR) technique (as shown in Fig.2.5). For linear polarization resistance (LPR) technique, also known as the polarisation resistance method, relies on the relationship between the corrosion potential of a piece of corroding steel and an external potential or current applied to it. Close to the corrosion potential the polarisation curve is linear. By measuring the polarisation curve experimentally in a small range around the equilibrium potential, the slope ΔE/ΔI of the curve can be obtained. This slope is defined as polarisation resistance Rp, which is related to the corrosion current by the Stern-Geary-equation:

$$i_{corr} = \frac{b_{ax}.b_{red}}{b_{ax} + b_{red}} \cdot \frac{1}{R_p} \quad (2.4)$$

This equation is often expressed in a simplified way as:

$$i_{corr} = \frac{B}{R_p} \quad (2.5)$$

Where Rp is the polarization resistance ($\Omega.cm^2$); i_{corr} is the corrosion current density ($\mu A/cm^2$), and B is the Stern–Geary constant. The Stern–Geary constant generally assumed to be 0.026 V at all measurements, which assuming that corrosion always occurred although should be determined empirically. The i_{corr} was converted to the corrosion rate to surface area of the steel rebar.

This technique is non-destructive and very fast, but in order to detect the initiation of active reinforcement corrosion, a significant corrosion rate has to be defined. The schematic diagram of the electrical circuit of the polarization technique is shown in Fig. 2.5. Table 2.4 shows a qualitative guide for assessing corrosion rates of structures based on the CEB standard [2.7]. Significant corrosion is characterized by an averaged sustained corrosion rate higher than 0.1 to 0.2 $\mu A/cm^2$ in concrete which contains substantial moisture and oxygen. It has to be noted that the measured corrosion rate is an average value over the exposed steel area. The local current density inside the pit is typically very high.

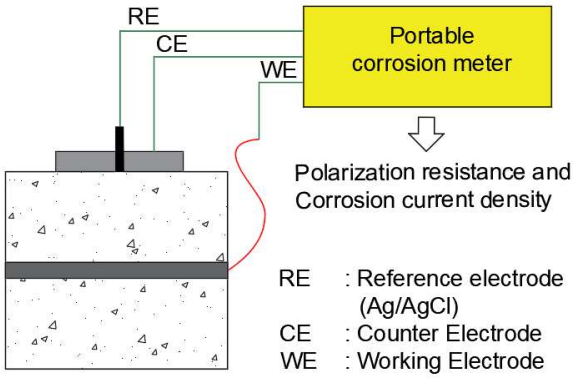

(a) rebar corrosion meter

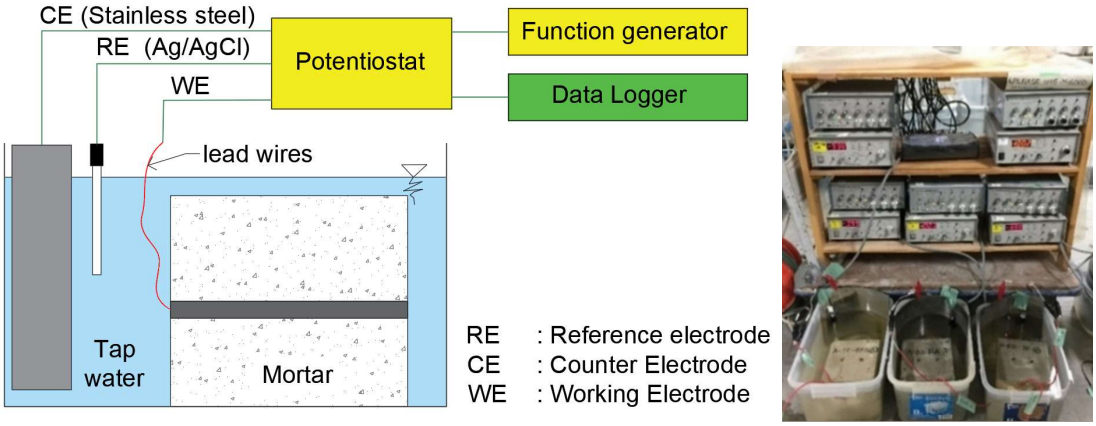

(b) linear polarization resistance (LPR) technique

Fig. 2.5—The schematic diagram of the electrical circuit of the portable corrosion meter and polarization technique

Table 2.4—Qualitative guide for the assessment of corrosion rates [2.7]

Polarization resistance, kΩ cm^2	Corrosion rate, μA/cm^2	Judgment of corrosion rate
Less than 26	Larger than 1.0	Severe and high corrosion rate
26 - 52	0.5 – 1.0	Corrosion rate of moderate to high degree
52 - 130	0.2 - 0.5	Corrosion rate of low to moderate degree
Larger than 130 - 260	Less than 0.1 - 0.2	Passive state

2.3.3 Anodic-cathodic polarization

Reactions at the anodes and cathodes are widely referred to as half-cell reactions. The anodic reaction is the oxidation process, which results in dissolution or loss of metal

while the cathodic reaction is the reduction process which results in reduction of dissolved oxygen forming hydroxyl ions. For steel embedded in concrete, following are the possible anodic reactions depending on the pH of interstitial electrolyte, presence of aggressive anions, and the existence of an appropriate electrochemical potential at the steel surface:

$$3Fe + 4H_2O \rightarrow Fe_3O_4 + 8H^+ + 8e^-$$
$$2Fe + 3H_2O \rightarrow Fe_2O_3 + 6H^+ + 6e^-$$
$$Fe + 2H_2O \rightarrow HFeO_2^- + 3H^+ + 2e^+$$
$$Fe \rightarrow Fe^{2+} + 2e^- \quad (2.6)$$

The possible cathodic reactions depend on the availability of O_2 and on the pH in the vicinity of the steel surface. The most likely reactions are as follows:

$$2H_2O + O_2 + 4e^- \rightarrow 4OH^-$$
$$\text{Or } 2H^+ + 2e^- \rightarrow H_2 \quad (2.7)$$

Anodic polarization curve is related to the quality of passivity film. When the current density becomes larger, the grade of passivation film becomes worse. On the other hand, cathodic polarization is related to diffusion of oxygen. When the current density becomes larger, it is indicating that the level of oxygen supply becomes larger [2.8]. The information on the passivity of steel bar is very important in the maintenance of existing RC structures. Anodic-cathodic polarization curve is one method for the evaluation of passivity. Polarization curve can be conducted in immersion and contact method. The immersion method is a measuring method in which the measurement is carried out with the specimen to be immersed in a solution. The mortar specimen was immersed in tap water, and two electrodes (counter and reference electrodes) were arranged and connected with the instrument in the solution. The standard saturated calomel electrode (SCE) and metal electrode (stainless steel) were used as the reference electrode and counter electrode, respectively. In addition, contact method is a measuring method using double-layer counter electrode contacted on the specimen surface.

In the measurement of anodic-cathodic polarization curve, the potential of the steel bar (E_{corr}) was shifted to ±700 mV from the natural potential with a sweep rate of 50 mV/min. The current was recorded continuously. The schematic diagram of the electrical circuit of polarization technique is shown in Fig. 2.5b. The maximum current density obtained from anodic polarization curve was then used to judge passivity grade based on Fig. 2.6 and Table 2.5 [2.8].

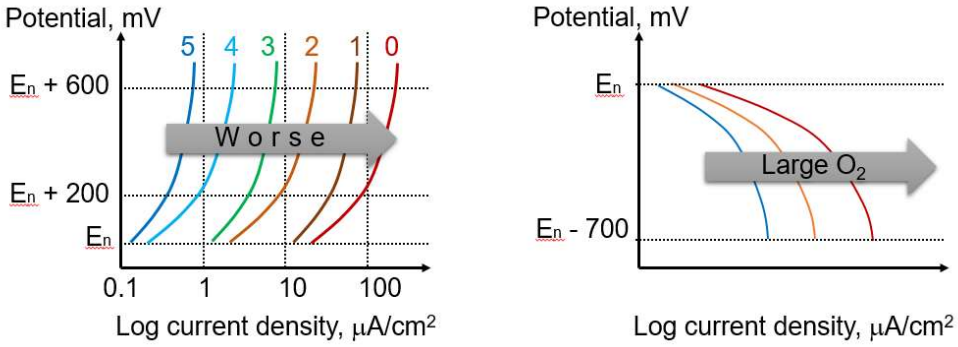

a. grade of passivity from anodic polarization curve [2.8]

b. oxygen supply from cathodic polarization curve [2.8]

Fig. 2.6— Evaluation of polarization curve

Table 2.5—Grade of passivity film associated anodic polarization curve [2.8]

Grade	Polarization curve	Condition
Grade 0	potential 0.2-0.6V, current density is over 100μA/cm² at least one time	no passivity exist
Grade 1	potential 0.2-0.6V, current density is 10-100μA/cm²	certain degree of passivity exist
Grade 2	potential 0.2-0.6V, current density is over 10μA/cm² at least once but not to qualified to	
Grade 3	potential 0.2-0.6V, current density is 1-10μA/cm²	
Grade 4	potential 0.2-0.6V, current density is over 1μA/cm² at least once but not qualified to Grade 1, 2 and 3.	
Grade 5	potential 0.2-0.6V, current density is less than 1μA/cm²	excellent passivity exist

2.3.4 Electrical resistivity

Electrical resistivity is a measure of the ability of concrete to resist the passage of electrical current. Concrete resistivity influences the corrosion rate of embedded steel once favorable conditions for corrosion exist. The four-point Wenner probe is commonly used to measure resistivity and consists of four equally spaced probes, which contact the concrete surface. This method passes between the two outermost probes use a small alternating current, and determine the resistivity of the concrete by measuring the resulting potential difference between the inner two probes (shown in Fig. 2.7). Interpretation of resistivity measurements for depassivated steel is shown in Table 2.6. Resistivity measurements are more used to complement other techniques and should not be seen as a definitive measure of corrosion activity.

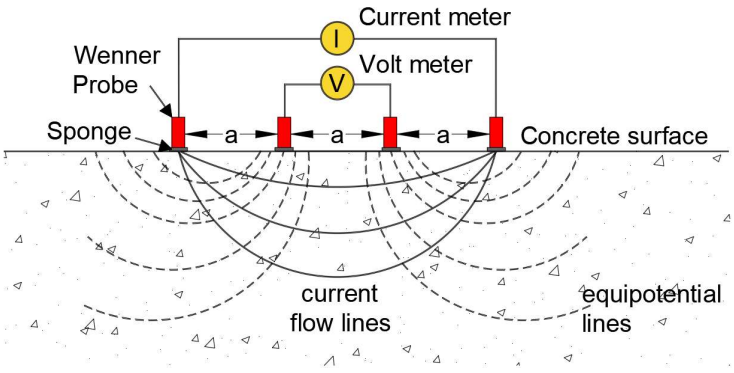

Fig. 2.7—Principle of Wenner probe measurement of concrete resistivity

Table 2.6—Relationship between resistivity and corrosion risk [2.9]

Resistivity (k Ω-cm)	Risk level
> 100 – 200	Very low corrosion rate even if chloride contaminated
50 – 100	Low corrosion rate
10 – 50	Moderate to high corrosion rate
< 10	High corrosion rate; Resistivity is not the controlling

2.4 Corrosion initiation

Chlorides penetrating concrete and carbonation of concrete can both cause the steel (or part of it) to be depassivated and start to corrode actively which is called "corrosion initiation". This monograph is concerned mainly with chloride-induced corrosion since it is invariably much damage and destructive to RC. However, carbonation-induced corrosion will also be covered briefly for completeness.

2.4.1 Chloride-induced corrosion

Chloride ions in sufficient concentration in concrete may depassivate the steel locally by breaking down the protective layer of γ-Fe_2O_3. Chlorides (Cl^-) are not consumed in the corrosion process but they help to break down the passive layer and greatly accelerate corrosion. The chloride ions act as a catalyst for the oxidation of iron through the formation of the $FeCl^-_3$ complex which is unstable and can be drawn into solution where it reacts with the available hydroxyl ions to form $Fe(OH)_2$ (see Fig. 2.8). This results in the release of Cl^- back into the solution and consumption of hydroxyl ions, as shown in the following equations:

$$2Fe + 6Cl^- \leftrightarrow 2FeCl^-_3 + 4e^-$$

followed by:

$$2FeCl + 4OH^- \leftrightarrow 2Fe(OH)_2 + 6Cl^- \quad (2.8)$$

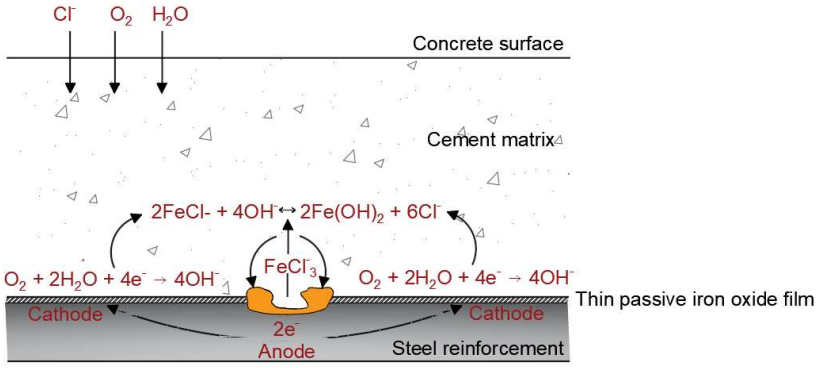

Fig. 2.8—Corrosion of reinforcement in concrete exposed to chloride ions [2.10]

Intense localized pitting corrosion as the result of corrosion is usually of the macrocell type. The acidic conditions created and the recycling of chloride ions by hydrolysis of the chloride compounds causing the process is self-propagating. In addition, chlorides reduce the resistivity of the concrete, which results in higher corrosion rates. Passivity should not be viewed as complete protection of the underlying metal but rather as a limiting value of corrosion. Indeed, some corrosion of the steel is required to form the passivating layer of oxide. The passive layer is in a continual state of breakdown and repair under normal conditions. Chloride ions contribute towards the breakdown of the passive layer while other anions such as OH^- are responsible for its stability and have inhibiting properties. There is a point therefore at which the concentration of aggressive ions overcomes the inhibiting ions and corrosion can initiate. This point is known as the chloride threshold level (see below), represented by the pitting potential, below which passivity is maintained [2.10].

Photo 2.2—Chloride-induced corrosion in a marine environment

Therefore, the tidal and splash zones in a marine environment are the areas with the highest risk for chloride-induced corrosion (as shown in Photo 2.2). Other sources of chlorides can be de-icing salts, which can generate chloride-induced corrosion on large concrete surfaces.

2.4.2 Carbonation-induced corrosion

Carbonation occurs in concrete when atmospheric carbon dioxide, CO_2, penetrates the concrete by diffusion and reacts mainly with the water and calcium hydroxide in the concrete to form calcium carbonate, $CaCO_3$. This results in the lowering of the pore solution pH from above 12 to between 8.5 and 9.0.

$$CO_2 + Ca(OH) + H_2O \rightarrow CaCO_3 + 2H_2O \quad (2.9)$$

The reduced alkalinity leads to the depassivation of steel in contact with the carbonated zones. The reaction front progresses in a step-wise fashion into the concrete. Once this carbonation front reaches the steel, the corrosion process begins, provided there are sufficient moisture and oxygen present. Carbonation usually induces a generalized (microcell) type of corrosion, where there are no distinct anodes or cathodes.

The statistical analysis by Das et al. that carbonation potential of concrete decreases with increase of compressive strength of concrete. The results indicated that using a decrease in the charge passed through concrete as a measure of carbonation could lead to misleading results in evaluation of the service life of concrete structures [2.11]. It was also observed that a low water-to-cement ratio concrete with Portland pozzolana cement has higher resistance to carbonation and rapid chloride ion permeability compared with ordinary Portland cement. A variety of interrelated factors influence the carbonation depth in concrete, including cover thickness, carbonation resistivity, effective CO_2 diffusion coefficient, binding capacity for CO_2, curing condition, age, cement type, cement composition, calcium oxide (CaO) content in cement, surface concentration of carbon dioxide, time of wetness, ambient temperature, and relative humidity. Environmental conditions, such as sheltered versus exposed and underground versus atmospheric, also have an essential impact on concrete carbonation process.

The most common method to measure carbonation depth is to spray a 1% phenolphthalein solution on to a freshly broken concrete surface. Where the pH is greater than 9, the concrete turns purple with gradually lightening shades of pink for pH of 8-9.

Colorless concrete represents the practical depth of carbonation where the pH is at or below approximately 8. Cross-section of concrete showing the carbonated and carbonated zones is shown in Fig. 2.9.

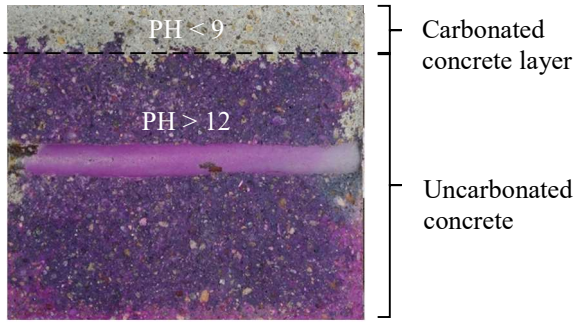

Fig. 2.9—Cross-section of concrete showing the carbonated and uncarbonated zones

2.5 Chloride Threshold

2.5.1 Chloride threshold value

It was mentioned previously that 'sufficient' chlorides are needed at the steel surface to initiate corrosion. The concentration of chlorides necessary to break down the passive film on the steel surface and initiate corrosion called chloride threshold value (CTV). Two different ways of defining CTV are common [2.12-2.13]: From a scientific point of view, the CTV can be defined as the chloride content required for depassivation of steel (namely Definition 1), whereas from the practical engineering point of view CTV is usually the chloride content associated with acceptable or visible deterioration of the RC structure (namely Definition 2). It has to be emphasized that two definitions are related to different phenomena: the depassivation-criterion in Definition 1 only considers to the initiation stage, whereas in the case of Definition 2 with acceptable or visible deterioration as a criterion, also the propagation stage is included in this definition. As a result, two definitions lead to different of CTV. Fig. 2.10 illustrates this by combining Tuutti's corrosion model [2.14] with the assumed curve representing chloride concentration at steel bar vs. time. This figure clearly shows that using the practical definition leads to higher CTV. It is essential to understand that this is only the result of a long time passing until chloride content is set on. The rate at which corrosion proceeds has a significant influence on when this is done and thus significantly affects to CTV when applying this definition. Definition 1 is more precise since it interprets the chloride content that is directly related to depassivation. In Definition 2, the chloride content

related with an acceptable degree of corrosion has no theoretical background: the amount of chloride that is measured at that time has nothing to do with the degree of corrosion or the corrosion rate. Also the term “acceptable degree” is imprecise and thus Definition 2 results in a larger scatter of CTV. In the literature, these two definitions are often mixed up. Care has, therefore, to be taken when comparing and evaluating results reported by different researchers.

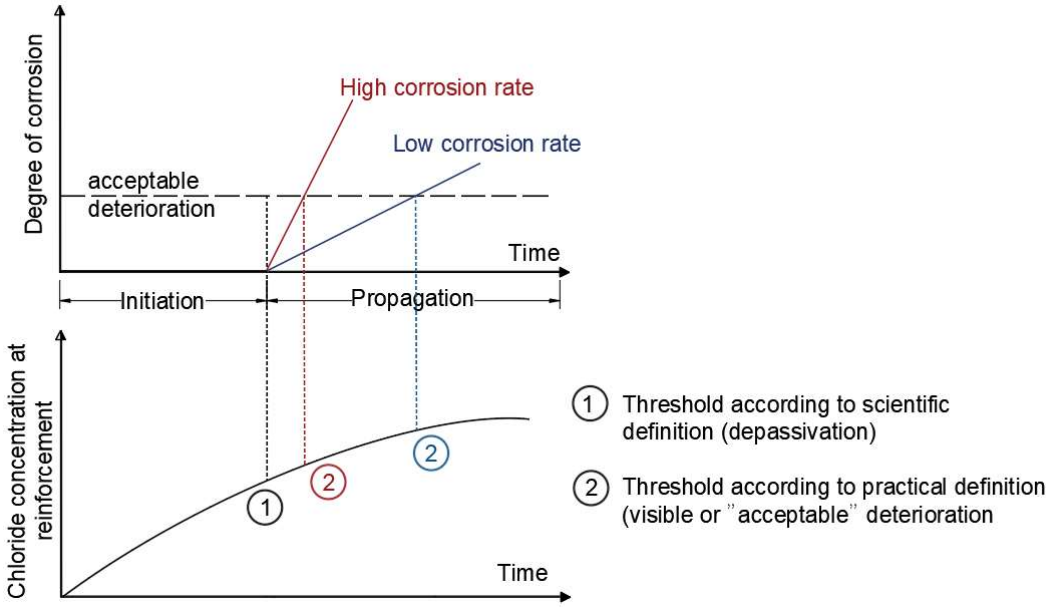

Fig. 2.10—Definitions for chloride thresholds (based on Tuutti's model) [2.14].

The chloride threshold level is not a single value for all types of concretes, steels and environments, but is affected by factors such as cover thickness, temperature, relative humidity, the electrical potential of the reinforcement, chemistry of the binder, proportion of total chlorides to free chlorides, and chloride to hydroxyl ion ratio. Since some of these factors change with time, the chloride threshold value may also change with time. All chlorides (both bound and free) can potentially influence corrosion, and so it is usually the total chlorides in the concrete that are considered for the chloride threshold. Different approaches have been used to express the chloride threshold level. These include:

1. The proportion of free chlorides (an over-simplification).
2. The ratio between free chloride and hydroxyl ion concentration, which expresses the ratio of aggressive to inhibitive ions influencing corrosion initiation. However, other factors such as the inhibitive effect of the cement matrix related to a denser hydration product layer on the steel surface are also important.

3. Total chloride (acid-soluble) content. This is the most widely used approach.

The otal chloride content relative to the weight of cement is most commonly expressed as the CTV. Relatively simple and well documented in standards is the main reason for this is the fact that the measurement of total chloride content [2.15-2.16]. Since the quantification of the binder content in hardened concrete can be difficult, it is sometimes referred to express CTV as total chloride content relative to the weight of the concrete. Generally, a large scatter is found in the literature on the minimum total chloride content that is required at the steel to initiate corrosion. Values vary from 0.02 to 3.08% total chlorides by mass of binder. A conservative value of 0.4% total chlorides by mass of binder is given by most authors. The increased use of mineral extenders such as fly ash and slag also makes the prediction of the CTV in concrete difficult.

2.5.2 Effect of mineral admixtures and water to binder ratio on CTV

Cement extenders generally higher the chloride threshold level, attributed to the reduction in alkalinity and the presence of sulfides in any slag blended binders. Table 4. show varying chloride threshold values for concretes with different binders. However, it must be stressed that different researchers have arrived at very different values for the chloride threshold level in concretes with different binders.

For example, Thomas [2.17] found that the threshold chloride value decreased with increasing substitution of PC by FA in reinforced concrete specimens after exposure to a marine environment for up to four years. Similarly, Oh et al. measured lower chloride threshold levels with increasing addition of FA. In comparison with PC, lower chloride threshold values have also been reported for silica fume containing binders [2.19, 2.20]. The partial replacement of PC with SF reduces the aluminate phases and thereby the ability of the cement to bind chlorides. However, since the addition of SF also leads to pore refinement, the effect of physical adsorption is more pronounced in SF-containing binders. Work by Gouda and Halaka [2.21] gave lower chloride threshold values for specimens containing slag when compared to specimens containing PC. The use of GGBS increases the chloride binding capacity due to improved chemical and physical binding [2.22-2.24].

Lastly, low threshold values for the blended cement may also be attributed to the slow early hydration process leading to higher short-term concrete permeability. In the long term, the denser pore structure in these concretes tends to result in a substantial

decrease in corrosion rate or a stifling of the corrosion process. For concrete in a moist environment, the cathodic reaction depends on the availability of oxygen at the cathode, and the corrosion rate may, therefore, be limited by the cathodic reaction. With a decrease in w/b ratio, oxygen ingress decreases due to lower concrete permeability, thus suppressing the cathodic reaction. Also, the concrete resistivity increases with a decrease in the w/b ratio. Corrosion rate may also be controlled by the alkalinity, which is higher in concrete that has a lower w/b ratio.

2.5.3 Free and bound chlorides

Not all of the chlorides in concrete are free or mobile and thus available for corrosion. Some are bound to the cement matrix. Free chlorides are those dissolved in the concrete pore solution, and their concentration reduces with time due to chloride binding. Binding is the removal of chloride ions from the pore solution through interaction with the cement matrix. Chlorides in concrete can be bound chemically through a reaction with the aluminate phases (C_3A and C_4AF) to form calcium chloro-aluminates. They can also be physically bound to hydrate surfaces by adsorption [2.25]. All cement bind chlorides to some degree and this strongly influences the rate at which chlorides penetrate the concrete from an external source.

Bound chlorides exist in chemical equilibrium with the free chlorides, which means they can be released under certain conditions to become free chlorides again. Such a condition occurred when chloride contaminated concrete subsequently carbonates, which causes a release of the bound chlorides. Thus, bound chlorides also present a corrosion risk. While chloride binding retards chloride penetration, it also allows the build-up of higher chloride contents that can increase the corrosion risk in some situations. The nature of cement chemistry is essential in chloride binding. In exposure conditions where chlorides are a problem such as marine conditions, choice of binder type is critical.

The effect of chloride binding on corrosion initiation is twofold: (1) the rate of chloride transport in concrete is reduced by binding since the number of mobile ions (free chlorides) is reduced and (2) the reduction of free chlorides results in lower amounts of chlorides accumulating at the reinforcing steel and therefore it takes longer to reach the chloride threshold level. The increased time to corrosion initiation cannot only be attributed to chloride binding effects, since other effects such as the denser pore structure in the blended cement may also contribute to the longer time to corrosion initiation. Even

after corrosion has started, the rate will continue to be affected by binding as there is a slower increase in chloride level which in turn limits the increase in corrosion rate.

2.6 Seawater mixing

Fig. 2.11 demonstrates literature reviews to the contribution of various mechanisms affecting the durability, which were reviewed more than 400 references [2.26]. From this figure, it was seen that carbonation and chloride attack mechanism were the most significant percentage affecting durability. It means that the majority deterioration cases of concrete are connected to corrosion of reinforcing steel bars due to carbonation or chloride-induced corrosion. The literature-based investigations of seawater-mixed concrete have widely been discussed by Nishida et al. [2.27]. They reported that from 1974 to 2011, 68 papers had been published regarding seawater mixing, as shown in Fig. 2.12. From this figure, it implies that the properties and durability of concrete mixed with seawater have been investigated in several aspects, widely.

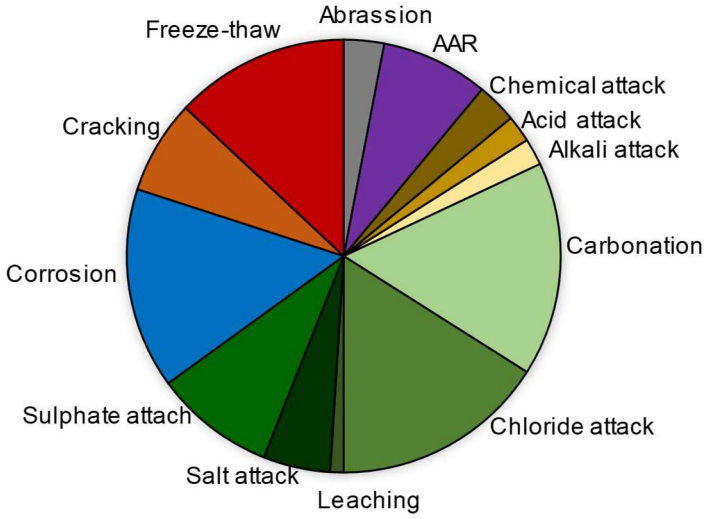

Fig. 2.11—Contribution of various mechanisms influencing durability [2.26]

In regard to strength, Tarek et al. [2.28] have stated that there was no significant difference in compressive strength of concrete for concrete mixed with seawater tap water, after exposure 20 years in the tidal environment. The concrete strength after 20 years' exposure under the marine environment is not affected by mixing water as stated by Fukute et al. [2.29]. Ghorab et al. [2.30] also reported that the compressive strength of plain concrete cubes ages up to 17 months is unaffected by mixing and curing water. A

similar tendency is also revealed by Mori [2.31] that the difference in the strength of concrete mixed with seawater and freshwater is small after ten years' exposure test.

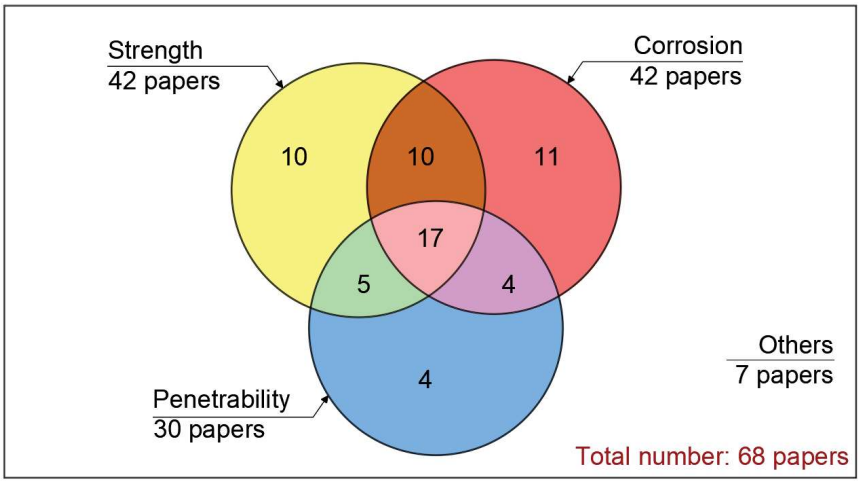

Fig. 2.12—Investigated items related to seawater mixed concrete [2.27]

Regarding strength, the concrete strength after 20 years' exposure under the marine environment is not affected by mixing water as stated by Fukute et al. [2.28]. Tarek et al. [2.29] have reported that there was no significant difference in compressive strength of concrete for concrete mixed with seawater tap water, after exposure 20 years in the tidal environment. Mori [2.30] also found the difference in the strength of concrete mixed with seawater and freshwater is small after ten years' exposure test. A similar tendency is also found by Ghorab et al. [2.31] that the compressive strength of plain concrete cubes ages up to 17 months is unaffected by mixing and curing water.

However, Donald et al. [2.32] concluded that natural seawater does not deteriorate plain concrete; strength is generally increased with salinities up to nearly three times. A similar finding was also found by Otsuki [2.33] that mixing with seawater decreases the number of pores, and then strength BFS cement with seawater is increased. It is also concluded by Taylor et al. [2.34] that the compressive strength of concrete is enhanced by the presence of sodium chloride or ocean salts in the mixing water. The early strength of seawater and unwashed sea sand concrete (total chloride ion content: around 4.5 kg/m^3) is high, long-term strength is also retained at a high level by Katano et al. [2.35]. On the other hand, Kausik et al. [2.36] expressed that seawater affects the gain in strength of cement when used for mixing, it increases the early strength up to 7 days, but ultimately the strength decreases about 13% at 28 days.

2.7 Issues addressed in this study

Chloride-induced corrosion is recognized as one of the primary cause of deterioration of RC structures, particularly in the marine environment. The chloride penetrates concrete then after reached some amount of value then corrosion initiate. Several standards code described the chloride threshold for breakdown passivity film of steel bar. JSCE, RILEM and ACI define threshold values to forecast the beginning of the propagation period of the corrosion process in RC structure. JSCE standard suggested that 1.2 kg/m^3 of chloride by weight concrete as chloride threshold. While, RILEM and ACI recommended that 0.2~0.5% and 0.2% of chloride by weight %-cement as chloride threshold, respectively. The previous study based on Hamada et al. [2.37] indicated that 0.4% of chloride by weight %-cement as chloride threshold. The optimal design regarding durability for long-lasting performance of seawater in RC structure was necessary because it provides a demonstration of the long-term behavior of a commonly used construction material, permitting the prediction of the behaviors of existing structures and the more informed design and study of structures to be built. Therefore, this study is using mineral admixture to determine chloride threshold value and completing an extended evaluation of the corrosion-related deterioration of RC beams exposed to naturally corrosive environments. The result of this study is expected to propose reliable ranges of threshold chloride concentration causing active corrosion of steel using mineral admixture and an overview assessment of seawater mixing regarding durability consideration of concrete member and become issues addressed in this study.

Chapter 3 and **Chapter 4** are laboratory case for corrosion evaluation of mortar due to chloride attack. Influence of water to binder ratio and utilization of mineral admixture on CTV provide great necessary information for durability evaluation. Further, field case by performing long-term exposed of RC beam in tidal and splash zone are described in **Chapter 5** and **Chapter 6**. Influence of concrete cover, water to binder ratio, seawater mixing, and bending moment in marine environment will provide necessary information regarding durability, performance evaluation and future applicability of seawater mixing.

Finally, based on comprehensive analysis was conducted in **Chapter 3, 4, 5** and **6**, an overview assessment was offered in the last section on **Chapter 6** for long-lasting performance concrete structures particularly in marine environmental condition. An overview of durability assessment from long-lasting performance may guide for future

durability design. In addition, the resulting data set provides a clear demonstration of the effects seawater on corrosion reinforcement and proper measures to prevent reinforcement from corrosion.

References

[2.1] Neville, Adam. "Seawater in the mixture." *Concrete international* 23.1 (2001): 48-51.

[2.2] JSCE, Standard Specification for Concrete Structures (Part: Maintenance), Japan Society of Civil Engineers, Japan, 2007.

[2.3] O. T. de Rincón, Y. Hernández-López, A. de Valle-Moreno, A. A. Torres-Acosta, F. Barrios, P. Montero, P. Oidor-Salinas, J. R. Montero, Environmental influence on point anodes performance in reinforced concrete, Construction and Building Materials 2008;22(4):494-503.

[2.4] Richardson, Mark G. Fundamentals of durable reinforced concrete. CRC Press, 2002.

[2.5] Liu, Youping. Modeling the time-to corrosion cracking of the cover concrete in chloride-contaminated reinforced concrete structures. Diss. Virginia Tech, 1996.

[2.6] ASTM C876, Standards test method for half-cell potentials of reinforcing steel in concrete; 1991.

[2.7] CEB. "Strategies for Testing and Assessment of Concrete Structure" Bulletin n.243, 183 pp., 1998.

[2.8] Otsuki, N. "A study of effectiveness of chloride on corrosion of steel bar in concrete." Report of Port and Harbor Research Institute (1985): 127-134.

[2.9] Andrade, C., and Cruz Alonso. "Corrosion rate monitoring in the laboratory and on-site." Construction and Building Materials 10.5 (1996): 315-328.

[2.10] Broomfield, John P. Corrosion of steel in concrete: understanding, investigation and repair. CRC Press, 2003.

[2.11] Das, B. B., D. N. Singh, and S. P. Pandey. "Rapid chloride ion permeability of OPC-and PPC-based carbonated concrete." Journal of Materials in Civil Engineering 24.5 (2011): 606-611.

[2.12] P. Schiessl, M. Raupach, Influence of concrete composition and microclimate on the critical chloride content in concrete, Proc. 3rd Int. Symp. “Corrosion of Reinforcement in Concrete”, Elsevier Applied Science, Wishaw, UK, 1990, pp. 49–58.

[2.13] Schiessl, P., and S. Lay. "Influence of concrete composition." Corrosion in reinforced concrete structures (2005): 91-134.

[2.14] Tuutti, Kyösti. Corrosion of steel in concrete. Cement-och betonginst., 1982.

[2.15] ASTM, C. "1152 (2004)“Standard Test Method for Acid-Soluble Chloride in Mortar and Concrete,”." ASTM International, West Conshohocken, PA.

[2.16] Andrade, C., and M. Castellote. "Recommendation of RILEM TC 178-TMC:" Testing and modelling chloride penetration in concrete": Analysis of total chloride content in concrete." Materials and structures 35.9 (2002): 583-585.
[2.17] Thomas, Michael. "Chloride thresholds in marine concrete." Cement and concrete research 26.4 (1996): 513-519.
[2.18] Oh, Byung Hwan, Seung Yup Jang, and Y. S. Shin. "Experimental investigation of the threshold chloride concentration for corrosion initiation in reinforced concrete structures." Magazine of Concrete Research 55.2 (2003): 117-124.
[2.19] Pettersson, K. "Chloride threshold value and the corrosion rate in reinforced concrete." Proc. of the Nordic Seminar. 1994.
[2.20] Manera, Marco, Øystein Vennesland, and Luca Bertolini. "Chloride threshold for rebar corrosion in concrete with addition of silica fume." Corrosion Science 50.2 (2008): 554-560.
[2.21] Gouda, V. K., and W. Y. Halaka. "Corrosion and corrosion inhibition of reinforcing steel: II. Embedded in concrete." British Corrosion Journal 5.5 (1970): 204-208.
[2.22] Arya, C., N. R. Buenfeld, and J. B. Newman. "Factors influencing chloride-binding in concrete." Cement and Concrete research 20.2 (1990): 291-300.
[2.23] Dhir, R. K., M. A. K. El-Mohr, and T. D. Dyer. "Chloride binding in GGBS concrete." Cement and Concrete Research 26.12 (1996): 1767-1773.
[2.24] Luo, Rui, et al. "Study of chloride binding and diffusion in GGBS concrete." Cement and Concrete Research 33.1 (2003): 1-7.
[2.25] Boddy, Andrea, et al. "An overview and sensitivity study of a multimechanistic chloride transport model." Cement and concrete research 29.6 (1999): 827-837.
[2.26] Basheer, P. A. M., S. E. Chidiact, and A. E. Long. "Predictive models for deterioration of concrete structures." Construction and Building Materials 10.1 (1996): 27-37.
[2.27] Nishida, Takahiro, et al. "Some considerations for applicability of seawater as mixing water in concrete." Journal of Materials in Civil engineering 27.7 (2013): B4014004.
[2.28] Fukute, T., K. Yamamoto, and H. Hamada. "Study on the Durability of Concrete Mixed with Sea water." Report of the Port and Harbour Research Institute 29.3 (1990).
[2.29] Mohammed, Tarek Uddin, Hidenori Hamada, and Toru Yamaji. "Performance of seawater-mixed concrete in the tidal environment." Cement and concrete research 34.4 (2004): 593-601.
[2.30] Mori, Y. "10 years exposure test of concrete mixed with seawater under marine environment." Journal of cement association 35 (1981): 341-344. (in Japanese).
[2.31] Ghorab, Hanna Youssef, M. S. Hilal, and A. Antar. "Effect of mixing and curing waters on the behavior of cement pastes and concrete Part 2: Properties of cement paste and concrete." Cement and concrete research 20.1 (1990): 69-72.
[2.32] Donald F. Griffin and Robert L. Henry, “The Effect of Salt in Concrete On Compressive Strength, Water Vapor Transmission, and Corrosion of Reinforcing Steel”, Technical Report of U.S. Naval Civil Engineering Laboratory, 1964.

[2.33] Otsuki, Nobuaki, Tsuyoshi Saito, and Yutaka Tadokoro. "Possibility of sea water as mixing water in concrete." Conference on Our World in Concrete & Structures. Tokyo Institute of Technology, Japan. 2011.

[2.34] Taylor, Michael A., and Adam Kuwairi. "Effects of ocean salts on the compressive strength of concrete." Cement and Concrete Research 8.4 (1978): 491-500.

[2.35] Katano, Keisaburo, et al. "Properties and application of concrete made with sea water and un-washed sea sand." Proceedings of Third International Conference on Sustainable Construction Materials and Technologies. 2013.

[2.36] Kaushik, S. K., and S. Islam. "Suitability of sea water for mixing structural concrete exposed to a marine environment." Cement and Concrete Composites 17.3 (1995): 177-185.

[2.37] Hamada, Hidenori, et al. "An experimental study on relationship between chloride content in mortar and passivity condition of embedded steel bar." 4th International Symposium on Life-Cycle Civil Engineering, IALCCE 2014. CRC Press/Balkema, 2015.

CHAPTER 3 CORROSION MONITORING OF STEEL BAR IN OPC MORTAR FROM MODERATE TO HIGH CORROSION RATE

3.1 Introduction

Generally, the corrosion initiation time is quite long (decades) than that of the propagation stage (years) for the RC structures. In such situations, the accuracy of predicting the overall service life of the structure depends on the accurate prediction of the initiation period [3.1]. However, few RC structures show corrosion initiation early in their service life with more extended corrosion propagation stage, which emphasizes the need for accurate prediction of the variability in the corrosion propagation. The early corrosion can occur in case of new structures with preexisting narrow cracking, which has caused corrosion to initiate relatively early. In most cases, preexisting of close cracking on the concrete surface due to hydration heat after hardening. Where the factors that influence are type, total content, and chemical composition of cement, ambient temperature and admixtures used so that chloride can promote corrosion initiation. Once reinforcement corrosion is initiated, its propagation is governed mainly by the oxygen supply, moisture content and resistivity of concrete [3.2]. It progresses almost at a steady rate and shortens the service life of the structure, by causing surface cracking and subsequently spalling of the cover concrete due to the expansion of the corroding steel. The rate of corrosion directly affects the extent of the remaining service life of a corroding RC structure. Within recent decades, some researchers placed much focus on studying the initiation as well as propagation of corrosion processes in RC structures. In particular, concerning the propagation of reinforcement corrosion, electrochemical analysis still necessary for developing to evaluate corrosion processes in RC structures.

Various techniques for detecting and measuring corrosion will provide data on the causes, detection, or rate of corrosion [3.3]. The electrochemical methods could be used to estimate the corrosion rate in RC structures to show the speed at which steel bar already corroded and to identify vulnerable locations. Determination of electrochemical parameters is,

however, often difficult or necessary highly accuracy for in situ RC structures. By reviewing the literature in Chapter 2, the values of corrosion potential, corrosion current density and grade passivity are a highlight as significant parameters in the analysis predictions of corrosion.

The main objective of this study was to identify and determine corrosion behavior and the extent of corrosion of OPC mortar during the early period of the propagation stage using several corrosion measurement methods. Four corrosion measurement methods (corrosion potential, corrosion current density, grade passivity and electrical resistance) were chosen to assess the corrosion behavior of steel bar embedded in chloride contaminated mortar. The corrosion state of the steel bar in mortar was analyzed within specified limits of corrosion current density by 0.5-1.0 μA/cm² which indicate corrosion rate moderate to a high degree as per classification of corrosion rate by CEB [3.4]. From the present test results, the factors influence of corrosion behavior of OPC mortar with difference chloride contaminated from moderate to high corrosion rate is proposed. The interesting issue, the sensitivity of the corrosion potential against chloride content tends to be decreased after a certain period of exposure. Therefore, from moderate to high corrosion rate, after 8-years exposure for OPC mortar has increased the probability from pitting to generate corrosion.

3.2 Experimental method

3.2.1 Materials and mix proportions

Ordinary Portland Cement (OPC) was used in the mortar specimens. The physical properties and chemical analysis are shown in Table 3.1. Washed sea sand was used as fine aggregates. Specific gravity, water absorption, and fineness modulus of sand were 2.49 g/cm^3, 1.42 %, and 2.8, respectively. Japanese Industrial Standard steel bars (JIS SR 235) were used. The chemical compositions of steel bars are shown in Table 3.2.

Table 3.1—Physical and chemical compositions of cement

Specific gravity	Blaine fineness, cm^2/g	Ignition loss, %	Al_2O_3, %	MgO, %	SO_3, %	Cl^-, %
3.16	3250	2.04	0.51	1.29	2.08	0.018

Note: OPC satisfied JIS R5210

Table 3.2—Chemical compositions of steel bar

C, %	Si, %	Mn, %	P, %	S, %
0.18	0.18	0.64	0.015	0.021

Note: Steel bar satisfied JIS G3112

3.2.2 Specimens

The specimens were exposed for almost 8-years in the laboratory ambient condition (T: 20±2°C, RH: 60%). The size of the specimens is 120x135x135 mm. Round steel bars 13 and 135 mm in diameter and length, respectively, were embedded at cover depths of 50 mm clear distance from the measuring surface. The copper wires were connected to the steel bar for electrochemical measurement. The end of steel bar was covered with resin to avoid corrosion and to ensure the connection between steel bar and copper wire.

Five sides of the specimen were coated with epoxy resin and the remaining side was kept uncoated for CO_2 diffusion and as a measuring surface (Photo 4.1).

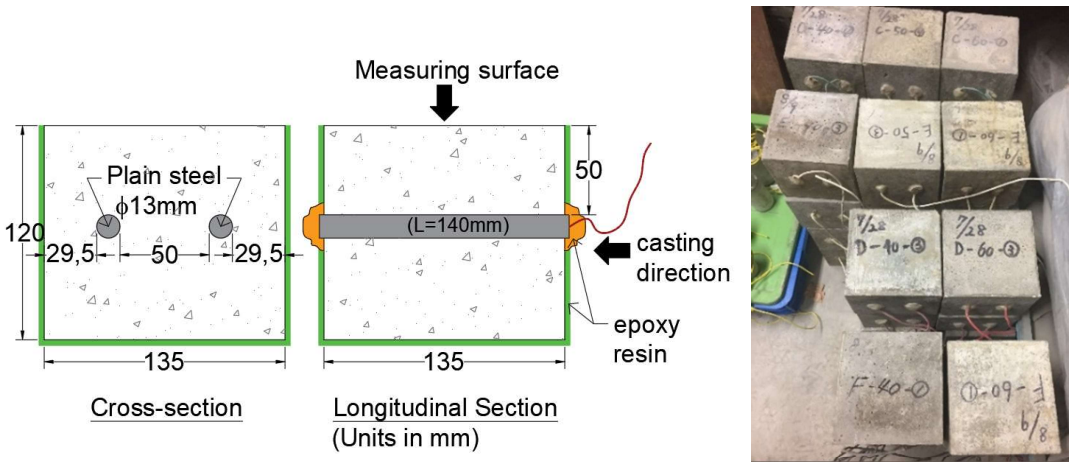

Fig. 3.1—Appearance and details of specimen

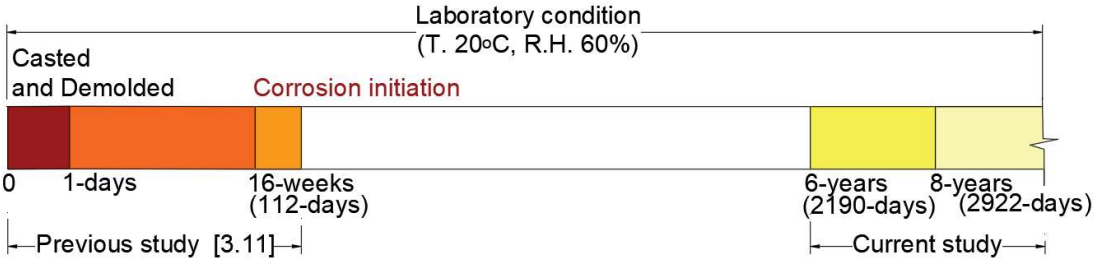

Fig. 3.2—The schematic of the exposure condition

3.2.3 Proportions of mixture

Four series of mortar mixtures with three types of water-to-cement ratio (W/C) of 0.4, 0.5, and 0.6 was set for mixing mortar. Two influencing parameters of chloride content in mortar were used. One is interpreted in %-cement (mass ratio of cement), another is interpreted in kg/m^3 (total chloride weight in mortar). Water-to-cement ratio (W/C) of 0.5 was selected as a reference. In this reference, chloride content in mortar are 1.46 kg/m^3, 2.18 kg/m^3 and 2.91

kg/m^3 in accordance to 0.29%-cement, 0.43%-cement and 0.57 %-cement, respectively. In the specimen B, D and F, chloride content is fixed in kg/m^3. And, in the specimen A, C and E, chloride content is fixed in %-cement. All cases of chloride content for each mix and mix proportions of specimen are shown in Table 3.3 and Table 3.4, respectively. Notable, electrochemical data for specimen in Series A and B are only available until 140-days.

Table 3.3—Design of chloride content

Specimen code	W/C	Chloride content		Remark
		Total content in mortar, kg/m^3	Weight ratio of cement, %-cement	
A	0.4	1.66	0.29	A40
	0.5	1.46		AB50
	0.6	1.3		A60
B	0.4	1.46	0.25	B40
	0.5		0.29	AB50
	0.6		0.32	B60
C	0.4	2.49	0.43	C40
	0.5	2.18		CD50
	0.6	1.94		C60
D	0.4	2.18	0.38	D40
	0.5		0.43	CD50
	0.6		0.48	D60
E	0.4	3.32	0.57	E40
	0.5	2.91		EF50
	0.6	2.59		E60
F	0.4	2.91	0.5	F40
	0.5		0.57	EF50
	0.6		0.64	F60

Table 3.4—Mixture proportions of mortar

W/C	W, kg/m^3	C, kg/m^3	S, kg/m^3
0.4	232	581	1508
0.5	255	510	1508
0.6	272	454	1508

Note: W = Water, C = Cement, and S = Sand.

3.3 Experimental Methods

3.3.1 Corrosion potential

The corrosion potential (E_{corr}) was taken as an average of two steel bars and measured by using the silver/silver chloride reference electrode (Ag/AgCl) after 30-min pre-wetting of mortar surface. Then, the potential value was converted to the value against copper/copper sulfate reference electrode (CSE). The specified limits of E_{corr} (-500 mV) are considered to be severe corrosion as per ASTM C876 [3.5]. Fig. 3.3 shows the details of the measurement.

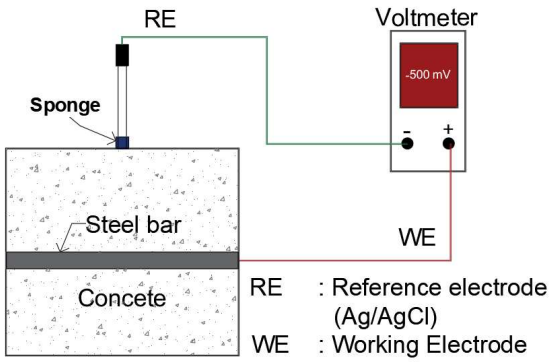

Fig. 3.3—Measurement of corrosion potential

3.3.2 Corrosion current density

The polarization resistance was taken as an average of two steel bars and measured by using the silver/silver chloride reference electrode (Ag/AgCl) and portable corrosion meter after 30-minutes pre-wetting. Figure 3.4 shows the details of the measurement. The following equation was used to calculate the I_{corr} using the Stren-Geary Formula [3.6].

$$I_{corr} = \frac{B}{R_p} x\ 10^6 \qquad (3.1)$$

Where I_{corr} is corrosion current density ($\mu A/cm^2$), Rp is polarization resistance ($\Omega.cm^2$) and B is 0.026V considering steel inactive condition [3.7, 3.8]. The specified limits of corrosion current density (0.5-1.0 $\mu A/cm^2$) are considered to be moderate to high corroding as per CEB Standard [3.4].

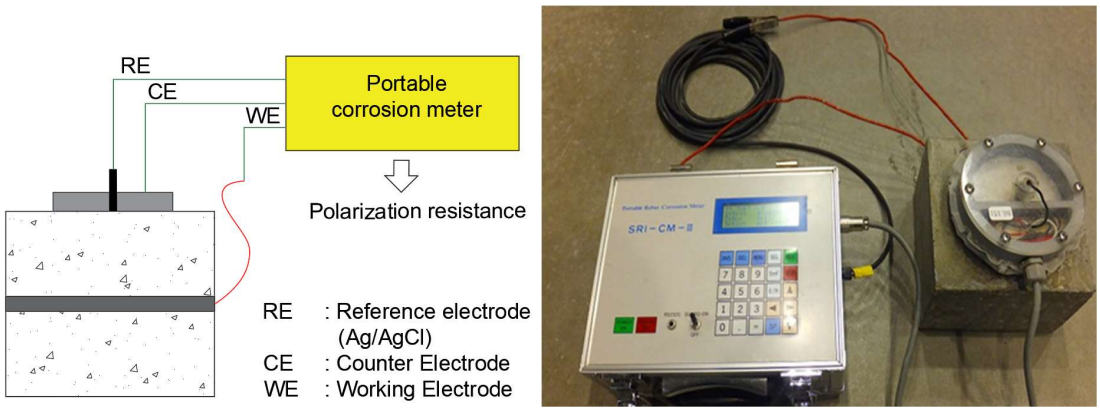

Fig. 3.4—Measurement of micro-cell corrosion

3.3.3 Grade passivity and oxygen permeability

The anodic polarization curve (APC) is related to the passivity condition of steel bar. When the current density becomes larger, the grade of passivity film of steel bar becomes worse [3.9]. The cathodic polarization curve (CPC) is related to diffusion of oxygen. When

the current density becomes larger, the level of oxygen diffusion becomes larger. For this, similar testing equipment as for polarization behavior test was used. The mortar specimen was immersed in tap water, and two electrodes (counter and reference electrodes) were arranged and connected with the instrument in the solution. The standard saturated calomel electrode (SCE) and metal electrode (stainless steel) were used as the reference electrode and counter electrode, respectively. The rest potential of the steel bars gradually shifted to +700 mV for APC and -700mV for CPC with a scan speed of 50 mV/min by a potentiostat. The maximum current density obtained from APC was then used to judge passivity grade in Chapter 2 (Fig. 2.6 and Table 2.5) [3.9]. Fig. 3.5 shows the details of the measurement.

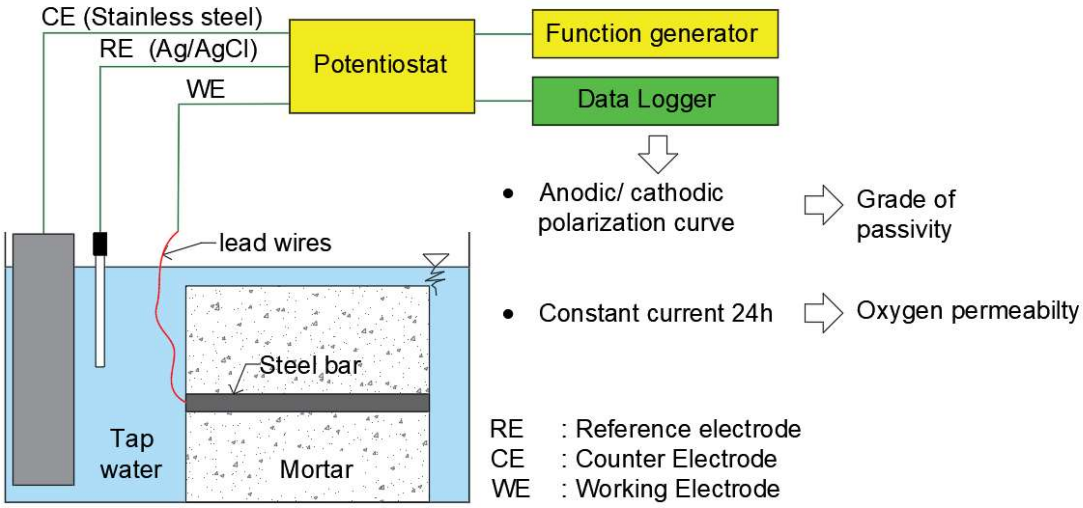

Fig. 3.5—The schematic diagram of the electrical circuit of polarization technique

The constant current density (i_{lim}) over the steel bars was measured. The i_{lim} was measured by using a potentiostat. The potential of the steel bar was set to -1,000 mV and held constant then the current was recorded continuously. When measurements began, current was a maximum then gradually falling until reaching an almost constant value after kept in 24-hours. The rate of oxygen permeability was obtained from the i_{lim} using the following Eq. (3.2)

$$\frac{dQ}{dt} = -\frac{i_{lim}}{n.F} \tag{3.2}$$

where (dQ)/(dt) is the oxygen permeability in mole/cm^2/s (on steel surface); i_{lim} is the limiting cathodic current density in A/cm^2; n is 4, and F is the Faraday's constant (96,500 coulombs/mole). Fig. 3.5 shows the details of the measurement.

3.3.4 Electrical resistivity

The electrical resistivity was measured by using the Wenner probe. The resistivity of mortar specimen from the average of three times measurement was determined. The specified limits of electrical resistivity (10-50 kΩ-cm) are considered to be moderate to high corroding base on Andrade and Alonso [3.10].

3.3.5 Corroded area

For physical evaluation of corrosion, the corroded area of the steel bars was measured followed by cutting and splitting of corrosion test specimens. A transparent paper was wrapped carefully on the circumferential surface of corroded steel bars. Then using a permanent black marker pen corroded area was sketched. An image of transparent paper has been produced by scanning the paper. Then the corroded area of steel bar was calculated using computer image analysis software (Image Jv1.49).

3.4 Results

3.4.1 Corrosion potential

The difference value of corrosion potential at the age of 6-years and 8-years and the time dependence changes of corrosion potential during 8-years are shown in Fig. 3.6 and Fig. 3.7, respectively. The HCP data of 6-years was already reported in previous study [3.13]. From both figures, the potential of all specimens in Series C~F value was dropped to more negative value than -400mV after 6-years (2190-days). The potential of all specimen crossed a threshold value based on the ASTM standard [3.8] which is categorized as 90% probability of corrosion. After 8-years, the potential did not change too much from 6-years. The higher negative values of corrosion potential of all the specimens implied that specimens have started to corrode which was confirmed by the visual observation later. In addition, the potential tends to be more negative value linearly with the increase in W/C ratio.

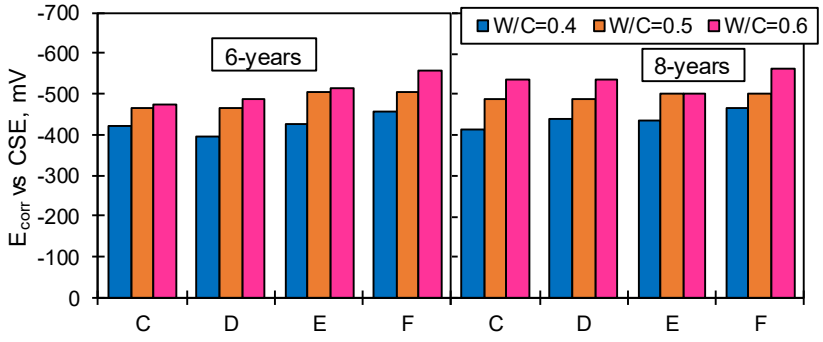

Fig. 3.6—Corrosion potential at the age of 6-years and 8-years

Fig. 3.8 shows the relationship between chloride content and corrosion potential at 6-years and 8-years, together with the 16-weeks data based on previous data [3.10]. The chloride content in mass percent versus unit cement mass and total weight of unit mortar volume are shown in Fig.3.5. These figures both indicate that corrosion potential shows a clear linear relationship with chloride content. The relationship is interpreted with the following equations (3.3) and (3.4) at 6-years and 8-years, respectively, which the equation constructed from the linear regression function (least-squares estimation).

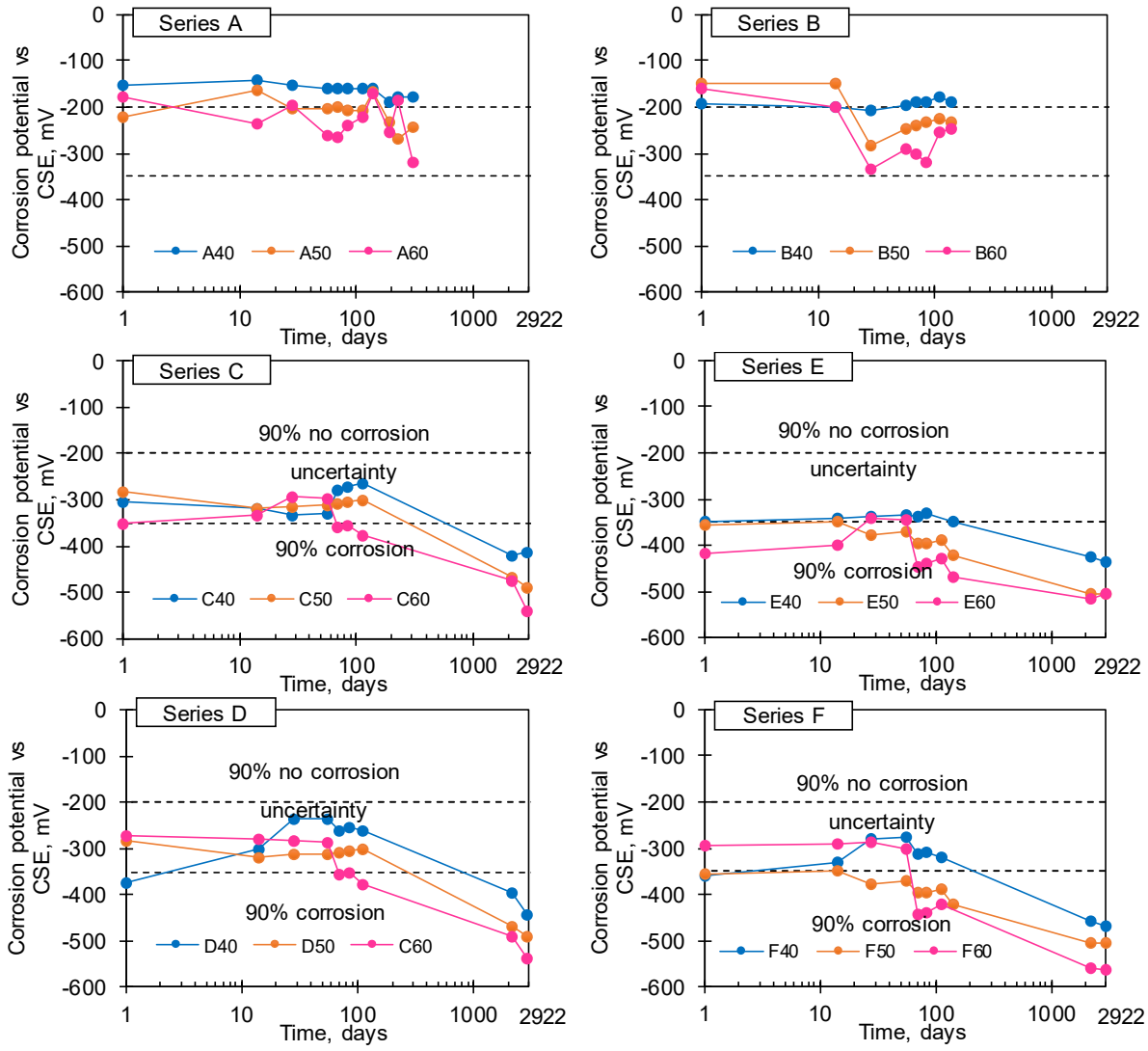

Fig. 3.7—Time dependence change of E_{corr}

Equation for 6-years old:

$$E_{corr} = -182\ Cc - 339 \qquad (W/C=0.4)$$
$$E_{corr} = -260\ Cc - 355 \qquad (W/C=0.5)$$
$$E_{corr} = -388\ Cc - 305 \qquad (W/C=0.6)$$

E_{corr} = -31 Ct - 341 (W/C=0.4)
E_{corr} = -50 Ct - 358 (W/C=0.5)
E_{corr} = -84 Ct - 308 (W/C=0.6) (3.3)

And equation for 8-years old:

E_{corr} = -69 Cc - 407 (W/C=0.4)
E_{corr} = -100 Cc - 446 (W/C=0.5)
E_{corr} = -104 Cc - 488 (W/C=0.6)
E_{corr} = -12 Ct - 408 (W/C=0.4)
E_{corr} = -19Ct - 447 (W/C=0.5)
E_{corr} = -22 Ct - 489 (W/C=0.6) (3.4)

Where E_{corr} is corrosion potential in mV (CSE), Cc is chloride content in %-cement and Ct is chloride content in kg/m^3.

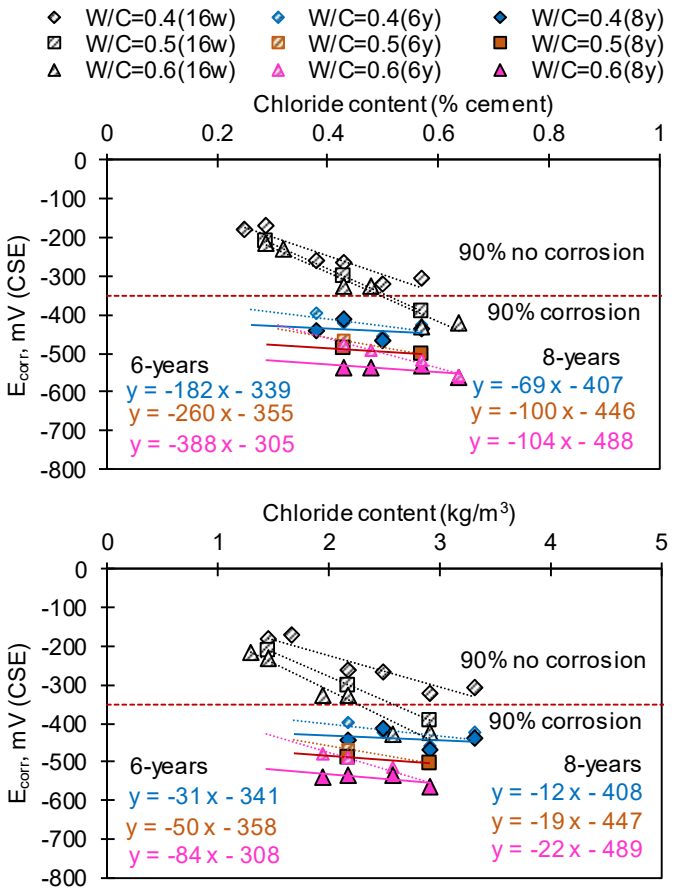

Fig. 3.8—Relationship between E_{corr} and chloride content

3.4.2 Corrosion current density

The previous study refers to Hamada et al. [3.11], the E_{corr} values were used as a criterion for estimating the corrosion level of steel bars embedded in mortar specimens. For all the specimen series, -350 mV of potential was used as a threshold limit for defining the

start of active corrosion. After more than 6-years (2190-days) exposure, the potential value seems almost similar and chloride contaminated in mortar become less effectiveness. Therefore, in this study, the corrosion potential, corrosion rate and grade passivity also were used as a criterion for identification of corrosion level of steel bar after more than 6-years exposure.

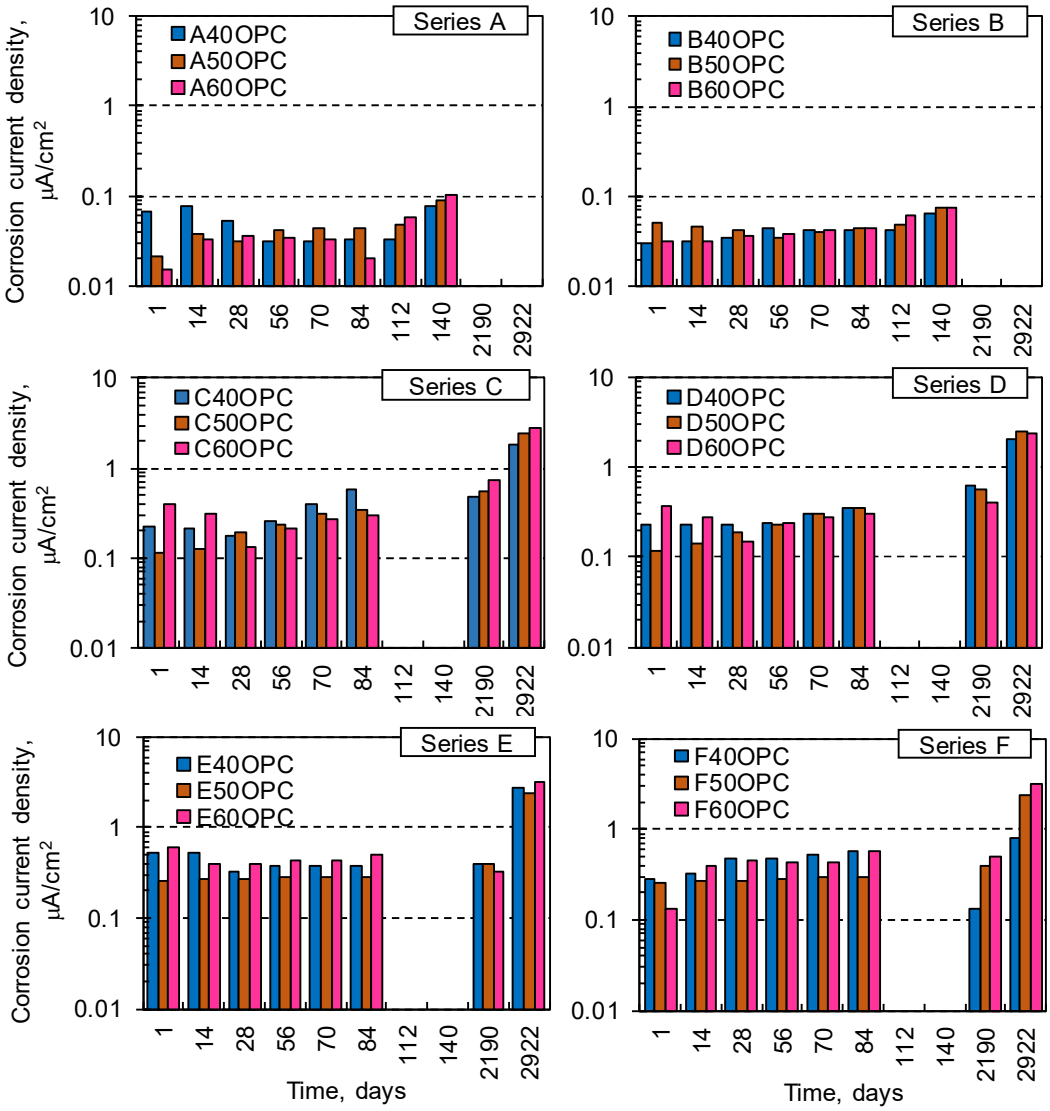

Fig. 3.9—Time dependence change of corrosion current density

The time dependence change of I_{corr} for all series is shown in Fig. 3.9. It was observed that the value of the I_{corr}-time graph for Series C, D, E and F series are quite steep as compared to A and B series. The I_{corr} of A and B (1~140 days) shows less than 0.1 μA/cm^2, which is categorized as a passive state based on CEB standard [3.4]. Series C~F (1~84 days) shows around 0.1~0.5 μA/cm^2, which is classified as low corrosion level. It should be noted that Series C~F at the age of 112 and 140-days data was not available. Further, mortar specimens

of series C and D after reaching the specified criteria of 0.5~1.0 μA/cm² as moderate corrosion was found to be after 6-years. After 8-years (2922-days) exposure, I_{corr} for each series (C~F) reach more than 1 μA/cm^2 and indicated high corrosion level. The electrochemical evaluation by I_{corr} was confirmed and strong correlated on actual corrosion at the age of 6-years and 8-years which explain later. The actual corrosion at the age of 6-years on surface steel bar surface can be observed only small amount and after 8-years it was increased to a large amount of corrosion. No significant influence amount of chloride was found after 8-years. It implies that each specimen showed the same behavior during the corrosion propagation stage.

3.4.3 Grade passivity

The APC of the steel bars at the age of 16 weeks, 6-years and 8-years are shown in Fig. 4.10. From the figures, the anodic curve towards higher current region with the increase in W/C ratio. When the current density becomes larger, the grade of passivation film becomes worse [3.9]. For quantitative evaluation, the passivity grades (scaled from 0 to 5) were also evaluated based on the procedure developed by Otsuki et al. [3.9]. The Grade 0 means complete loss of passivity and Grade 5 means excellent passivity.

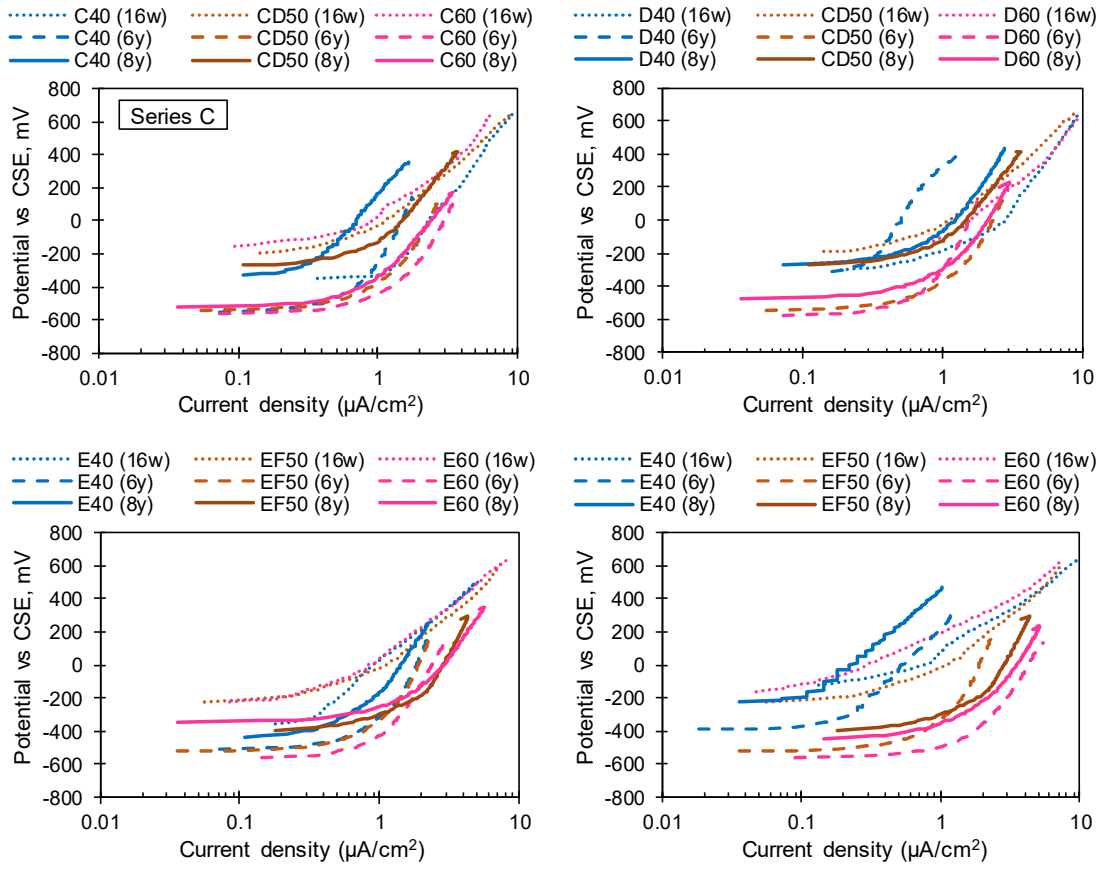

Fig. 3.10—Anodic polarization curves

From the APC, the maximum current density of anodic and passivity grade for each series was determined and are listed in Table 3.5. From this table, it was found that the higher chloride contaminated shows the lower passivity grade. Indicates that there is an influence of amount of chloride to passivity grade. At the age of 16-weeks (initiation corrosion starts) the steel bar categorized in Grade 4 (good condition) and Grade 3 (poor condition). In contrary, after 6-years exposure, the grade passivity of steel bar was Grade 4 and Grade 5 which represents good and an excellent passivity, respectively; the steel bars are supposed to be in a passive condition for this case. This implies the passivity become recover after necessary certain period, even contaminated with higher chloride. Also, this may be due to the hydration of cement was complete which consume all of oxygen and water trapped, that is, the concrete resistance increase and promote the passivity film recovery. However, after 8-years exposure, the grade passivity around the steel bar dropped again into Grade 4 (good condition) and 3 (poor condition). Therefore, it implies that current situation enters to propagation stage, which confirms from I_{corr} data and by visual observation of steel bars after removal from mortar specimen. After certain period, once anodic grade recover, however after that, continuous to falling down. It can be understanding that environmental condition dramatically affects the passivity grade of steel bar.

Table 3.5—Anodic current density at 200 mV and 600 mV and passivity grade

Specimen code	Current in $\mu A/cm^2$								
	16-weeks			6-years			8-years		
	200mV	600mV	GP	200mV	600mV	GP	200mV	600mV	GP
C40	1.87	4.18	4	0.82	1.56	4	0.51	1.27	4
C50	1.15	4.56	4	1.12	2.48	4	1.16	3.01	3
C60	1.05	4.48	4	1.41	3.12	4	1.05	2.83	4
D40	1.78	5.04	3	0.42	0.91	5	1.02	2.39	4
D50	1.15	4.56	4	1.12	2.48	4	1.16	3.01	3
D60	1.29	5.23	3	0.83	1.60	4	1.09	2.61	3
E40	0.61	2.30	4	1.00	2.03	4	0.76	1.89	4
E50	1.02	4.36	4	1.00	2.05	4	1.78	3.81	3
E60	0.82	3.63	4	1.22	2.50	4	1.85	4.72	3
F40	1.02	5.84	3	0.31	0.98	5	0.22	0.80	5
F50	1.02	4.36	3	1.00	2.05	4	1.78	3.81	3
F60	0.40	4.14	3	2.01	3.53	4	1.70	4.53	3

3.4.4 Oxygen permeability

The oxygen permeability data at the age of 8-years is shown in Fig. 3.11. The result showed that the oxygen permeability through the cover concrete for each series was higher as

increasing the amount of chloride. Also, oxygen permeability increased as increased of W/C ratio. Higher oxygen permeability was found in specimen E50, E60, F50 and F60 which indicated a large amount of chloride.

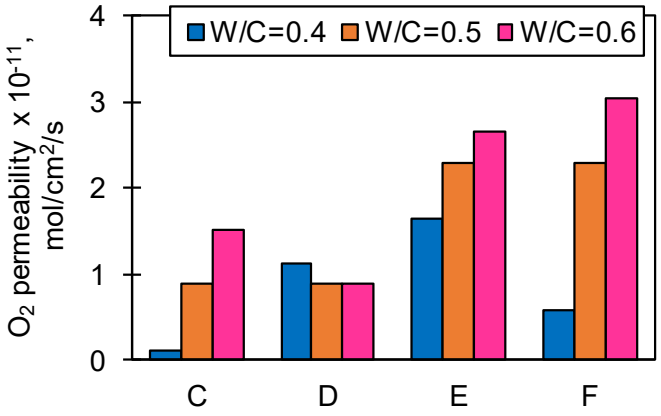

Fig. 3.11—Oxygen permeability through concrete cover

3.4.5 Electrical resistance

The concrete resistance for each series at the age of 6-years and 8-years are shown in Fig. 3.12. It was shown that concrete resistance was increased as decreased of W/C ratio. No significant difference value was found and the amount of chloride less effective after certain period (6-years and 8-years). The concrete resistance at the age of 8-years was lower (decreased) than 6-years. It is implying that the quality of concrete become reduce. The concrete resistance at the age of 6-years was higher than 50 kΩ–cm and categorized low corrosion rate based on Andrade and Alonso [3.10]. But after 8-years, the concrete resistance reduces to 10~50 kΩ–cm which categorized moderate to high corrosion rate (except W/C= 0.4).

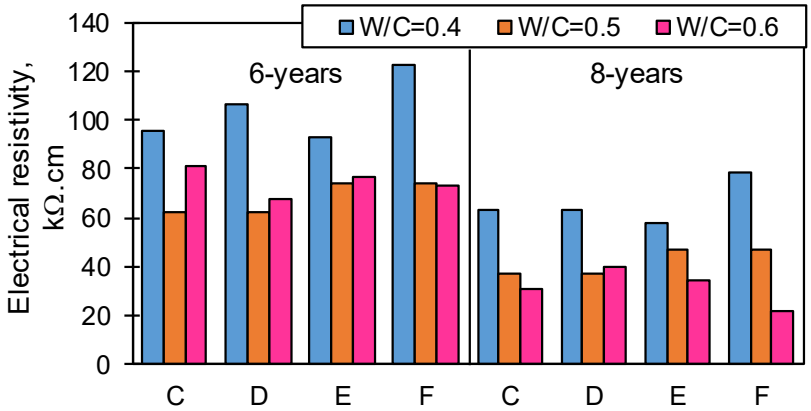

Fig. 3.12—Concrete resistance

3.4.6 Physical evaluation of corrosion

After each electrochemical investigation was conducted entirely, the specimens were split open to see the actual condition of the steel bars as well as the split-open mortar surface surrounding the steel bars. The appearance of split-open mortar and corrosion conditions of steel bars for each specimen at the age of 6-years and 8-years are shown in Fig. 3.13 and 3.14. The electrochemical data of 6-years was already reported in the previous study [3.14].

All steel bars showed more corrosion at the end of the bars. It should be noted the corrosion area was measured except the 1 cm edge from the top and bottom of steel bar to avoid unexpected corrosion due to un-perfect coating in the top and bottom edge of the steel bar. From Fig. 3.14, all of the specimens were showed corrosion at the age of 6-years and 8-years. After 8-years, it is almost generated corrosion that indicates which passivity film of steel bar was broken due to the increase of black colored corrosion product. Compared to 6 years, just pitting corrosion exited on the steel surface. The result corresponded with the result of I_{corr} in Fig. 3.9 where at 6-years the current density was lower than 8-years. The results indicate that under the small current density, the passivity of steel can be enhanced by environmental improvement effects after certain periods, in this case, 6-years exposure. Moreover, the higher chloride content shows in a larger corrosion area. That means corrosion area of steel bar depends on the chloride content in mortar.

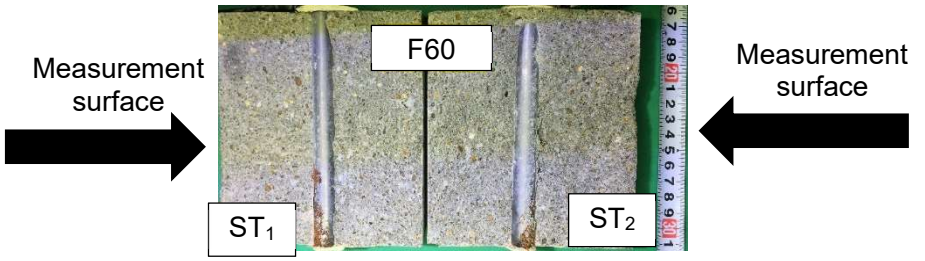

(a) 6-years

(b) 8-years

Fig. 3.13—Appearance of split-open mortar at the age of 6-years and 8-years

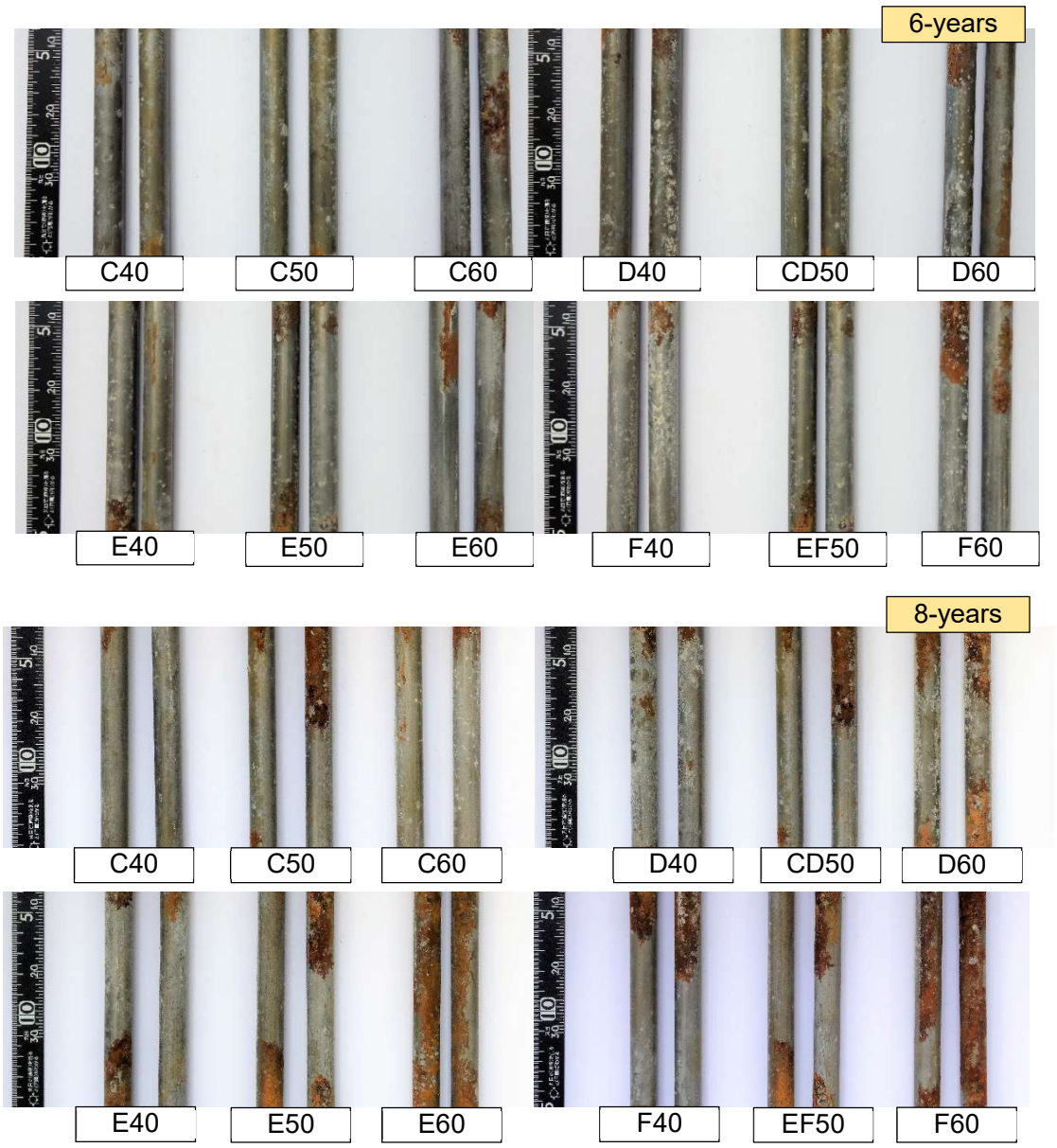

Fig. 3.14—Appearance of steel corroded at 6-years and 8-years

The total corroded area at the age of 6-years and 8-years is summarized in Fig. 3.15. From this figure, after 8-years exposure, the total corroded area was rapidly increased about 1.6-4 times from 6-years for all cases of W/C, but for C40, D40 and C60 the total corroded area was decreased. It was considered that W/C and amount of chloride were an important parameter for concrete resistance. Further, the results also support the electrochemical data explained previously. The corrosion of steel bars is controlled due to the remarkably higher concrete resistance which lower amount of chloride, that is, the absence of conversion (Fig. 3.12). As can be noted from the concrete resistance data as well as other electrochemical and physical data related to the corrosion of steel bars. The high quality of concrete is considered to provide the environment more favorable for pitting corrosion [3.12].

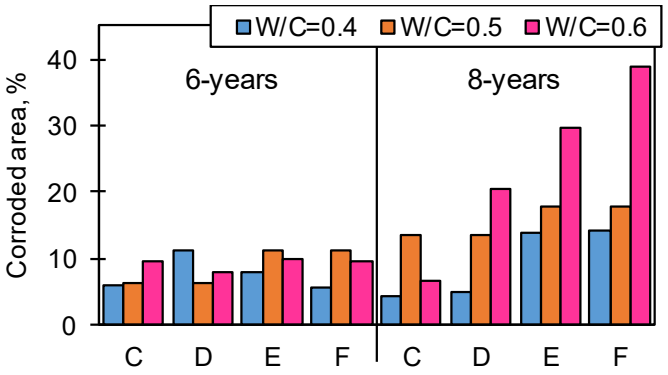

Fig. 3.15—The corroded area

3.5 Discussion

From the practical point of view, the behavior of steel bar due to an increase of corrosion should mean the developing of active corrosion that remains with time. This situation can be detected by electrochemical analysis and confirm by visual observation. Therefore, this study has proposed to identify corrosion behavior of OPC mortar from moderate to high corrosion. The limits of corrosion potential, corrosion current density and grade passivity were specified to generate a specific degree of corrosion. In spite of, the current density value more than 1 μA/cm^2 and corrosion potential lower than -500mV is generally considered as the criteria to classified the higher corrosion degree which are defined by CEB and ASTM standard, respectively [3.4, 3.8]. However, this study proposed the deterioration stage which determined from electrochemical analysis which confirmed by actual observation.

Relationship between electrochemical and physical analysis is shown in Fig. 3.16. From this figure, it was clearly seen that after 8-years exposure, the behavior of steel bar become worse as confirm from grade passivity data (categorized into Grade 3= poor condition), I_{corr} data (more than 1 μA/cm^2= high corrosion) and E_{corr} data (more than -500 mV= severe corrosion). And, from the worse criteria, the dashed line vertical was taken and this study found the relationship between an electrochemical measurement with corroded area. The value is 13~15% of total corroded area can be defined as high corrosion degree and categorized into propagation stage. Moreover, clear relationship between I_{corr}-corroded area and E_{corr}-corroded area was as found only after 8-years exposure. Implies after entering propagation stage, total corroded area is more effective to evaluate. The relationship is interpreted with the following equations (3.5) and (3.6) for I_{corr} and E_{corr} with total corroded area, respectively, which the equation constructed from the linear regression function (least-squares estimation).

$$I_{corr} = 0.041CA + 1.717 \quad (3.5)$$

$$E_{corr} = -2.96CA - 441.95 \quad (3.6)$$

Where, I_{corr} = corrosion rate, $\mu A/cm^2$; E_{corr} = corrosion potential, mV(CSE), and CA = total corroded area (%).

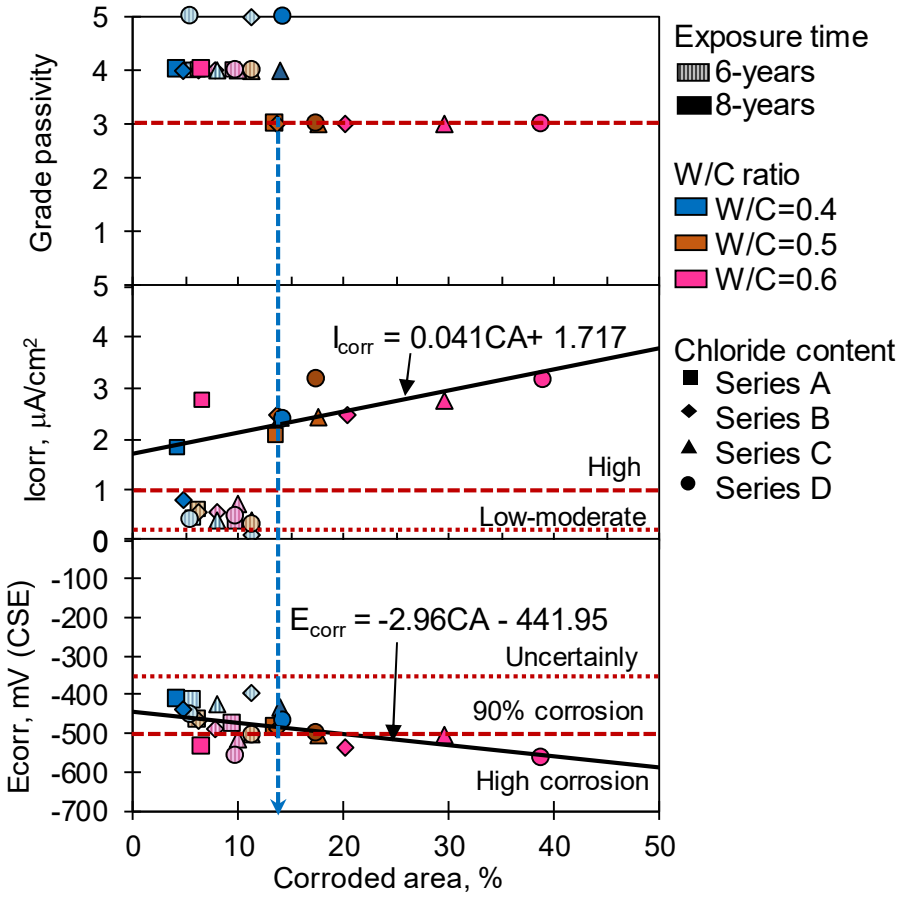

Fig. 3.16—Relationship between electrochemical and physical analysis

3.6 Conclusion

In this study, water-to-cement ratio and chloride content in mortar were set as an experimental parameter, and the effectiveness of these experimental parameters on electrochemical measurements, such as corrosion potential, corrosion current density, grade passivity and corrosion area were experimentally evaluated. Finally, the following conclusions were obtained.

1. At the age of 6-years and 8-years, the sensitivity of the corrosion potential against chloride content tends to be decreased compared to the 16-weeks. Implies after entering propagation stage, amount of chloride content less effective.
2. From moderate to high corrosion rate, after 8-years exposure for OPC mortar has increased the probability from pitting to generate corrosion.

3. The value is 13~15% of corrosion area can be defined as high corrosion degree and categorized into propagation stage by using Equation:

$$CA = 24.39\ I_{corr} + 41.88 \text{ and } CA = 149.31 - 0.34\ E_{corr}$$

4. Electrochemical method (corrosion potential, current density and passivity grade) has reliable to evaluate corrosion during enter initiation and early propagation stage.

Reference

[3.1] Mullard, J. A., & Stewart, M. G. (2011). Corrosion-Induced Cover Cracking: New Test Data and Predictive Models. ACI Structural Journal, 108(1).

[3.2] Tuutti, K. (1982). Corrosion of steel in concrete. Cement-och betonginst..

[3.3] Bjegovic, D., Miksic, B. A., & Stehly, R. D. (2000). Test protocols for migrating corrosion inhibitors (MCI®) in reinforced concrete. Materials and Corrosion, 51(6), 444-452.

[3.4] CEB. (1998). Strategies for Testing and Assessment of Concrete Structure. Bulletin n.243, pp.183.

[3.5] Stern, M., & Geary, A. L. (1957). Electrochemical polarization I. A theoretical analysis of shape of polarization curves. Journal of the electrochemical society, 104(1), 56-63.

[3.6] Andrade, C., & González, J. A. (1978). Quantitative measurements of corrosion rate of reinforcing steels embedded in concrete using polarization resistance measurements. Materials and Corrosion, 29(8), 515-519.

[3.7] Pech-Canul, M. A., & Castro, P. (2002). Corrosion measurements of steel reinforcement in concrete exposed to a tropical marine atmosphere. Cement and Concrete Research, 32(3), 491-498.

[3.8] ASTM C876. (2015). Standards test method for half-cell potentials of reinforcing steel in concrete.

[3.9] Otsuki, N. (1985). A study of effectiveness of Chloride on Corrosion of Steel Bar in Concrete. Report of Port and Harbor Research Institute, 127-134.

[3.10] Andrade, C., & Alonso, C. (1996). Corrosion rate monitoring in the laboratory and on-site. Construction and Building Materials, 10(5), 315-328.

[3.11] Hamada, H., Yamamoto, D., Sagawa, Y., & Ikeda, T. (2015, January). An experimental study on relationship between chloride content in mortar and passivity condition of embedded steel bar. In 4th International Symposium on Life-Cycle Civil Engineering, IALCCE 2014 (pp. 1479-1484). CRC Press/Balkema.

[3.12] Busba, E., & Sagüés, A. A. (2013, March). Critical Localized Corrosion Penetration of Steel Reinforcement for Concrete Cover Cracking. In NACE conference and Expo

[3.13] Patah, D., Hamada, H, Sagawa, Y, and Yamamoto, D. (2017). Half-cell Potential of Steel Bar in Mortar due to Chloride Ion Content at Age of 6 Years. JSCE 19th International Summer Symposium 2017.

[3.14] Patah, D., Hamada, H, Yamamoto, D. and Sagawa, Y. (2018). 6-Years Evaluation of Electrochemical Characteristic of Steel Bar in Chloride Contaminated Mortar. Journal of Cement Science and Concrete Technology Vol.7.1, pp. 402-409.

CHAPTER 4. THE EFFECTIVENESS OF MINERAL ADMIXTURE ON CORROSION RESISTANCE OF STEEL BAR IN MORTAR

4.1 Introduction

The corrosion of steel reinforcement in concrete has been a concern in recent years as durability has become more important in concrete structures. Especially, chloride-induced corrosion of reinforcing steel is increasingly important in many countries due to the increasing use either sea sand and seawater for heavy construction of marine structures. Although many researchers (Table 4.1) have studied the mechanism of chloride-induced corrosion, the concentration of chloride ions which causes the initiation of steel corrosion in concrete – the most important parameter in determining the durability life and/or service life of concrete structures – is still ambiguous and needs further study. A sustained level of chloride content on steel reinforcement surface which causes depassivation is called as chloride threshold value (CTV). The chloride threshold value has been represented in three different forms in the literature, as a ratio of chloride ion to hydroxyl ion ($[Cl^-]/[OH^-]$), as free chloride content and as total chloride content.

Since assessment and the prediction of CTV are interdependent, many researchers suggested highly elaborated scatter plots to estimate CTV based on certain conditions. This chloride threshold concentration for corrosion initiation is not fixed and known to be affected by several factors including cement content, type of binder, binding capacity of cement, concentration of hydroxyl ions, moisture and oxygen, etc. [4.1]. RILEM has recommended that 0.2~0.5% of chloride by weight %-cement as chloride threshold [4.2]. The JSCE standard also has recommended the level of CTV as 0.4% for RC structures [4.3]. Further, factors such as mineral admixture material used, presence of surface cracks, impurities present in concrete, w/c ratio, steel surface condition, type of measurement used and units adopted for measurement significantly influence the chloride threshold values. Despite the influence of these factors, in general, 0.2 to 0.4% weight of cement is used as a conservative estimate of CTV during the analytical design for the service life of RC structures [4.4–4.8].

Table 4.1—Literature reviews

Reference	Steel condition	Binder type	W/B ratio	Depassivation detection	CTV % wb.
Richartz [4.9]	Smooth	OPC	0.45	Visual inspection	0.4
Gouda and Halaka [4.10]	Smooth	OPC	0.6	Anodic polarization, potential	3
		GGBS			1
Gouda and Halaka [4.10]	Smooth	OPC	-	Anodic polarization, potential	2.4
		GGBS			1.2
Hansson and Sorensen [4.11]	Cleaned, smooth	OPC, FA, SRPC, SF, RHPC	0.4-0.6	Current between WE & Passive external CE	0.4–1.37
Takagi et al [4.12]	-	SF	-	Potential	0.125
Schiessl & Breit [4.13]	Ribbed	GGBS or FA	0.5-0.7	Macrocell current	1.0–1.5
Thomas [4.14]	Ribbed	OPC, FA	0.32-0.68	Weight loss	0.2–0.65
Breit [4.15]	Smooth	OPC, SRPC, SF, FA, GGBS	0.5-0.6	Potentiostatic, visual inspection	0.25–0.75
Alonso et al [4.16]	Ribbed,	OPCs	0.5	LPR, potential	1.24–3.08
Whiting et al[4.17]	Cleaned	FA	0.4-0.6	LPR	0.4
Oh et al. [4.18]	Smooth	OPC, FA and 30% GGBS	0.35-0.55	Potential	0.68–0.97
Manera et al [4.19]	Smooth, ribbed	OPC	0.5	LPR, potential	1.1–2.0
		OPC, SF	0.6		0.6–1.2
Mohammed and Hamada [4.20]	Smooth, ribbed	OPC	0.5	LPR, potential	0.4-0.8
Locke & Siman [4.21]	ribbed,	OPC	0.4	LPR	0.4-0.8
Hansson and Sørensen [4.22]	smooth, cleaned	OPC, FA, SRPC, SF, RHPC	0.4-0.6	current between WE and passive external CE	0.4-1.37
Schiessl & Raupach [4.23]	not reported	OPC, FA, SF, GGBS	0.4-0.6	Macrocell current	0.5-2.0
Pettersson [4.24]	cleaned	OPC, SF, FA	0.4-0.6	LPR	0.5-1.8
Pettersson [4.25]	ribbed	OPC, SF,	0.3-0.75	LPR	
Schiessl and Breit [4.26]	ribbed	OPC	0.5-0.7	Macrocell current	0.5-1.0
		GGBS, FA			1.0-1.5
Thomas et al.[4.27]	ribbed	OPC	0.32-0.68	Weight loss	0.7
		FA			0.2-0.65
Breit [4.28]	smooth	OPC, SF, FA, SRPC, GGBS	0.5-0.6	Potentiostatic, visual inspection	0.25-0.75
de Rincón et al.[4.29]	NR	OPC, FA, SF	0.58	Potential, LPR	0.4
Hamada [4.30]	smooth	OPC	0.4,-0.6	Potential, anodic polarisation	0.3-0.4

This study is focused on the corrosion of steel bars induced by internal chlorides in concrete at early ages. The main objective of this study is to determine the threshold chloride concentration causing depassivation and onset of active corrosion of steel bar embedded in

mortar. To this end, a comprehensive experimental program has been set up, and a large number of specimens have been evaluated. In this study the factor influence on chloride threshold of corrosion initiation in concrete such as the type of cement (chloride binding capacity) and the W/B ratio was taken into consideration and another influence was neglected. Corrosion potential and corrosion current density were conducted to examine the threshold chloride concentration. The amount of chloride was determined according to the added amount of chlorides, type of mineral admixtures and W/B ratios.

From the present test results, the factors influencing threshold chloride concentration are investigated, and the reliable ranges of threshold chloride concentration causing active corrosion of steel bar are proposed. Further, the effects of the W/B ratios and type of mineral admixtures on the threshold chloride concentration have been clarified. Another interesting issue, the effects of W/B ratio of 0.4 for replacement cement with 5% of silica fume on the chloride threshold also need to be identified. Therefore, establish the threshold total and free chloride ion concentration using mineral admixtures for the initiation of corrosion steel bars in concrete structures become the main contributions of this study.

4.2 Test Program

4.2.1 Material

The specimens were made with Ordinary Portland Cement (OPC), Type B fly ash cement (FB), Type A silica fume cement (SA), Type B blast-furnace slag cement (BB), and metakaolin cement (MKP). These cements are specified in Japan. The physical properties and chemical analysis are presented in Table 4.2. The classifications of the cement depending on the blended content are presented in Table 4.3. Washed sea sand was used as fine aggregate. Specific gravity, water absorption, and fineness modulus of sand were 2.49 g/cm^3, 1.42%, and 2.8, respectively. Japanese Industrial Standard (JIS) steel bars were used and its chemical compositions are presented in Table 4.4.

Table 4.2—Physical and chemical compositions of cement

Items	OPC	FB	SA	MKP	BB
Specific gravity	3.16	2.26	2.35	2.75	3.02
Blaine fineness, cm^2/g	3400	3.97	1800	9.03	3.86
Ignition loss, %	1.97	2.4	1.22	-	1.46
SiO_2, %	-	60.60	95.50	52.37	34.10
MgO, %	1.31	-	0.56	1.04	3.26
SO_3, %	2.14	-	0.18	7.56	2.04

Note: OPC satisfied JIS R5210; FA satisfied JIS A 6201; SF satisfied JIS A 6201 and BB satisfied JIS R5211.

Table 4.3—Classifications of fly ash, silica fume, and blast furnace slag cement

Type	Mass, %	Code
Fly ash Type B	20 to 40	FB
Silica Fume Type A	5 to 10	SA
Blush furnace slag Type B	40 to 45	BB

Table 4.4—Chemical compositions of steel bar

C, %	Si, %	Mn, %	P, %	S, %
0.18	0.18	0.64	0.015	0.021

4.2.2 Specimens

Mortar cubic specimens 120x135x135mm were investigated. The layout of the specimens is shown in Fig. 4.1. Two round steel bars 13 mm in diameter were embedded in each specimen at a cover depth of 50 mm from the measuring surface. The mortar was demoulded one day after casting, then moisture curing by wrapping with wet towel and plastic sheet until 91 days in a controlled room maintained at 20ºC, R.H. 60% was conducted. Afterward, five sides of specimen were masked by epoxy resin and the remaining side was kept as a measuring surface. Then the specimens were stored in laboratory with the temperature from 5ºC in winter to 35ºC in summer. After one year of exposure, because there is no sign of corrosion the specimens were exposed in accelerated carbonation condition at 20ºC, R.H. 60% and CO_2 concentration 5 % until the sign of corrosion initiating. Corrosion behavior of natural exposed was already reported saperatly [4.62]. The schematic diagram of curing and exposure time of the specimen is shown in Fig. 4.2. The accelerated carbonation of concrete was carried out in accordance with JIS A 1153-03. Photo 4.1 depicts accelerated carbonation chamber was used.

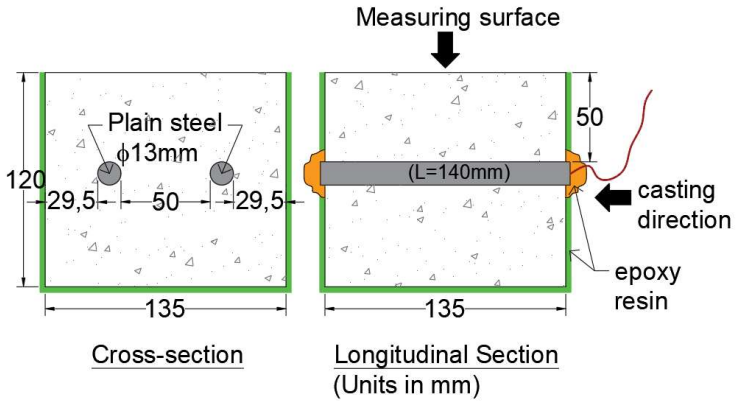

Fig. 4.1—Details of specimen

Photo 4.1—Carbonation chamber

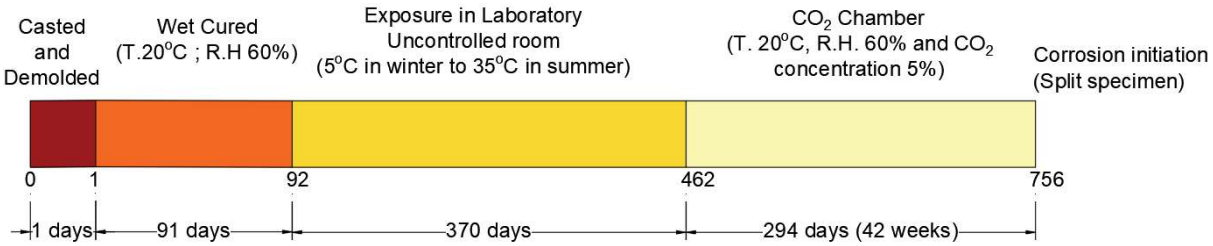

Fig. 4.2— The schematic diagram of curing and exposure time of the specimen

4.2.3 Proportions of mixture

Three series of mortar mixtures with three types of W/B ratio of 0.4, 0.5, and 0.6 was set for mixing mortar. Electrochemical techniques evaluated corrosion of steel bars embedded in chloride-contaminated mortar, thus mortar specimens contained 0.29%, 0.57%, and 0.86% chloride by weight of cement. Mix proportions of specimen and all cases of chloride content for each mix and are presented in Table 4.5 and Table 4.6, respectively. The chloride-contaminated mortar with OPC only referred to as a control specimen and chloride-contaminated mortar with additional admixture by FB-20%, SA-5%, and BB-45% by cement weight was determined. In addition, chloride-contaminated mortar with BB-80% and MKP-20% marked as BBMKP was also determined.

Table 4.5—Mixture proportions of mortar

W/B	W, kg/m^3	C, kg/m^3	S, kg/m^3
0.4	232	581	1508
0.5	255	510	1508
0.6	272	454	1508

Note: W=Water, C=Cement, and S=sand.

Table 4.6—Design of chloride content

Series	W/B	Total chloride addition		Remark
		Total content in mortar, kg/m^3	Weight ratio of cement, %-binder	
A	0.4	1.68	0.29	A40
	0.5	1.48		A50
	0.6	1.32		A60
B	0.4	3.31	0.57	B40
	0.5	2.91		B50
	0.6	2.59		B60
C	0.4	5.00	0.86	C40
	0.5	4.39		C50
	0.6	3.90		C60

4.3 Experimental Methods

4.3.1 Compressive strength and porosity

The compressive strength of mortar was measured as per JIS A1108. The size of cylinder specimen is ϕ50x100mm. After curing 91 days, the average compressive strength of three specimens was determined.

The porosity of mortar was measured. After curing for 91 days, mortar pieces cut into five mm-thick cube slice samples. The sample was immersed in acetone for 15 min to stop the hydration of cement and then dried in the vacuum desiccator for two days. Then the porosity of concrete was evaluated by mercury intrusion porosimeter (MIP). The average compressive strength of two specimens was determined.

4.3.2 Corrosion potential and corrosion current density

The corrosion potential (E_{corr}) was taken as an average of two steel bars and measured by using the silver/silver chloride reference electrode (Ag/AgCl) after 30-min pre-wetting of mortar surface. Then, the potential value was converted to the value against copper/copper sulfate reference electrode (CSE). The threshold limit of E_{corr} is assumed to be -350 mV as per ASTM C876 [4.31]. The measurement setup is illustrated in Fig. 4.3.

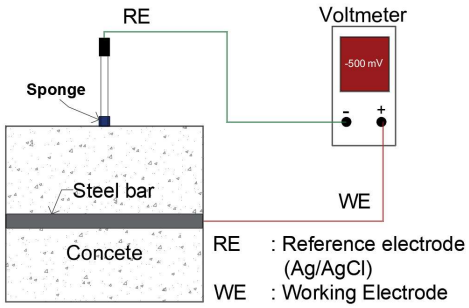

Fig. 4.3—Measurement setup for corrosion potential

Linear polarization resistance (LPR) measurement was conducted to observe the corrosion current density (I_{corr}) of steel. The schematic diagram of the electrical circuit of polarization technique is shown in Fig. 4.4. The mortar specimen was immersed in tap water, and two electrodes (counter and reference electrodes) were arranged and connected with the instrument in the solution. The standard saturated calomel electrode (SCE) and metal electrode (stainless steel) were used as the reference electrode and counter electrode, respectively. The polarization resistance was measured by Potentiostat machine using high frequency at 15 kHz of alternating current with scan speed of 50 mV/min, and the following equation was used to calculate the I_{corr} using the Stren-Geary Formula [4.32].

$$I_{corr} = \frac{B}{R_p} x \ 10^6 \qquad (4.1)$$

Where I_{corr} is corrosion current density, μA/cm^2; Rp is polarization resistance, Ω.cm^2 and B is 0.026 V considering steel inactive condition [4.46]. A detailed description of the measurement of LPR can be obtained from Literature Chapter 2. A sustained corrosion current density of 0.2 μA/cm^2 is generally accepted as the value above which the reinforcement is considered to be actively corroding as per CEB Standard [4.33].

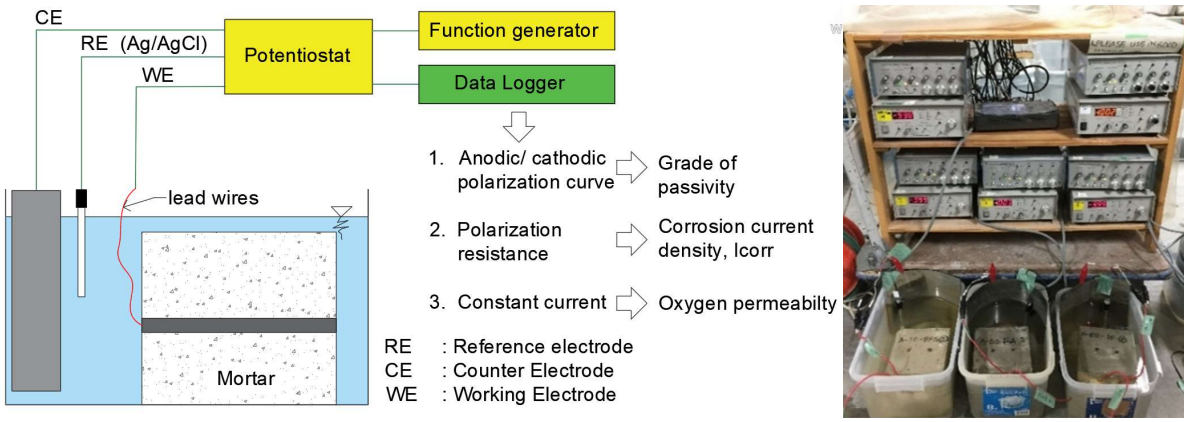

Fig. 4.4—The schematic diagram of the electrical circuit of the polarization technique

4.3.3 Electrical resistivity and permeability

The electrical resistivity and permeability were measured by using the Wenner probe and Torrent, respectively. The resistivity and permeability of mortar specimen from the average of three times measurement were determined.

4.3.4 Oxygen Permeability

The constant current density (i_{lim}) over the steel bars was measured. The i_{lim} was measured by using a potentiostat. The potential of the steel bar was set to -1,000 mV and held constant then the current was recorded continuously. When measurements began, current was a maximum then gradually falling until reaching an almost constant value after kept in 24-hours. Fig. 4.4 shows the details of the measurement. The oxygen permeability was calculated by using the following equation [4.34]:

$$\frac{dQ}{dt} = -\frac{i_{lim}}{n.F} \tag{4.2}$$

where (dQ)/(dt) is the oxygen permeability in mole/cm^2/s (on steel surface); i_{lim} is the limiting cathodic current density in A/cm^2; n is 4, and F is the Faraday's constant (96,500 coulombs/mole).

4.3.5 Physical analysis and visual inspection

At the end of the experiments, the steel bars were removed from the specimen. Then, the presence of rust spots on the steel surface was visually observed. It was noticed that those specimens having I_{corr} values at range 0.149-0.2 μA/cm^2 showed visible corrosion, different mineral admixture has different corrosion passivity limit.

4.3.6 Carbonation

After 42 weeks of carbonation, the carbonation depth of each specimen was evaluated after spraying 1% phenolphthalein solution on a freshly cut or broken surface. In the carbonated areas, the color of the solution does not change (colorless), while in the noncarbonated areas, the color solution is changed to purple-red. The distance between the color change boundary to the concrete surface was measured as the carbonation depth. The accelerated carbonation of concrete was measured according to JIS A1152-02. Twenty readings were recorded from the measuring surface. The average reading was taken to represent the carbonation depth for each specimen.

4.3.7 Chloride analysis

In case of initiation mortar specimens, after confirmation of corrosion initiation, chloride analysis was carried out to estimate the total chloride and water-soluble chloride in mortar by using Japan concrete institute methods (JCI-SC4). Mortar specimens were taken and cut in an approximately 5 mm surround the steel bar. The total chloride was extracted by analyzing the chloride ion concentration of HNO_3 (2 mol/l) solution that mortar melt into, and water-soluble chloride was extracted by analyzing the chloride ion concentration from mortar melt into water. Solutions are at 50°C. Chloride ion concentration of mortar was measured using an automatic chloride ion titration device. A detailed description of the measurement of chloride analysis can be obtained from Literature Chapter 2.

4.4 Result and discussion

4.4.1 Result of the previous study

Chloride threshold value (CTV) for OPC mortar already conducted by the previous study by Hamada et al. [4.30]. Time dependence change of corrosion potential (E_{corr}) and corrosion current density (I_{corr}) are shown in Fig. 4.5. From this figure, even in same chloride content, higher of W/C ratio shows more negative of corrosion potential. The relationship between polarization resistance and chloride content at 16 weeks is shown in Fig. 4.6. From this figure, it showed that difference polarization resistance due to difference in chloride expression is not clear. However, it can be found that polarization resistance is decreased quickly at the chloride content of 0.4% versus cement mass, or 1.2 kg/m^3 chloride weight in unit mortar volume. This performance of polarization resistance is clearly different from corrosion potential. Further, difference due to W/B ratio cannot be found.

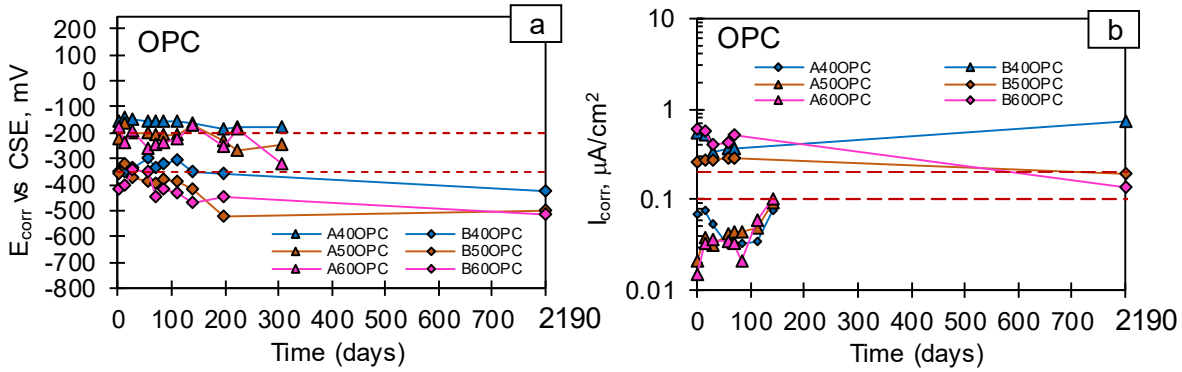

Fig. 4.5—Time dependences changes of E_{corr} and I_{corr} for OPC mortar

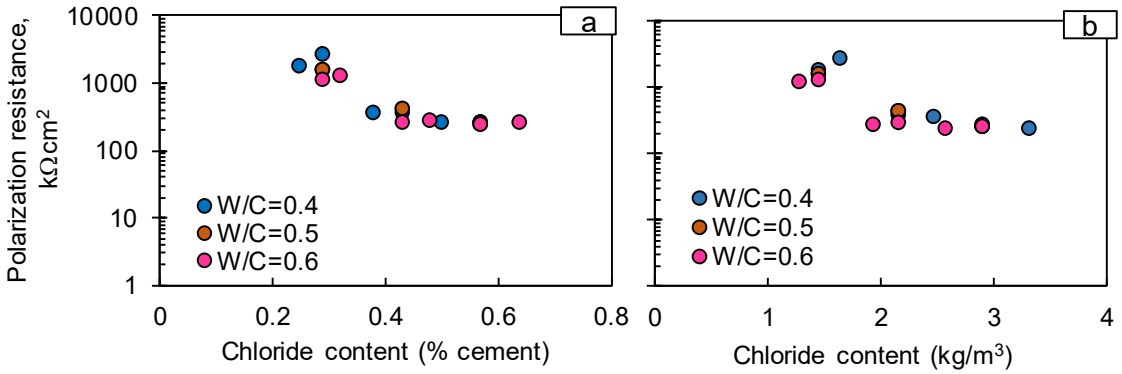

Fig. 4.6—Polarization resistance as a function of chloride content

4.4.2 Compressive strength and porosity

The compressive strength is shown in Fig. 4.7. From these figures, the compressive strength was different, depending on W/B ratio and type of mineral admixture. Results of compressive strength showed that specimens presented higher strength, which was deeper for lower W/B ratios. No significant influence in amount chloride addition to compressive strength. The SA mortar showed higher strength values to other mineral admixture. Following BBMKP and BB mortar showed almost same strength. In contrary to the result of the FB mortar, it gave lower strength and it was related to the properties of FB mortar that declines the heat of hydration process. Almusallam [4.35] reported determined all mechanical characteristics of hardened fly ash concrete by replacing 20% fly ash and concluded that the inclusion of fly ash results in higher compressive strength on later ages. The slow reactivity and lesser surface area of the fly ash are the reason for slower the rate of hardening and compressive strength gain [4.35].

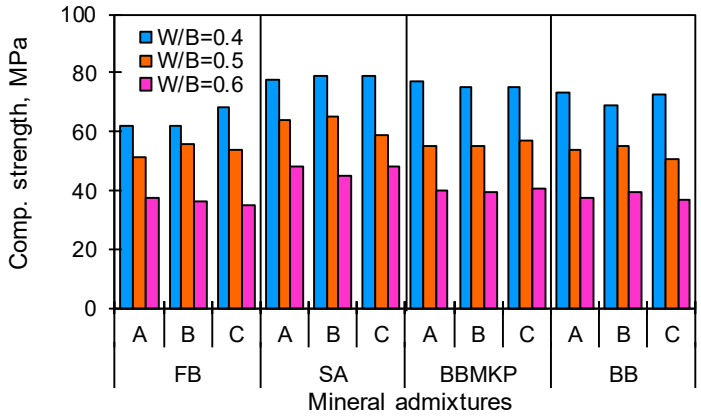

Fig. 4.7—Compressive strength

Total pore volume for each mineral admixture is shown in Fig. 4.8. From the figure, the specimen presented lower total pore volume correspond which were lower of W/B ratios.

No significant influence in amount chloride addition to porosity. Also, no significant difference in total pore volume value of each mineral admixture. Only SA mortar showed the lower porosity value in all cases of W/B ratio. For BB mortar in W/B ratio of 0.4 also showed lower porosity value compared to other mineral admixture.

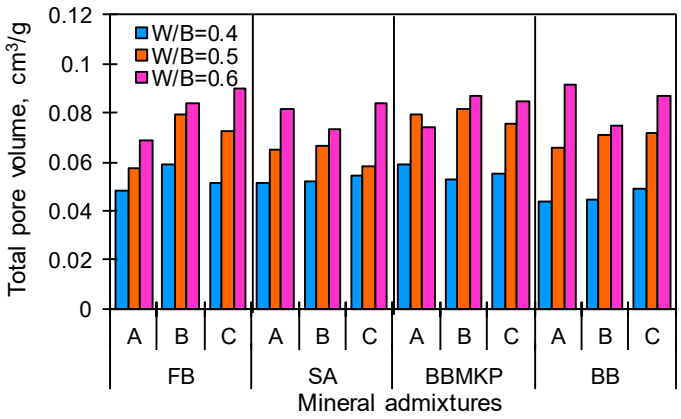

Fig. 4.8—Total pore volume

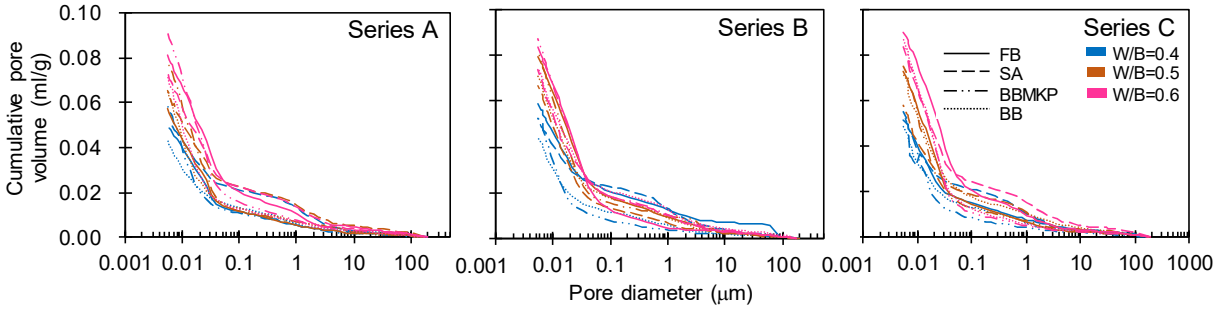

Fig. 4.9—Cumulative pore volume as a function of pore diameter of the specimen

The pore size distribution for each mineral admixture is shown in Fig. 4.9. From this figure, distribution pore of becoming harmless with decreasing W/B ratio. No significant influence of amount chloride addition to distribution pore volume. The BBMKP mortar show harmless pore compared to other mineral admixture. Following BB and FA mortar had almost similar distribution pore. In contrary, the SA mortar shows harmful pore compare to other mineral admixture in all cases W/B ratio even SA mortar had higher compressive strength.

4.4.3 Corrosion potential, corrosion current density

Time dependences changes of corrosion potential (E_{corr}) and corrosion current density (I_{corr}) for various of each mineral admixture are shown in Figs. 4.10-4.13. The indicates line for active and passive state of corrosion separates the regions between 0.1 and 0.2 μA/cm^2 in

the I_{corr} figure and same indicate lines between -200 and -350mV in the E_{corr} figure, according to the critical value of I_{corr} (CEB Standard) and E_{corr} (ASTM). From Fig.s 4.10a-4.13a, on the first day just after demolding, the potential for all specimens fallen down to more negative than -350 mV in all case of W/B ratio. However, the potential tends to recover after 91 days (i.e., finish curing time) in specimens with mineral admixture in all case of W/B ratio and categorized as 90% no corrosion. Difference result was showed with the specimens for OPC only (see Fig. 4.5), the potential was stable or even tends to be more negative, categorized as uncertainty or 90% corrosion (Series A and B). After 721 days, the potential value of mineral admixture starts to drop. The starting time of corrosion for each specimen was same at 721 days which E_{corr} value started to drop and reach to critical value. Same signal with I_{corr} value which starts to shift to critical value (see Fig. 4.10b-4.13b). It was considered that initial chloride content induced by mineral admixture as mortar material increased the duration to reach corrosion threshold chloride content compared to OPC mortar which much shorter (initiation time: 112 days/16 weeks). On the other hand, in case for mortar with mineral admixture had similar resistance against corrosion. It was considered that similar duration length was necessary to reach critical value of I_{corr}.

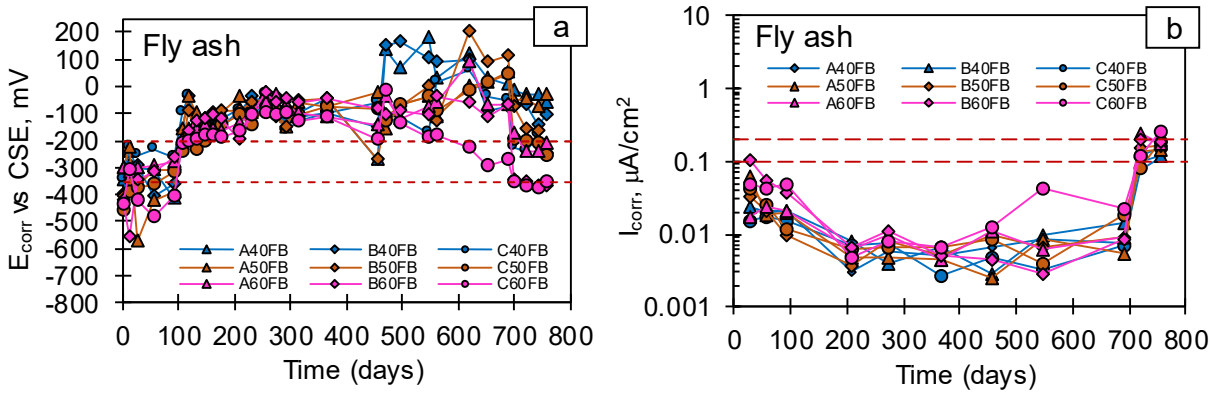

Fig. 4.10—Time dependences changes of E_{corr} and I_{corr} for FB

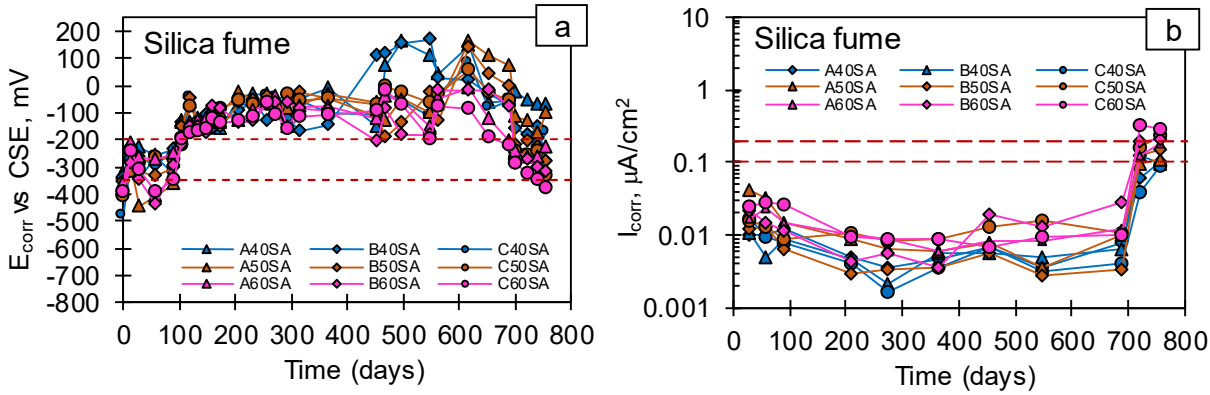

Fig. 4.11—Time dependences changes of E_{corr} and I_{corr} for SA

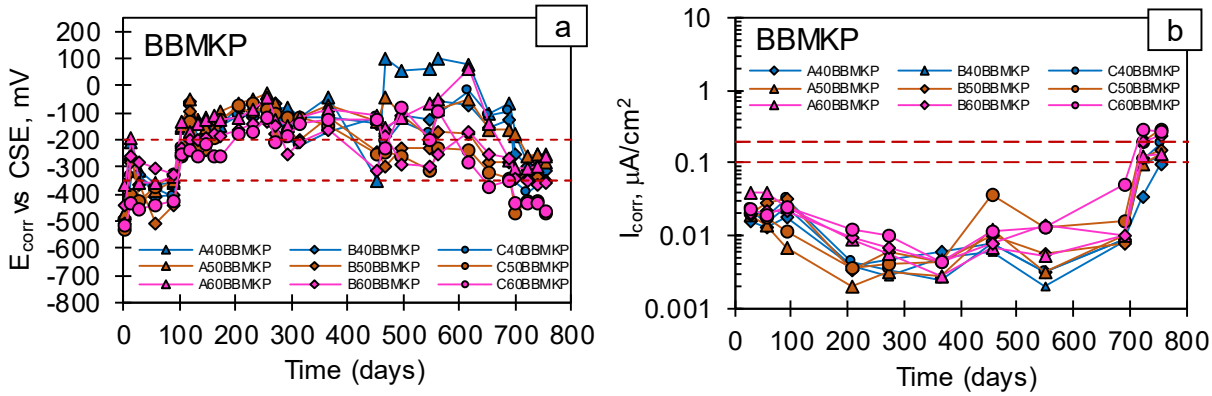

Fig. 4.12—Time dependences changes of E_{corr} and I_{corr} for BBMKP

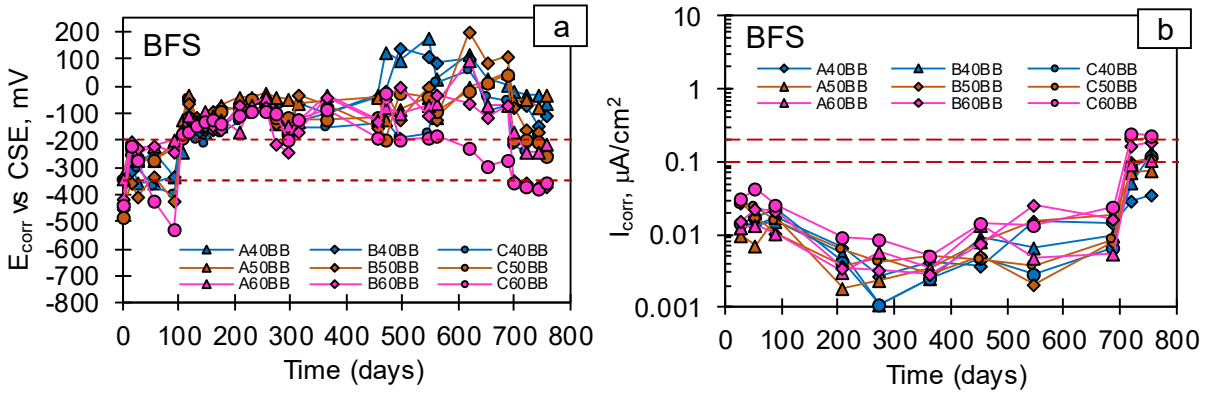

Fig. 4.13—Time dependences changes of E_{corr} and I_{corr} for BB

The corrosion initiation was determining when E_{corr} dropped below and I_{corr} shifted to the threshold value at the last measurement time where no significant drop in E_{corr} and shift in I_{corr} were observed. E_{corr} and I_{corr} at the age of 756 days are summarized in Table 4.7.

Table 4.7—Corrosion potential (E_{corr}) and corrosion current (I_{corr}) at depassivation time

Series	E_{corr} vs CSE, mV				I_{corr}, µA/cm²			
	FB	SA	BBMKP	BB	FB	SA	BBMKP	BB
A40	-145.26	-72.26	-253.26	-62.26	0.112	0.100	0.096	0.036
B40	-128.26	-281.26	-315.26	-108.26	0.118	0.094	0.129	0.138
C40	-308.26	-177.74	-354.26	-257.26	0.155	0.092	0.189	0.123
A50	-228.26	-198.26	-280.26	-34.24	0.149	0.112	0.136	0.079
B50	-281.26	-276.26	-352.26	-248.26	0.160	0.149	0.149	0.112
C50	-321.26	-331.26	-468.26	-219.26	0.193	0.236	0.286	0.222
A60	-326.76	-230.26	-261.26	-212.26	0.178	0.181	0.135	0.109
B60	-352.26	-314.76	-354.26	-266.26	0.186	0.205	0.239	0.185
C60	-382.26	-380.00	-461.26	-355.26	0.250	0.297	0.271	0.225

4.4.4 Electrical resistance

After a sign of corrosion initiate, the electrical resistivity was conducted. The electrical resistivity for each series of mineral admixture as a function of W/B ratio is shown in Fig. 4.14. In series A, mineral admixture had substantial influence on the concrete resistivity. The value of resistance was more than 100 kΩ–cm and categorized low corrosion. According to type of mineral admixture, the electrical resistance tends to increase in the following order: BBMKP > FB > BFS=SF. BBMKP mortar had a bigger reduction in resistivity between 0.4 and 0.6 and the values are between 340 kΩ–cm at W/B ratio of 0.4 and 250 kΩ-cm at W/B ratio of 0.6, while other mineral admixtures showed small difference at the same W/B ratio. In series B, FB mortar showed better performance than other mineral admixture but according to W/B ratio, a slight difference value in resistivity was found. The value of resistance was more than 100 kΩ–cm and categorized low corrosion. Then better performance followed by BBMKP at W/B ratio of 0.4 only (categorized low corrosion). BBMKP mortar also had a significant reduction in resistivity between 0.4 and 0.6 and the values were between 145 kΩ–cm at W/B ratio of 0.4 and 50 kΩ-cm at W/B ratio of 0.6. While BB and SA mortar showed small reduction and even steady at the same W/B ratio. The value of resistance was at range 50-100 kΩ–cm and categorized moderate corrosion, at all cased W/B ratio. The different result was showed in Series C, no significant difference of concrete resistivity to type of mineral admixture was found. Implies that with such higher of chloride contaminated mortar even use mineral admixture less effectiveness. The resistivity value of mineral admixture was less than 50 kΩ–cm and categorized high corrosion level, at all cased W/B ratio.

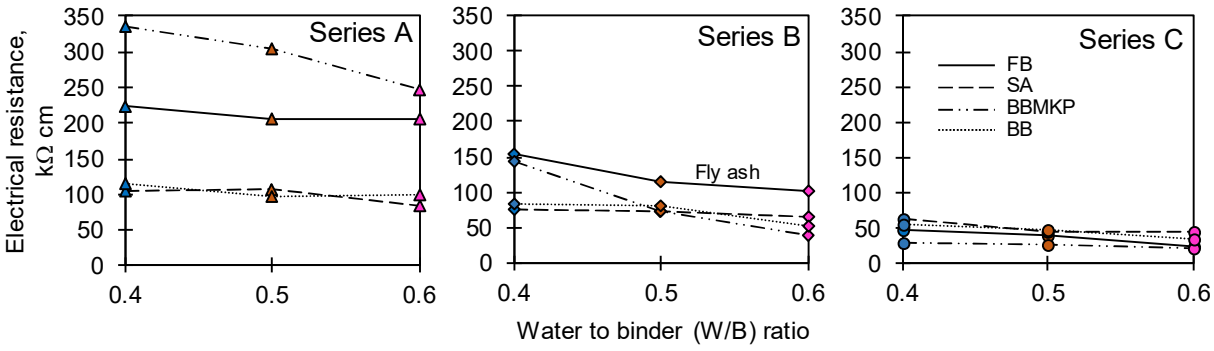

Fig. 4.14—Electrical resistivity as a function of W/B ratio of mineral admixture

From Fig. 4.14, it can be observed that lower of W/B ratio mortar provide higher resistivity. One possible reason that the amount of interconnected pores increases and due to increased ion mobility as the W/B ratio decreases [39]. The higher resistivity reflects the

higher imperviousness of the cement matrix produced by the hydration of the blended cement. However, increased level of chloride contamination resulted in significant reduction in electrical resistivity of mortars. The lower electrical resistivity the higher corrosion risk occurred on steel bar embedded in mortar. However, the utilization of BBMKP notably improved electrical resistivity of mortars, especially at level of chloride less than 0.3%-cement.

4.4.5 Oxygen permeability

After a sign of corrosion initiate, the permeability (on top surface) and oxygen supply (around the steel bar) were conducted. The permeability and oxygen permeability in mortar is shown in Fig. 4.15. In this figure, the significant influence of amount of chloride addition to permeability was found that higher chloride concentration can increase the permeability. It was also found that lower of W/B ratio mortar shows lower permeability. Same tendencies in oxygen supply were found. In Fig. 4.15a, the permeability of all specimen in Series A and B with all cases of W/B was categorized in good quality. Further, all specimen in Series C with all cases of W/B is in was categorized medium quality. The SA and BB mortar with W/B ratio of 0.6 and BBMKP with all cases of W/B ratio, were categorized in low quality. Fig. 4.15b shows the oxygen supply around the steel bar. From this figure, FB and BB mortar in series A with all cases of W/B ratio showed very lower oxygen supply compare to other mineral admixture. Further, in Series C with all cases of W/B ratio, FB mortar showed lower oxygen supply. Then following BB and BBMKP mortar. And the higher value of oxygen supply was found in SA mortar.

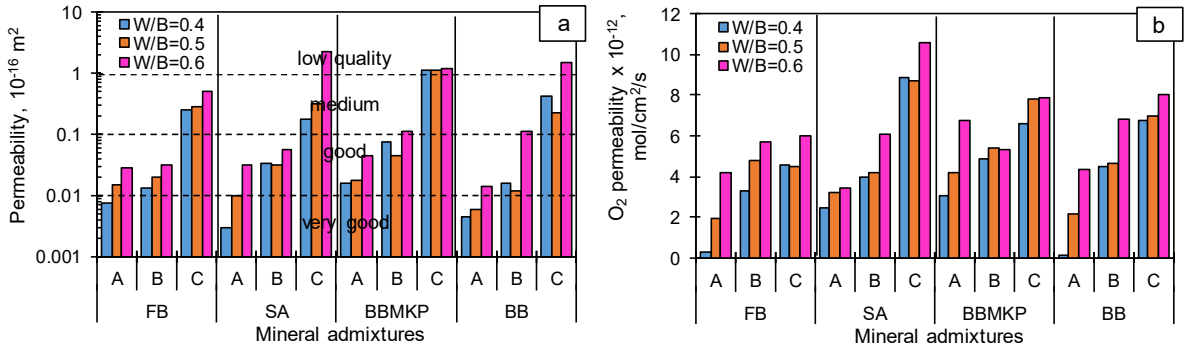

Fig. 4.15—Permeability and oxygen supply in mortar

Moisture and oxygen act as essential feeders for corrosion. Rust ($Fe(OH)_2$) is formed as a result of the increase in the level of OH^- ions. The available moisture content at the steel bar level acts as the electrolyte medium required for the corrosion process. Cathodic reaction

intensifies in by the presence of oxygen. Even at the stage of depassivation, without an adequate amount of oxygen, the progress of corrosion will halt, as there will not be enough oxygen for an active cathodic polarization. With higher oxygen permeability as well as concrete resistance, the cathodic reaction in mortar with bars will be faster. The result will cause more corrosion to depend on different mineral admixture.

4.4.6 Carbonation

The appearance and average depths of carbonation for all specimens are shown in Fig. 4.16 and summarized in Table 4.8. It can be observed that the carbonation depth did not influence by amount of chloride inside the mortar, regardless of the type of mineral admixture. Higher W/B ratio of mortar had lower resistance to carbonation which means carbon dioxide concentration increase. A similar tendency was also found by Parrot [4.36] that carbonation rate reduces 50% when the W/B ratio is reduced from 0.6 to 0.4. The carbonation depth of mortar replaced by SA and BB in the figure had lower and similar carbonation depth and the value was about 2 and 20~22 mm for 0.4 and 0.6 W/B ratio, respectively. At W/B of 0.5, the value of carbonation was about 5~8 and 9~11 for SA and BB mortar, respectively. Following FB mortar had lower carbonation depth but the value was slightly higher than BB and SA mortar. However, BBMKP mortar had higher carbonation depth from the other admixture. From this result, FA and BBMKP mortar showed lower performance against carbonation. Further, previous researchers have reported similar or lower carbonation for metakaolin concrete which it could be explained from fact that the replacement of cement by metakaolin and fly ash decreases the content of portlandite in hydrate product due to pozzolanic reaction [4.37, 4.38]. Carbonation rate is also strongly influenced by strength and permeability of mortar. Good quality, enough concrete cover, dense mortar delays the development of carbonation and slows down the first stage of the corrosion process.

Table 4.8—Average of carbonation depth after 42-weeks accelerated in CO_2 chamber

Series	Carbonation depth, mm			
	FB	SA	BBMKP	BB
A40	3.59	2.06	7.11	2.10
B40	2.17	1.90	8.80	2.10
C40	2.18	1.98	7.99	1.91
A50	12.29	6.03	20.45	9.62
B50	12.55	8.05	19.02	11.19
C50	14.01	5.40	23.09	10.48
A60	22.34	18.61	29.22	21.32
B60	22.44	20.91	28.63	21.84
C60	24.01	20.60	28.28	21.95

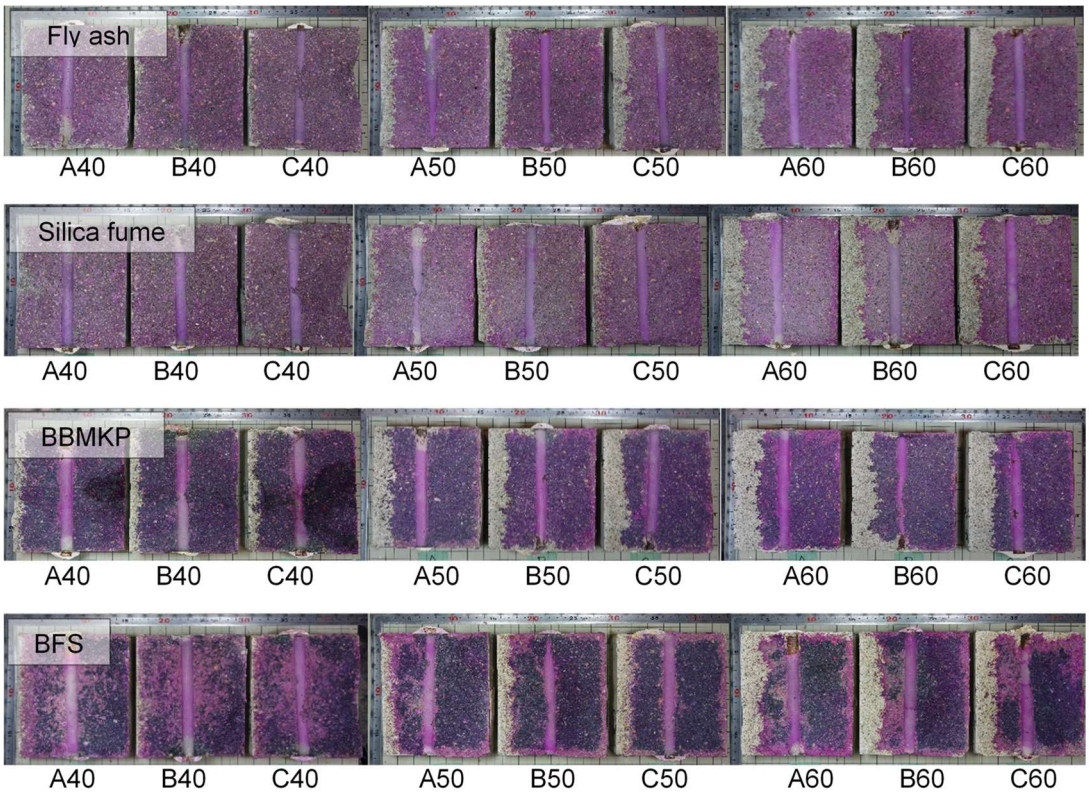

Fig. 4.16—Carbonation depth

4.4.7 Total chloride content values

A large amount of chloride may cause the corrosion of steel bars in mortar. Especially the quantity of water-soluble chloride is important factor in the corrosion of steel bars in mortar, because it destroys the passivation film directly around steel bars. However, the amount of water-soluble chloride in the steel bar surface to break down passivity still questionable. Therefore, it is necessary to clarify the water-soluble chloride content in mortar to understand the corrosion phenomena. The total chloride content and water-soluble chloride values by weight of cement and total weight in mortar, which was determined experimentally after accelerated in CO_2 chamber at the end of the experiment in all specimens, are shown in Fig. 4.17. From this figure, the total amount and water-soluble chloride content were varied, depending on W/B ratio and mineral admixture.

The amount of total chloride content was changed from initial total chloride addition for each mineral admixture due to carbonation. After the carbonation, hydration products are converted to calcium carbonate ($CaCO_3$), silica gel and alumina gel, and the pH value of the pore solution drops to about 9 [4.40]. The drop in pH value may decrease the degree of competition offered by hydroxyl, but increase the solubility of Friedel's salt and thus causes the release of bound chlorides [4.41-4.43]. The carbonation not only tends to neutralize the

alkalinity of the pore solution but also leads to the release of bound chlorides in the chloride contaminated mortar. The release of bound chlorides will increase the content of free chlorides and thus leads to the transport of free chlorides through the liquid phase of the mortar. These phenomena happen in each mineral admixture which makes total chloride addition in mixed mortar become change. From this figure (Fig. 4.17), water-soluble chloride of BBMKP was higher compared to other mineral admixture in all cases of W/B ratio, this because BBMKP had higher carbonation depth. Then followed order by SA>BB>FB. Further, water-soluble chloride increased as increased of W/B ratio.

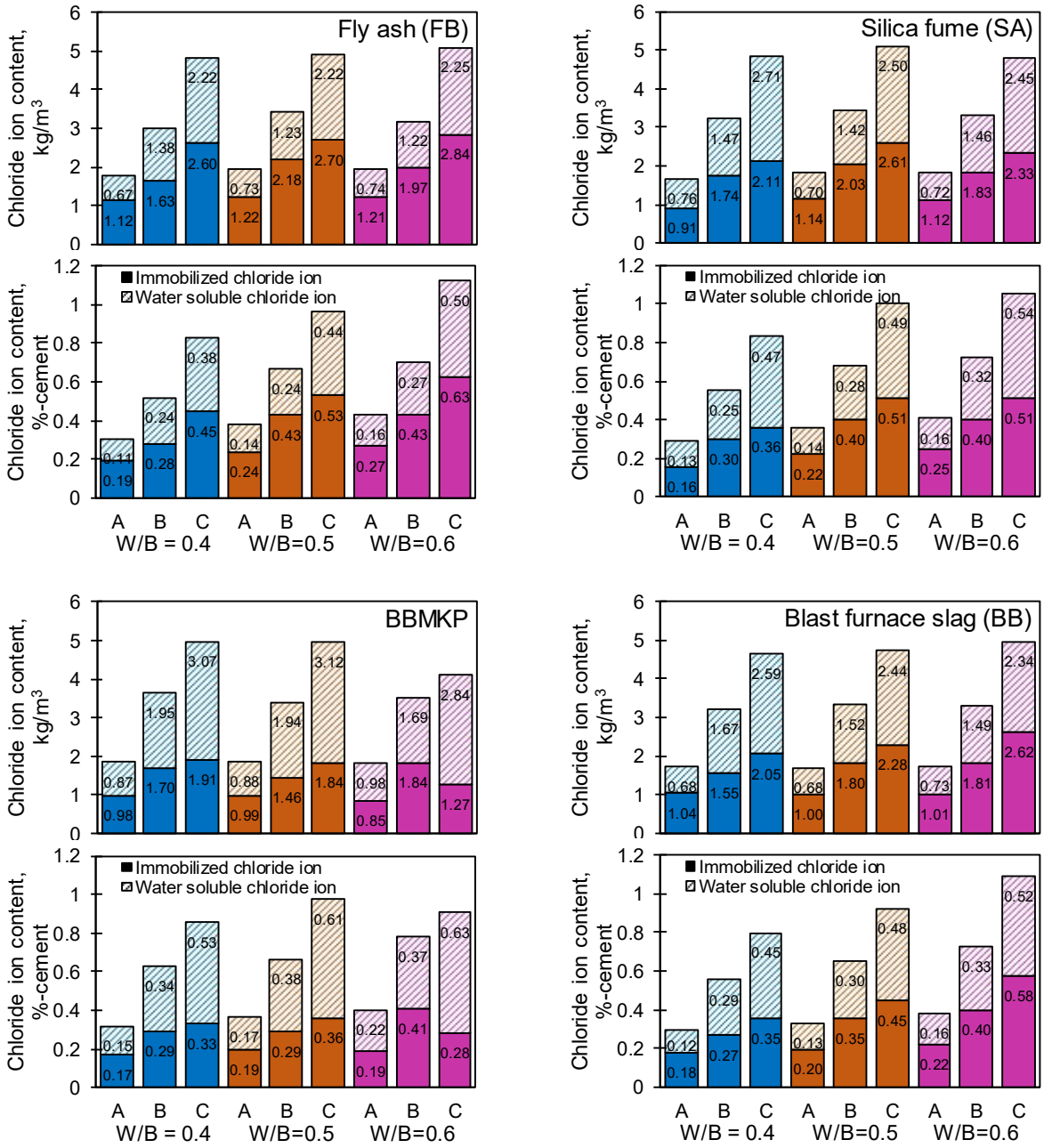

Fig. 4.17—Immobilized and water-soluble chloride for each mineral admixture

4.4.8 Visual observation

After electrochemical measurement was finished, all specimens were cut and split at the age of 756 days (at the last measurement time) to verify the changes observed with the electrochemical measurements and corrosion was confirmed by visualization. From the actual observation, the corroded area was measured except the 1.5 cm edge from top and bottom of steel bar to avoid unexpected corrosion due to un-perfect coating in the top and bottom edge of steel bar.

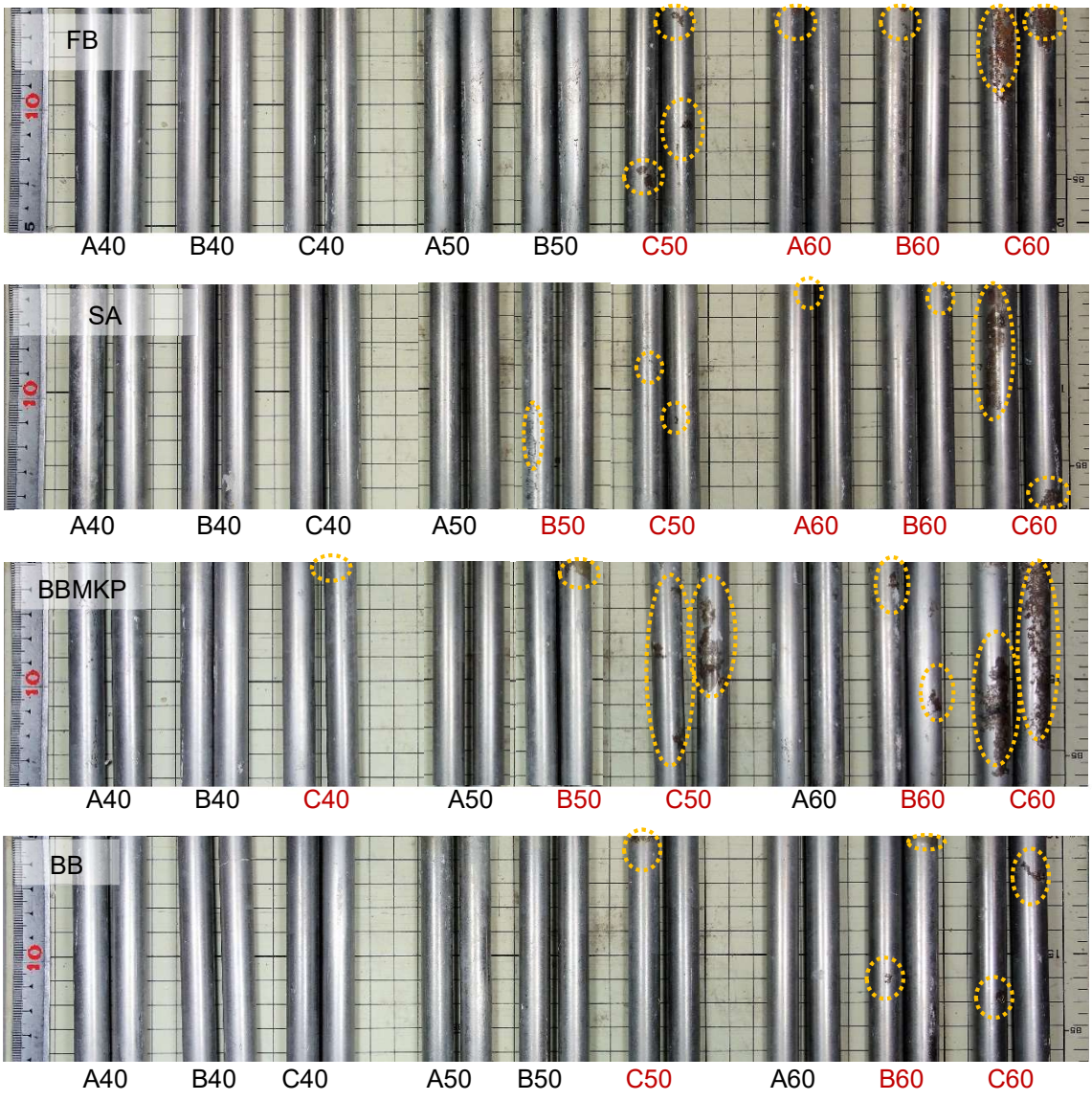

Fig. 4.18— Appearance of steel corroded

The visual observation and corroded area for each specimen are shown in Fig. 4.18 and Table 4.9, respectively. Rust spots were observed in those specimens showing range I_{corr} values 0.149~0.2 μA/cm^2 for all specimens. According to mineral admixture and W/B ratio,

the corroded area of all specimen was less than 1.00 cm^2. On the other hand, C60 and C50 of BBMKP showed large corrosion area and the value was 6.636 and 3.004 cm^2, respectively. Then C60 of FB also showed higher corrosion area with 4.095 cm^2. This indicated that corrosion already occurs before 721 days which earlier than other mineral admixture.

Table 4.9—The corroded area

Series	Corroded area, cm^2			
	FB	SA	BBMKP	BB
A40	0.000	0.000	0.000	0.000
B40	0.000	0.000	0.000	0.000
C40	0.000	0.000	0.406	0.000
A50	0.000	0.000	0.000	0.000
B50	0.000	0.437	0.218	0.000
C50	0.865	0.591	3.004	0.815
A60	0.333	0.300	0.000	0.000
B60	0.691	0.114	0.835	0.196
C60	4.095	2.353	6.636	0.791

4.5 Discussion

4.5.1 Proposed on chloride threshold

The definition of chloride threshold value still needs some consideration. From the practical point of view, depassivation should mean the developing of active corrosion that remains with time. This situation cannot be detected by visual observation only because the appearance of colored oxides may take some time to appear or, on the opposite, its appearance may not mean steady active corrosion.

To investigate the conditions of the onset of corrosion, Fig. 4.19 shows the relationship between the E_{corr} and I_{corr}. In these figures, wide analysis was carried out to obtain the passivity limit of I_{corr} for each mineral admixture, as indicator of corrosion initiation along with E_{corr}. It was observed the specimens in the passive limit showed higher I_{corr} and the values tend to increase at the start of the corrosion activity by actual observation. Further, I_{corr} increased to correspond with the drop of potential values indicating the onset of corrosion. Nevertheless, the indication from E_{corr} value was less accurate and probably misleading, either because the shift was not detected or because it also does not mean a significant activity. This confirmed from Fig. 4.18 (visual observation). These uncertainties recommend using I_{corr} only as an indicator parameter to define chloride threshold value (CTV), whose resistance shift as the corrosion investigates and as a result allows the current to pass through it. However, it should

be noted that the possible relation between corroding and passive areas. If the total exposed area is too large, the ratio of ΣAnodic/ΣCathodic may be too small that the total corrosion may not mean an increase beyond 0.2 μA/cm^2. In this situation, only spot corrosion observed along steel bar surface. In order to detect a significant increase, the total surface area has to be relatively small, as it is the case studied in present paper (less than 1 mm^2 corroded area for each mineral admixtures). With those small exposed areas indicates significant active corrosion not likely to repassivate but become steady. Therefore, I_{corr} has considered reliable to determine deppasivation of steel bar, however, followed by some precautions.

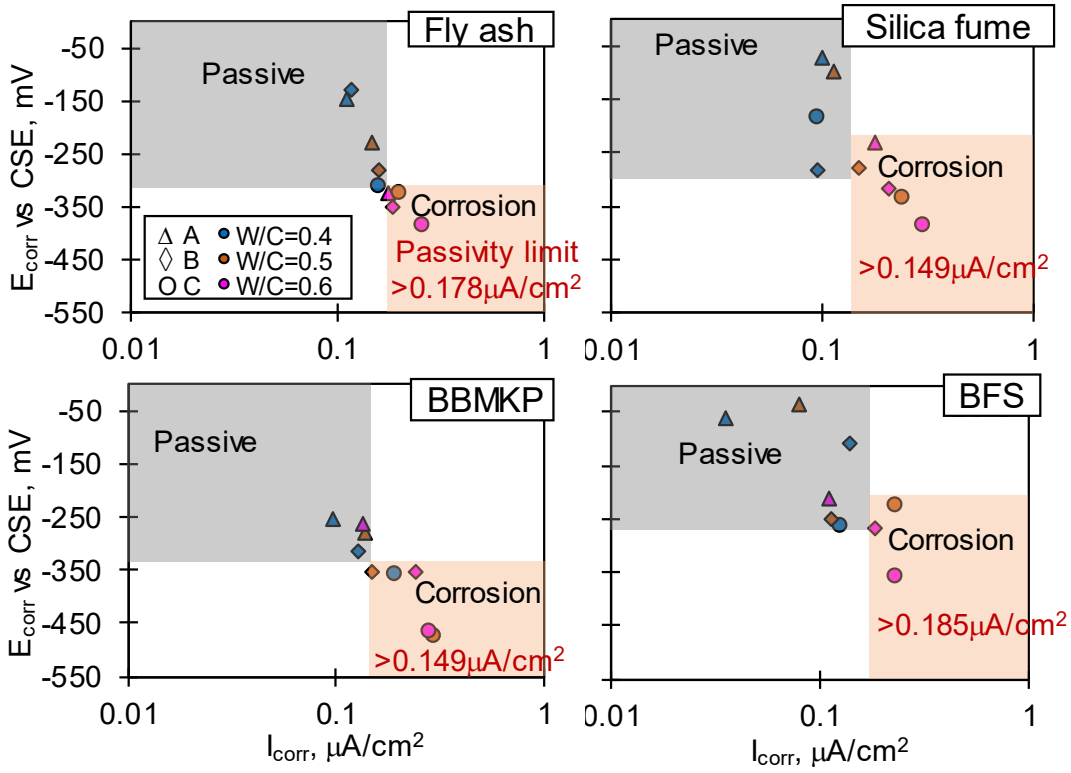

Fig. 4.19—Relationship between E_{corr} and I_{corr}

As shown in Fig. 4.19, according to W/B ratio it was noted that for FB, SA and BB mortar decreased in W/B ratio of 0.4 contributed delays the corrosion initiation but with a lower degree of probability (passive state). Only C40 of BBMKP was in corrosion state. Further, according to mineral admixture, few specimens are in the passive state at the I_{corr} value more than 0.149 μA/cm² (FB and BB). While on the other hand at the similar I_{corr} values, few specimens (SA and BBMKP) have also shown the corrosion initiation, which was even verified upon cutting the specimen. It was found that all specimen showed the corrosion initiation at different values of I_{corr} more than 0.178 μA/cm^2, 0.149 μA/cm^2, 0.149 μA/cm^2,

0.185 μA/cm^2 for replacement cement with FB, SA, BBMKP and BB, respectively (as shown in Fig. 4.19). Therefore, this study has proposed that corrosion can initiate even at such lower values of I_{corr}. In spite of, the current density of 0.2 μA/cm^2 is quite high and normally considered as the passivity limit of current density which is defined by CEB standard. However, this study proposed the CTV of the passivity limit which determined from current density which confirmed by actual corrosion.

4.5.2 Determination on of chloride threshold value (CTV)

The corrosion current density (I_{corr}) of total chloride and water-soluble content in mortar as function of the chloride content surround the steel bar after carbonation is plot in Figs 4.20 and 4.21, respectively. In these figures, the marked area with different color indicates the upper limit of the I_{corr} as a function of total chloride and water-soluble content in mortar. In order to compare the CTV for the initiation of spot corrosion of embedded steel, a chloride threshold was then defined as the range in the chloride content where I_{corr} measured between two-line passes from values 0.178 μA/cm^2, 0.149 μA/cm^2, 0.149 μA/cm^2, 0.185 μA/cm^2 for replacement cement with FB, SA, BBMKP and BB, respectively, to values less than 0.2 μA/cm^2. With such a method, a range of CTV was detected for each specimen with different mineral admixture and W/B ratio.

From Fig.s 4.20a and 4.20b of FB mortar with W/B ratio 0.6, the result of CTV is from 0.5% (at 0.178μA/cm^2) to 0.7% (at 0.2 μA/cm^2) of the total chloride by weight of binder. And when interpreted in weight of mortar, the CTV range from 2.2~3.1 kg/m^3. Further, from Fig.s 4.21a and 4.21b of FB mortar with W/B ratio 0.6, the result of CTV is from 0.2% (at 0.178μA/cm^2) to 0.28% (at 0.2μA/cm^2) of the water-soluble chloride by weight of binder. And when interpreted in weight of mortar, the CTV range from 0.9~1.3 kg/m^3. The same consideration for SA, BBMKP and BB mortar and the result of CTV of total chloride and water-soluble chloride were summarized in Table 4.10 and 4.11, respectively.

If we considered on actual structure and service life estimation, the range of CTV is necessary to fix. However, it was difficult to fix the value since the corrosion involved many factors such as environmental conditions and properties of the concrete structure. Consequently, this study proposed the minimum amount of total chloride ions and water-soluble chloride at a depth of reinforcement required to initiate corrosion are shown in Fig. 4.22 and 4.23, respectively.

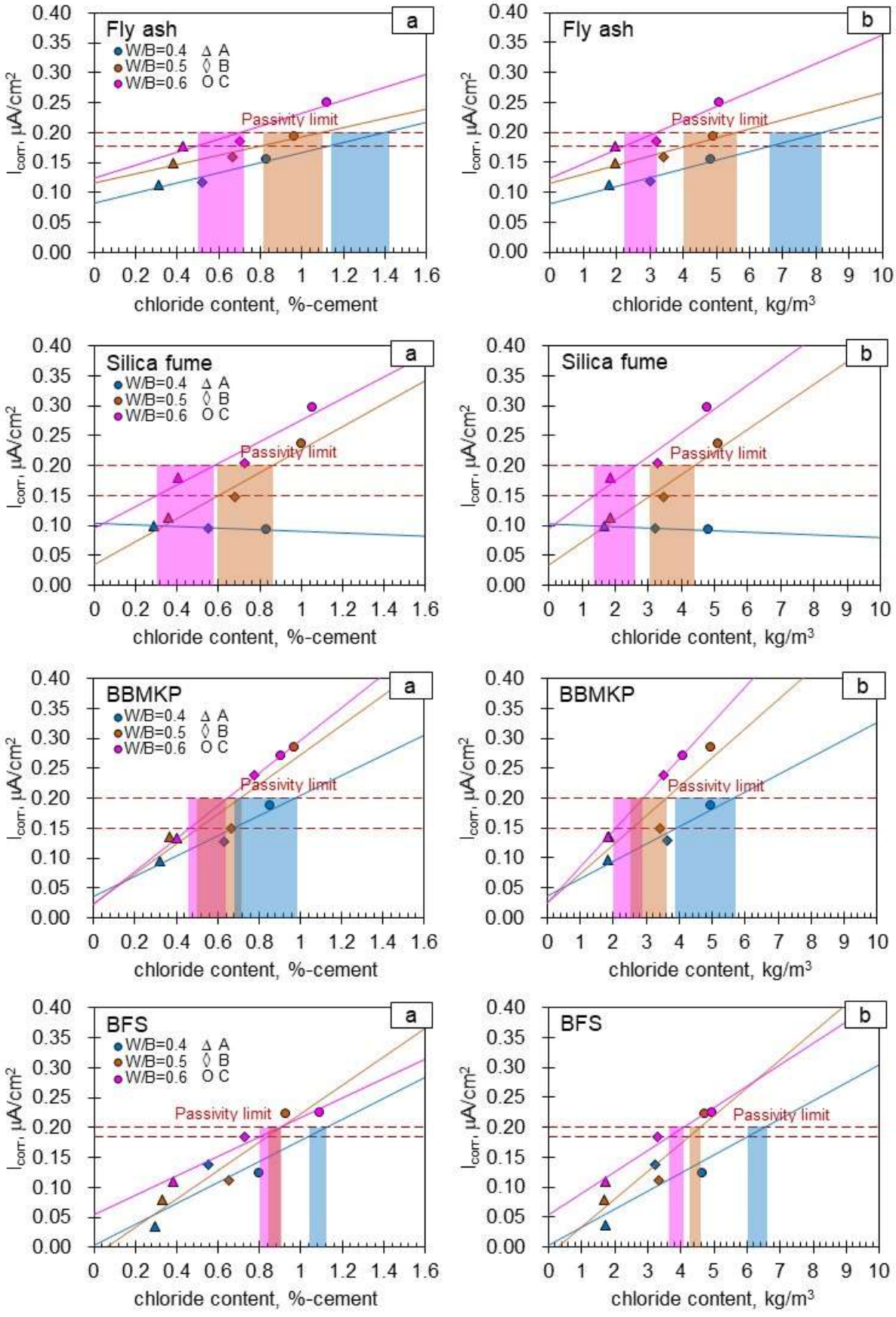

Fig. 4.20—Corrosion current density as a function of chloride content to determining the CTV of total chloride

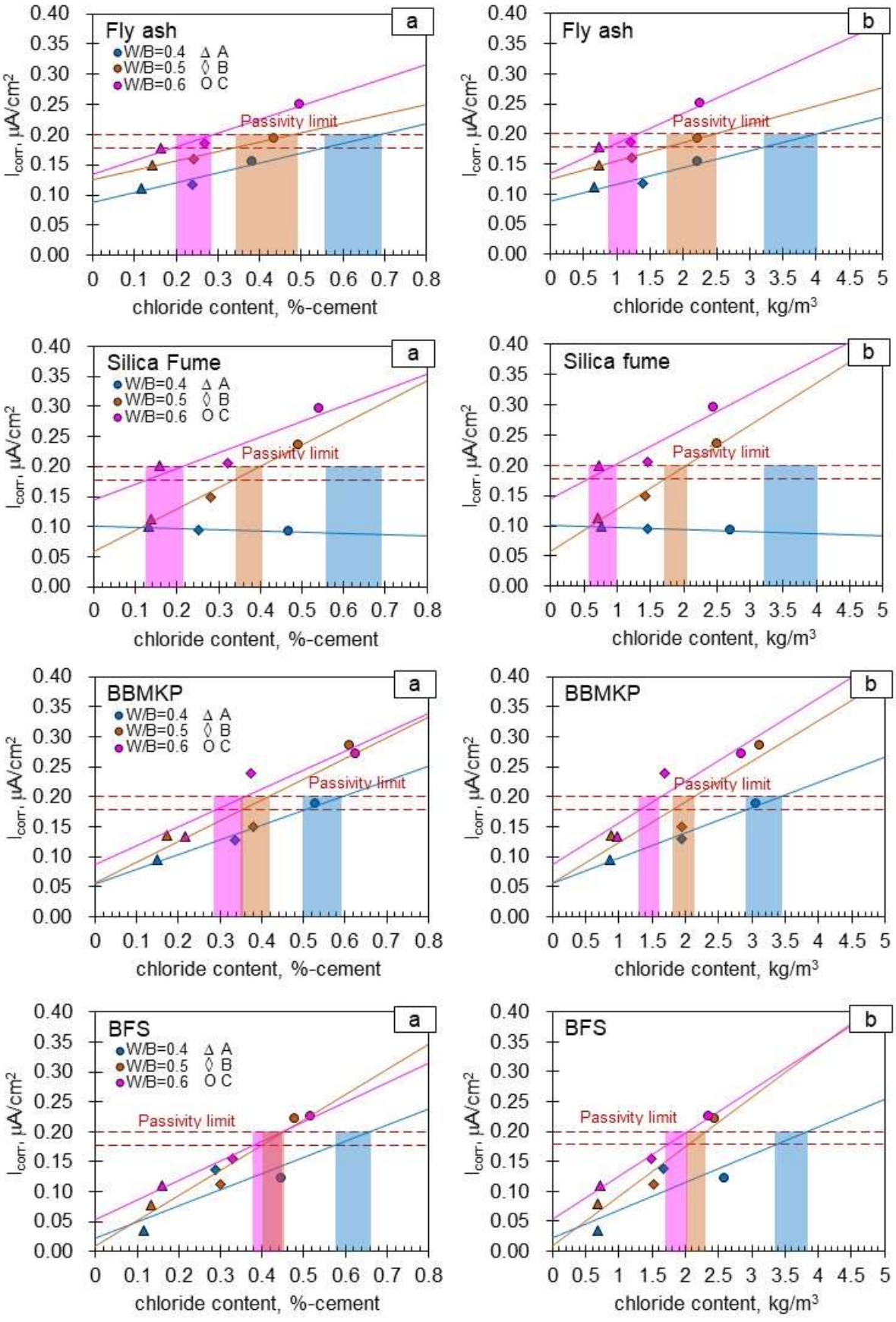

Fig. 4.21—Corrosion current density as a function of chloride content to determining the CTV of water-soluble chloride

Table 4.10—Chloride threshold value for total chloride

W/B	Weight of cement, %-cement				Total weight in mortar, kg/m^3			
	FB	SA	BBMKP	BB	FB	SA	BBMKP	BB
0.4	1.14-1.42	*	0.68-0.98	1.04-1.12	6.6-8.2	*	3.9-5.7	6.0-6.6
0.5	0.82-1.1	0.6-0.86	0.50-0.72	0.84-0.9	4.0-5.6	3.0-4.4	2.5-3.6	4.3-4.6
0.6	0.5-0.70	0.3-0.58	0.46-0.64	0.8-0.9	2.2-3.2	1.40-2.60	2.0-2.9	3.6-4.1

*out of the range

Table 4.11—Chloride threshold value for water-soluble chloride

W/B	Weight of cement, %-cement				Total weight in mortar, kg/m^3			
	FB	SA	BBMKP	BB	FB	SA	BBMKP	BB
0.4	0.56-0.69	*	0.5-0.59	0.59-0.68	3.2-4	*	2.9-3.45	3.35-3.85
0.5	0.34-0.49	0.34-0.4	0.35-0.42	0.4-0.45	1.75-2.5	1.7-2.05	1.8-2.1	2.0-2.3
0.6	0.2-0.28	0.12-0.21	0.28-0.35	0.38-0.44	0.9-1.3	0.6-1	1.3-1.6	1.7-2.0

*out of the range

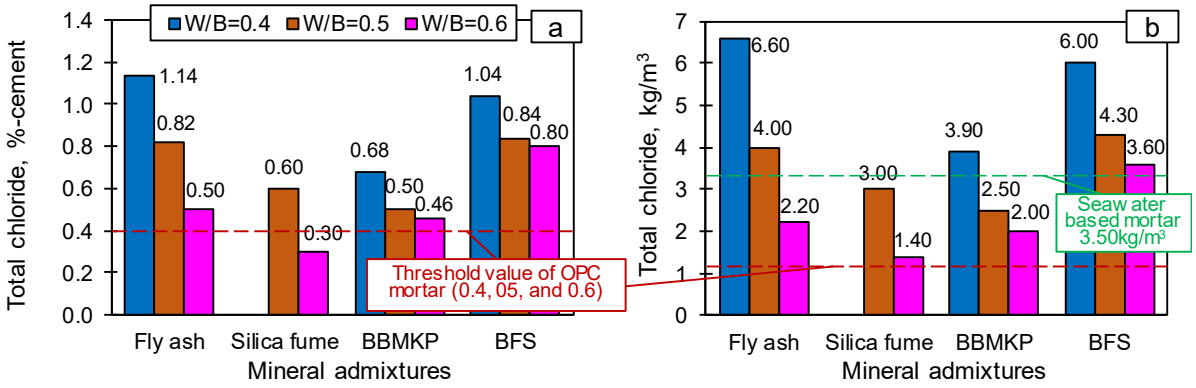

Fig. 4.22—Minimum chloride threshold value for total chloride

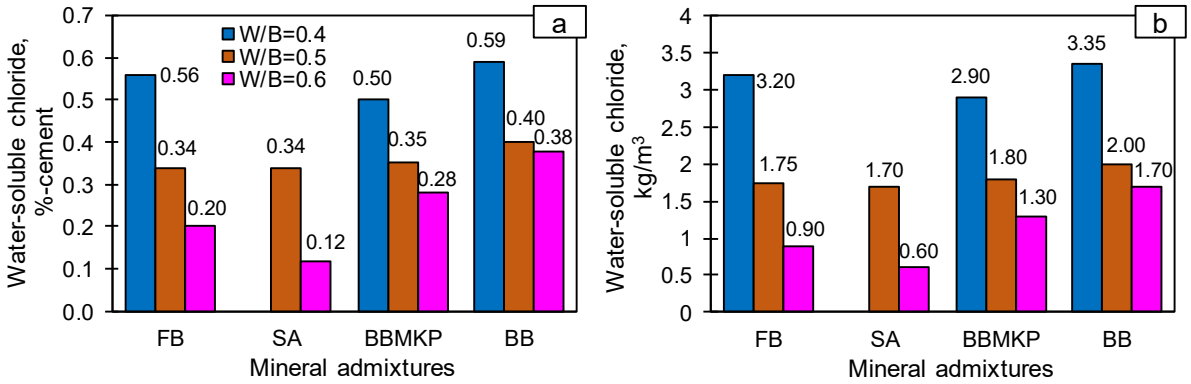

Fig. 4.23—Minimum chloride threshold value for water-soluble chloride

From Fig.s 4.22a and 4.22b, the CTV of BB and FB was larger compared to other mineral admixture, then following by BBMKP. These values for OPC mortar were higher in accordance with the previous study reported values [4.30]. Further, SA mortar had smaller

CTV than other mineral admixture. Also, the CTV of SA mortar with W/B ratio of 0.6 is less than CTV of OPC cement (dashed horizontal line shown in Fig. 4.22), it was 25% reduce from OPC. The effect of W/B ratio and mineral admixture on CTV was found and quite clear. The trend of decreased in CTV against the increase in W/B ratio of mortar contain mineral admixture, compared to OPC mortar from previously reported values was not found.

The effect of carbonation on the CTV is beyond the scope of this study. The pH value of the pore solution is one of the most important parameters that govern the passivation of the steel protecting it from risk of corrosion. The steel remains passive above a pH value of 13. However, as the chloride content in the pore solution reaches a limiting value, the depassivation process begins. At a pH value less than 11.5, corrosion is initiated. Percentage of chloride requirement to initiate the corrosion fluctuates highly as the pH level of the pore solution drops down [4.50]. Carbonation of the mortar does not in itself cause a loss of structural adequacy, but when the zone of carbonation extends to the steel, the protective action of the mortar is largely lost, primarily because calcium carbonate has a reduced PH value. This then allows positive Fe^{+2} ions to form which join with dissolved oxygen in the water to produce Fe_2O_3 (iron oxide or rust) and the process of corrosion of steel bar initiate [4.50]. The process of corrosion is greatly accelerated if chloride ions (from salt) are present. Chloride is not used in chemical reaction to form rust but seems to assist the formation of anode and cathode regions in metal.

4.5.3 Influence of mineral admixtures on chloride threshold value

Fly ash. From this study, replacement cement with 20% of fly ash has been found have a higher chloride binding capacity compared to other mineral admixture even mixed with same amount of chloride. This could be due to both physical adsorptions of chloride because of more gel formation and chemical binding due to the higher content of alumina [4.51]. The C_3A and C_4AF have greater affinity towards holding free chlorides. They bind chloride to form Friedel's salts and thus reduce the amount of free chloride available for further reaction with the pore solution. Nevertheless, an increase in C_3A also decreases the pH value of the pore solution [4.51, 4.52], making it susceptible to corrosion. Also the increasing in the CTV for FB mortar is mainly because of the reduction in the CH content. The CH present at the interface normally inhibits the corrosion initiation by the formation of passive film around the steel bar [4.55]. The reduced CH content in FB mortar is due to the decreased cement content and utilization of CH in the pozzolanic reaction. The lowered CH content ultimately drops the pH of FB mortar creating favorable environment for corrosion initiation. The mean CTV value

for prolonged curing of FB specimens was found to increase in spite of reduced CH content. In this case, the increased degree of pozzolanic reaction can reduce corrosion risk. Along with CH other hydrations products can also effectively act as a solid phase inhibitor to restrict the local fall in pH needed to maintain the corrosion process [4.56]. Also, this increase in CTV for prolonged curing may be due to the dense microstructure, increased binding effects of chlorides and new constituents acting as an inhibitor generated by the reaction [4.57].

Silica Fume. The use 5% of silica fume as replacement cement reduces the ability of chloride binding because of the reduction in the aluminate phases, which leads to the higher rate of corrosion in silica fume added mortar, in spite of the higher pore refinement. However, silica blended concrete mixtures have been reported to have lesser chloride binding capacity compared to OPC concrete [4.56]. The alkalinity of pore solution was found to decrease with increased addition of silica fume [4.52]. Some researcher found that CTV for silica fume blended concrete varies from 0.125~1.8% weight of cement, with most of the values coming under 0.4~0.8%. Although pore refinement due to addition of silica fume assists in increasing the CTV, the reduced alkalinity and chloride binding capacity offsets this effect and contributes to an overall reduction in CTV. Although further replacement of silica fume refines pores, it reduces alkalinity of the pore solution, resulting in a comparative reduction of chloride binding ability with formation of Friedel's salt, which is highly soluble at lower pH [4.52]. Therefore, lower CTV has been reported for silica fume compared to other mineral admixture.

Blast furnace slag. The replacement cement with BFS improves the physical and chemical binding properties of the mortar. Oh et al. [4.57] reported insignificant effect due to BFS addition on CTV. However, several researchers suggested CTV from 0.23 [4.58] to 2.5 [4.59] for BFS blended concrete. Dhir et al. [4.60] conducted extensive studies on the chloride binding capacities of BFS blended concrete. Unlike silica fume, the chloride binding capacity of the slag blended concrete was found to increase with the level of replacement. It is interesting to note that the chloride ion binding ability increased at higher chloride exposure concentrations. Therefore, higher values of chloride threshold have been reported for BFS blended concrete mixtures compared to silica fume and BBMKP.

Metakaolin. The replacement cement of BB (OPC and Slag) with metakaolin reduces the chloride binding ability because of the reduction content of portlandite in hydrate products due to pozzolanic reaction. This phenomenon makes metakaolin had lower performance to carbonation which reduces the alkalinity of the pore solution and release of bound chlorides. Bla [4.45] reported that the bound chloride of metakaolin increased if the chemical composition about 50% SiO_2 and 45% Al_2O_3. Different compositions of C-S-H, calcium

aluminate hydrates (C-A-H) and calcium alumino silicate hydrates (C-A-S-H) are the main hydration products for metakaolin systems and it is therefore expected that they would contribute to the binding capacity [4.45]. The chloride binding capacity of the metakaolin was found to increase with the level of replacement. For that reason, lower CTV has been reported for BBMKP compared to other mineral admixture.

4.5.4 Possibility of mineral admixture mixed with seawater

From the viewpoint of the immobilization of chloride ion and minimum CTV of total chloride of this study, it is estimated that FB and BB is the most efficient binder replacement cement against steel corrosion in mortar mixed with seawater. This study proposes the possibility to use seawater and if mortar mixed with blast furnace slag and fly ash with W/B ratio of 0.4~0.5. BBMKP is also efficient to use as replacement cement mixed with seawater with a maximum 0.4 of W/B ratio and cover depth of concrete should be increased. This similar recommended from ACI 201.2R guidelines [4.61] that slag is significant to use if quenched with seawater. With W/B ratio of 0.4~0.45 with concrete cover should be increased simultaneously. Additionally, it highlights the protective system against the corrosion, which is to be adopted based on different exposure conditions. However, this ACI 201.2R guidelines [4.61] reported that chloride content of the binder is typically very low when fly ash and silica fume are used as admixtures.

4.6 Conclusion

The following conclusions have been drawn from the present study.

1. Corrosion current density (I_{corr}) has reliable to evaluate and determine chloride threshold value (CTV).
2. A chloride threshold was estimated as the range of chloride content where the corrosion current density of steel passed difference value for each mineral admixture. The passivity limit to corrosion initiation of I_{corr} for replacement cement with FB, SA, BBMKP and BB being value at range 0.178 $\mu A/cm^2$, 0.149 $\mu A/cm^2$, 0.149 $\mu A/cm^2$, 0.185 $\mu A/cm^2$ respectively to the 0.2 $\mu A/m^2$.
3. The ranges of chloride threshold found, expressed in total and water-soluble chloride were the following:

a. Total chloride

W/B	Weight of cement, %-cement				Total weight in mortar, kg/m^3			
	FB	SA	BBMKP	BB	FB	SA	BBMKP	BB
0.4	1.14-1.42	*	0.68-0.98	1.04-1.12	6.6-8.2	*	3.9-5.7	6.0-6.6
0.5	0.82-1.1	0.6-0.86	0.50-0.72	0.84-0.9	4.0-5.6	3.0-4.4	2.5-3.6	4.3-4.6
0.6	0.5-0.70	0.3-0.58	0.46-0.64	0.8-0.9	2.2-3.2	1.40-2.60	2.0-2.9	3.6-4.1

*out of the range

b. Water-soluble chloride

W/B	Weight of cement, %-cement				Total weight in mortar, kg/m^3			
	FB	SA	BBMKP	BB	FB	SA	BBMKP	BB
0.4	0.56-0.69	*	0.5-0.59	0.59-0.68	3.2-4	*	2.9-3.45	3.35-3.85
0.5	0.34-0.49	0.34-0.4	0.35-0.42	0.4-0.45	1.75-2.5	1.7-2.05	1.8-2.1	2.0-2.3
0.6	0.2-0.28	0.12-0.21	0.28-0.35	0.38-0.44	0.9-1.3	0.6-1	1.3-1.6	1.7-2.0

*out of the range

4. The type of water to binder ratio seems to influence the threshold value significantly after depassivation.
5. In performance-based design determined by chloride attack and carbonation, it is possible to use seawater and if mortar mixed with BB or FA with maximum W/B ratio of 0.5. BBMKP is also efficient to use as replacement cement mixed with seawater with a maximum 0.4 of W/B ratio and cover depth of concrete should be increased.

Reference

[4.1] Hilsdorf, H., and Jorg Kropp. Performance criteria for concrete durability. CRC Press, 1995.

[4.2] Recommendation, RILEM Draft. "Draft recommendation for repair strategies for concrete structures damaged by reinforcement corrosion." Materials and Structures 27.171 (1994): 415-436.

[4.3] JGC16, "Standard Specification for Concrete Structures (Materials and Construction)," Japan Society of Civil Engineers, 2007.

[4.4] Alonso, Carmen, C. Andrade, and J. A. Gonzalez. "Relation between resistivity and corrosion rate of reinforcements in carbonated mortar made with several cement types." Cement and concrete research 18.5 (1988): 687-698.

[4.5] Feliu, S., et al. "Relationship between conductivity of concrete and corrosion of reinforcing bars." British corrosion journal 24.3 (1989): 195-198.

[4.6] Glass, G. K., C. L. Page, and N. R. Short. "Factors affecting the corrosion rate of steel in carbonated mortars." Corrosion Science 32.12 (1991): 1283-1294.

[4.7] Andrade, C., C. Alonso, and S. Goni. "Possibilities for electrical resistivity to universally characterise mass transport processes in concrete." Concrete 2000: Economic and durable construction through excellence 2 (2000): 1639-1652.

[4.8] Lopez, W., and J. A. Gonzalez. "Influence of the degree of pore saturation on the

resistivity of concrete and the corrosion rate of steel reinforcement." Cement and concrete research 23.2 (1993): 368-376.
[4.9] Richartz, W. "Die Bindung von Chlond bei der Zementerhartung." (1969): 447-456.
[4.10] Gouda, V. K. "Corrosion and corrosion inhibition of reinforcing steel: I. Immersed in alkaline solutions." British Corrosion Journal 5.5 (1970): 198-203.
[4.11] Hansson, C. M., and B. Sørensen. "The threshold value of chloride concentration for the corrosion of reinforcement in concrete." Corrosion Rates of Steel in Concrete (1989): 3-16.
[4.12] Takagi, N., et al. "Chloride corrosion of reinforcing steel in silica fume concrete exposed to marine environment. in: durability of concrete. second international conference. august 4-9, 1991, montreal, canada. volume i." durability of concrete. second international conference.. vol. 1. no. sp 126-25. 1991.
[4.13] Peter, Schieβl. "Local repair measures at concrete structures damaged by reinforcement corrosion-aspect of durability." corrosion of Reinforcement in Concrete Construction, Proceeding of the 4^< th> International Symposium, Cambridge UK 1-4 July. 1996.
[4.14] Thomas, Michael. "Chloride thresholds in marine concrete." Cement and concrete research 26.4 (1996): 513-519.
[4.15] Breit, W. "Critical chloride content-Investigations of steel in alkaline chloride solutions." Materials and Corrosion-Werkstoffe Und Korrosion 49.8 (1998): 539-550.
[4.16] Alonso, C., et al. "Chloride threshold values to depassivate reinforcing bars embedded in a standardized OPC mortar." Cement and Concrete research 30.7 (2000): 1047-1055.
[4.17] Whiting, David, Peter Clement Taylor, and Mohamad Nagi. Chloride limits in reinforced concrete. Portland cement Association, 2002.
[4.18] Oh, Byung Hwan, Seung Yup Jang, and Y. S. Shin. "Experimental investigation of the threshold chloride concentration for corrosion initiation in reinforced concrete structures." Magazine of Concrete Research 55.2 (2003): 117-124.
[4.19] Manera, Marco, Øystein Vennesland, and Luca Bertolini. "Chloride threshold for rebar corrosion in concrete with addition of silica fume." Corrosion Science 50.2 (2008): 554-560.
[4.20] Mohammed, Tarek Uddin, and Hidenori Hamada. "Corrosion of steel bars in concrete with various steel surface conditions." ACI Materials Journal 103.4 (2006): 233.
[4.21] "Locke, C. E., and A. Siman. ""Electrochemistry of reinforcing steel in salt-contaminated concrete."" Corrosion of reinforcing steel in concrete. ASTM International, 1980.
[4.22] Hansson, Carolyn M., and B. Sørensen."The threshold concentration of chloride in concrete for the initiation of reinforcement corrosion." Corrosion rates of steel in concrete. ASTM International, 1990.
[4.23] Schiessl, P., and M. Raupach. "Influence of concrete composition and microlimate on the critical chloride content in concrete." Third International Symposium on Corrosion of Reinforcement in Concrete Construction. 1990.
[4.24] Pettersson, Karin. "Corrosion threshold value and corrosion rate in reinforced concrete." CBI REPORT 2: 92 (1992).
[4.25] Pettersson, K. "Chloride threshold value and the corrosion rate in reinforced concrete." Proc. of the Nordic Seminar. 1994.

[4.26] Peter, Schieβl. "Local repair measures at concrete structures damaged by reinforcement corrosion-aspect of durability." corrosion of Reinforcement in Concrete Construction, Proceeding of the 4^< th> International Symposium, Cambridge UK 1-4 July. 1996.
[4.27] Thomas, M. D. A., JD MATTHEWS, and C. A. Haynes. "Chloride Diffusion And Reinforcement Corrosion In Marine Exposed Concrete Containing Pulverized-Fuel Ash. Corrosion Of Reinforcement In Concrete. Papers Presented At The Third International Symposium On" Corrosion Of Reinforcement In Concrete Construction", Belfry Hotel, Wishaw, Warwickshire, MAY 21-24, 1990." Publication of: CICC Publications (1990).
[4.28] Breit, Wolfgang. "Kritischer Korrosionsauslosender Chloridgehalt: Neuere Untersuchungsergebnisse.(TEIL 2): KAPITEL 8-10." Beton 48.8 (1998).
[4.29] de Rincón, O. "Comparison between chloride ion threshold and electrochemical measurements for reinforcement corrosion." 3rd International RILEM Workshop on Testing Modelling Chloride Ingress into Concrete. RILEM Publications SARL, 2004.
[4.30] Hamada, Hidenori, et al. "An experimental study on relationship between chloride content in mortar and passivity condition of embedded steel bar." 4th International Symposium Life-Cycle Civil Engineering, IALCCE 2014. CRC Press/Balkema, 2015.
[4.31] Astm, C. "876-15 Standard test method for half-cell potentials of uncoated reinforcing steel in concrete." ASTM Annual Book of ASTM Standards 4 (2015).
[4.32] Stern, Milton, and Al L. Geary. "Electrochemical polarization I. A theoretical analysis of the shape of polarization curves." Journal of the electrochemical society 104.1 (1957): 56-63.
[4.33] Comite Euro-International Du Beton. Durable Concrete Structures: CEB Design Guide. Comité Euro-international du Béton, 1985.
[4.34] S. Nagataki, N. Otsuki, A. Moriwake, S. Miyazato J. Mater., Concr. Struct. Pavements, 32 (544) (1996): 109-119.
[4.35] Demirboğa, Ramazan, İbrahim Türkmen, and Mehmet B. Karakoc. "Relationship between ultrasonic velocity and compressive strength for high-volume mineral-admixtured concrete." Cement and Concrete Research 34.12 (2004): 2329-2336.
[4.36] PARROT, LJ. "A review of carbonation in reinforced concrete. C&CA/BRE Report C/l-0987." British Cement Association (1987): 45.
[4.37] Vejmelkova, Eva, et al. "High performance concrete with Czech metakaolin: Experimental analysis of strength, toughness and durability characteristics." Construction and Building Materials 24.8 (2010): 1404-1411.
[4.38] Kim, Hong-Sam, Sang-Ho Lee, and Han-Young Moon. "Strength properties and durability aspects of high strength concrete using Korean metakaolin." Construction and building materials 21.6 (2007): 1229-1237.
[4.39] Hornbostel, Karla, Claus K. Larsen, and Mette R. Geiker. "Relationship between concrete resistivity and corrosion rate–a literature review." Cement and Concrete Composites 39 (2013): 60-72.
[4.40] Bertos, M. Fernández, et al. "A review of accelerated carbonation technology in the treatment of cement-based materials and sequestration of CO2." Journal of hazardous materials 112.3 (2004): 193-205.
[4.41] Goni, S., and A. Guerrero. "Accelerated carbonation of Friedel's salt in calcium

aluminate cement paste." Cement and Concrete Research 33.1 (2003): 21-26.
[4.42] Page, C. L., and Øisten Vennesland. "Pore solution composition and chloride binding capacity of silica-fume cement pastes." Matériaux et construction 16.1 (1983): 19-25.
[4.43] Suryavanshi, A. K., and R. Narayan Swamy. "Stability of Friedel's salt in carbonated concrete structural elements." Cement and Concrete Research 26.5 (1996): 729-741.
[4.45] Dousti, Ali, James J. Beaudoin, and Mohammad Shekarchi. "Chloride binding in hydrated MK, SF and natural zeolite-lime mixtures." Construction and Building Materials 154 (2017): 1035-1047.
[4.46] Maslehuddin, M., and O. S. B. Al-Amoudi. "Corrosion of reinforcing steel in concrete: its monitoring and prevention." Proceedings, Symposium on Corrosion its Control. 1992.
[4.47] Hussain, S. E., A. Al-Musallam, and A. S. Al-Gahtani. "Factors affecting threshold chloride for reinforcement corrosion in concrete." Cement and Concrete Research 25.7 (1995): 1543-1555.
[4.50] Gouda, V. K. "Corrosion and corrosion inhibition of reinforcing steel: I. Immersed in alkaline solutions." British Corrosion Journal 5.5 (1970): 198-203.
[4.51] Diamond, Sidney. "Effects of two Danish flyashes on alkali contents of pore solutions of cement-flyash pastes." Cement and Concrete Research 11.3 (1981): 383-394.
[4.52] Byfors, Kajsa. "Influence of silica fume and flyash on chloride diffusion and pH values in cement paste." Cement and Concrete Research 17.1 (1987): 115-130.
[4.53] Thomas, Michael. "Chloride thresholds in marine concrete." Cement and concrete research 26.4 (1996): 513-519.
[4.54] Whiting, David, Peter Clement Taylor, and Mohamad Nagi. Chloride limits in reinforced concrete. Portland cement Association, 2002.
[4.55] Hansson, C. M., and B. Sørensen. "The threshold value of chloride concentration for the corrosion of reinforcement in concrete." Corrosion Rates of Steel in Concrete (1989): 3-16.
[4.56] Larsen C K. "Chloride binding in concrete". Norwegian University of Science and Technology, NTNU, 1998.
[4.57] Oh, Byung Hwan, Seung Yup Jang, and Y. S. Shin. "Experimental investigation of the threshold chloride concentration for corrosion initiation in reinforced concrete structures." Magazine of Concrete Research 55.2 (2003): 117-124.
[4.58] Castellote, M., C. Andrade, and C. Alonso. "Accelerated simultaneous determination of the chloride depassivation threshold and of the non-stationary diffusion coefficient values." Corrosion Science 44.11 (2002): 2409-2424.
[4.59] Lambert, Page, C. L. Page, and P. R. W. Vassie. "Investigations of reinforcement corrosion. 2. Electrochemical monitoring of steel in chloride-contaminated concrete." Materials and Structures 24.5 (1991): 351-358.
[4.60] Dhir, R. K., M. A. K. El-Mohr, and T. D. Dyer. "Chloride binding in GGBS concrete." Cement and Concrete Research 26.12 (1996): 1767-1773.
[4.61] ACI 201.2R-01. "Guide to durable concrete". ACI, Committee, 2001.
[4.62] Patah, D., et al., (2018). Electrochemical Evaluation of Steel Bar in Chloride Contaminated Mortar with Several Kinds of mineral Admixtures throughout one year. Annual Conference of Japan Society of Corrosion Engineering held in Toyama.

CHAPTER 5. PERFORMANCE OF SEAWATER-MIXED CONCRETE IN NATURAL CORROSION ENVIRONMENTS

5.1 Introduction

The concrete industry uses large amounts of freshwater which are used annually in the mixing, curing, and cleaning around the world. Being the primary building material in construction, concrete production consumes several billion tons of fresh water every year which has caused increasing pressure on freshwater resources. In the viewpoint of saving freshwater, researchers continuously investigating other alternatives to freshwater for use in concrete and the possibilities of using seawater-mixed concrete should be investigated comprehensively as an alternative material. Further, if the use of seawater as mixing water in concrete is reliable, it would be very convenient and economical in construction, especially in coastal works and isolated island. JSCE committee [5.1] reported seawater as mixing water should be avoided to be used in RC structures because of the risk of early corrosion of reinforcement induced by chloride in seawater compounds. However, in the case of an unavoidable situation, seawater as mixing water is recommended only for plain concrete. Previous studies reported on corrosion evaluation of seawater mixed in concrete [5.2-5.4]. Furthermore, Mohammed et al. [5.6] reported that seawater mixing caused an earlier gain in the strength and improved the microstructure of concrete. compared to tap water mixing. In addition, the deterioration in concrete strength was not encountered due to the acceleration of hydration process in the presence of chlorides in the used seawater after 15 years of exposure in a tidal pool. Fukute and Hamada [5.7] reported the results of the long-term exposure tests conducted by Port and Airport Research Institute (PARI) in Japan indicated that the amount of Cl measured in concrete after 20-years of exposure is not affected by the mixing water and the negative influence of seawater used as mixing water is relatively decreasing with age [5.9].

This study performed several investigations on concrete mixed with seawater and tap water. Ten number of RC beams have been evaluated. The specimens were exposed to a tidal pool utilizing seawater directly from the sea. The major test variables include mixing water, various of cover depth, water to cement ratios, various bending load and exposure condition.

The effect of seawater mixing on corrosion of steel bar in 36-years old RC beams under marine tidal environment was reported already by Patah et al. [5.28]. The aim of the study is (1) to evaluate the effect of seawater mixing and exposure condition (tidal and splash) on deterioration and steel corrosion of RC beam under service load after 36-years of exposure; (2) to understand how far the contribution of seawater mixing and concrete cover on durability of RC structure after long-term exposure particularly in marine environment. Visual observation, chloride ingress, microstructure, and corrosion of steel bars in RC beams (electrochemical and physical) were evaluated and summarized in this paper. The results will be beneficial to understand the long-term performance of concrete mixed with tap water and seawater under marine environment.

5.2 Test Program

5.2.1 Exposure conditions

The investigations of ten RC beam specimens were carried out. The RC beam specimens were mixed with tap water and seawater. The cement type was Ordinary Portland Cement (OPC). The detailed information of mix proportions of concrete is unavailable. Water-cement ratios (W/C) were 45, 55 and 65%. The density of concrete was 2,398 kg/m^3. Three levels of stress of bar were applied that were 100, 200, and 300 MPa or if interpreted in bending load they were M=2.66, 5.32, and 7.97 kN.m, respectively. The summary of RC beam is shown in Table 5.1.

Table 5.1—Summary of RC beam specimens

Group	Type	W/C, %	M, kN-m	Mixing water	Exposure
Seawater	65-L1-SW-T	65	2.66 (L1)	Seawater (SW)	Tidal (T)
	45-L1-SW-T	45	2.66 (L1)	Seawater (SW)	Tidal (T)
	55-L2-SW-T	55	5.32 (L2)	Seawater (SW)	Tidal (T)
	55-L3-SW-T	55	7.97 (L3)	Seawater (SW)	Tidal (T)
	65-L1-SW-S	65	2.66 (L1)	Seawater (SW)	Splash (S)
	55-L1-SW-S	55	2.66 (L1)	Seawater (SW)	Splash (S)
	45-L1-SW-S	45	2.66 (L1)	Seawater (SW)	Splash (S)
Tap water	65-L1-TW-T	65	2.66 (L1)	Tap water (TW)	Tidal (T)
	55-L1-TW-T	55	2.66 (L1)	Tap water (TW)	Tidal (T)
	55-L3-TW-T	55	7.97 (L3)	Tap water (TW)	Tidal (T)

The layout details of the RC beam were shown in Fig. 5.1. Dimensions of beam were 12x15x120 cm. Three deformed steel bars of diameter 1 cm were embedded at 2, 3, and 5 cm of cover depth from the two sides in the beam. The four sides of the RC beam were noted “Side C” as compression side, “Side T” as tension side, “Side F” and “Side B as front and

backside respectively. The investigations were carried out after 36 years of exposure. The long-term exposure of concrete to marine environments has been studied by PARI since 1975 to evaluate the deterioration progress and performance degradation of RC beams as reported in previous studies [5.25-5.27]. The RC beams were cast and then stored in a tidal pool and artificial water splash under constant bending load at the Port and Airport Research Institute (PARI) laboratory in Yokosuka-Japan for 32-years. Then they were moved to exposure site at Kyushu University followed by four years' exposure under outside natural environment, without bending load (Fig. 5.2)

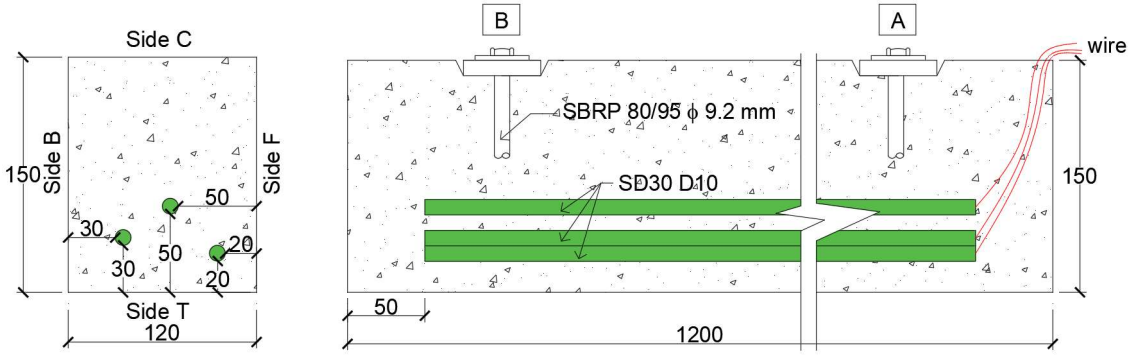

Cross-section Longitudinal section (unit in mm)

Fig. 5.1— Layout details of the RC beam

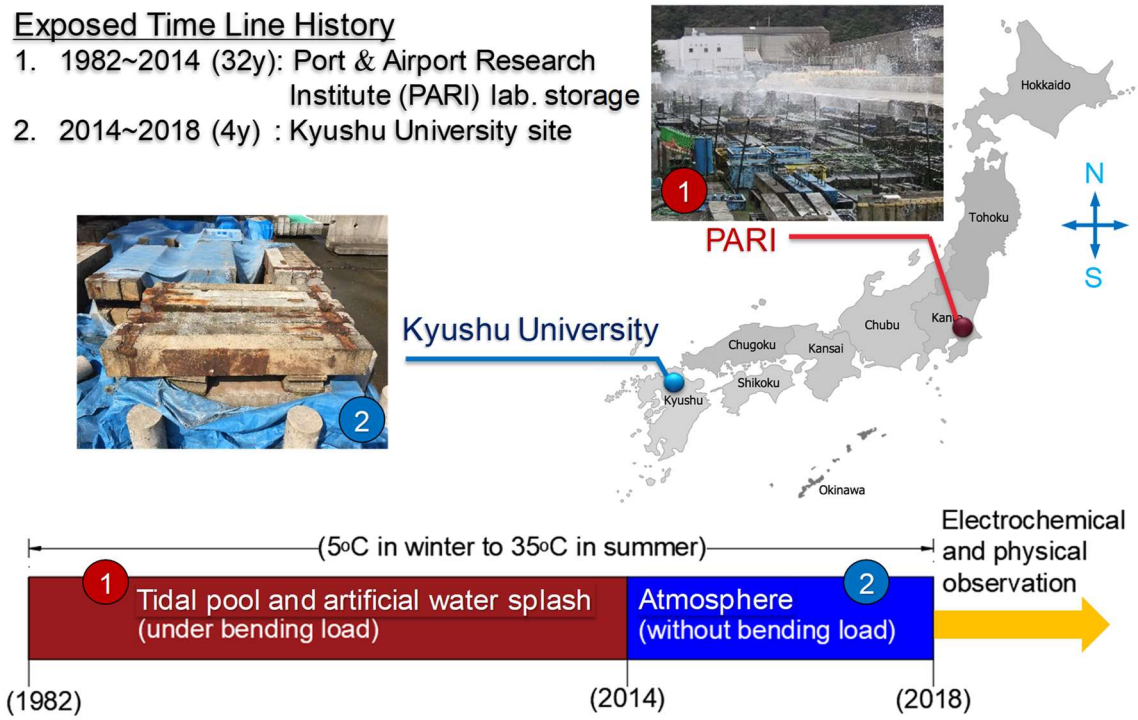

Fig. 5.2—Exposure condition

5.2.2 Experimental methods

(1) Visual observation-crack maps

For each side, crack maps are drawn, focusing on locations of longitudinal and transversal cracks due to corrosion cracking and service load, respectively. On these maps lengths, widths and depths of each referred crack are also indicated.

(2) Electrochemical analysis

For electrochemical evaluation of steel bars, half-cell potential (HCP), polarization curve, and oxygen permeability were measured in cover depths of 2, 3 and 5 cm. The HCP was measured by using the silver/silver chloride reference electrode (Ag/AgCl) after 30 min pre-wetting of beam surface. Then, the potential value was converted to the value against copper/copper sulfate reference electrode (CSE). The threshold limit of HCP is assumed to be -350 mV as per ASTM C 876-15 [5.8].

For polarization curve, the potential of the steel bar was swept to ±700mV from rest potential with a sweep rate of 50 mV/min by a potentiostat, and the current was recorded continuously. The maximum current from APC was a parameter to judge "grade of passivity" based on Otsuki [5.5] as shown in Fig. 2.6 and Table 2.5 in Chapter 2.

The constant current density (i_{lim}) over the steel bars at cover depth of 2, 3 and 5 cm were measured. The i_{lim} was measured by using a potentiostat. The potential of the steel bar was set to -1V and held constant then the current was recorded continuously. When measurements began, current was a maximum then gradually falling until reaching an almost constant value after kept in 24-hours. The rate of oxygen permeability was obtained from the i_{lim} using the following Eq. (5.1)

$$\frac{dQ}{dt} = \frac{-i_{lim}}{n.F} \tag{5.1}$$

where, dQ/dt is the oxygen permeability in mol/cm^2/s, i_{lim} is the constant current density in A/cm^2, n is the number of electrons (4) and F is Faradays constant (96,500 coulombs/mol).

(3) Carbonation and chloride analysis

The carbonation depth of the RC beam was evaluated after spraying 1% phenolphthalein solution on freshly cut or broken surfaces. Total and water-soluble chloride content, titration was measured at certain depths of specimens. Cylinder specimen was taken to measure chloride concentration by coring method. Then, specimens were cut in five layers from the surface of concrete through the depth with 1 cm thick for each layer and crushed into powder. The samples were powdered by a vibrating mill. Total chloride and water-soluble chloride concentration were measured based on JIS A1154 and JCI-SC4, respectively.

(4) Quality of concrete

For the quality of concrete, compressive strength, electrical resistivity and porosity were measured. The compressive strength of concrete was measured based on JIS A1108. Cylinder specimens in size of ϕ 5 x 10 cm were taken by coring method. The average of five-cylinder specimens was determined for each beam. The electrical resistivity was measured by using Wenner probe. The resistivity of concrete from the average of three times measurement was determined. The porosity of concrete was measured at depths of 6 cm from the surface. Mortar pieces were cut into five mm-thick cube slice samples. The sample was immersed in acetone for 15 min to stop the hydration of cement and then dried in the vacuum desiccator for two days. Then the porosity of concrete was evaluated by mercury intrusion porosimeter (MIP) with the pressure of 33,000 psi (227 MPa), and the surface tension and contact angle of mercury were 485 dynes/cm and 130^{o}, respectively.

(5) Physical analysis

For physical analysis, the corroded area, tensile test, and cross-sectional loss of the steel bars embedded at different cover depths were measured. Corroded area of steel bar was measured after completely removed from the RC beam specimen. The corroded area over the steel bars was traced over a transparent paper and then corroded area of steel bar was calculated using software ImageJ v1.49.

The extracted corroded reinforcing bars were cleaned by immersion in an aqueous solution of diammonium hydrogen citrate ($C_6H_{14}N_2O_7$) with a concentration of 10% for 24h. After the steel bars had been cleaned, it was found that corrosion around them was quite irregular and remain many corrosion pits at the and part of steel bars, but in middle part was almost clean. Because of the non-uniform distribution of corrosion, the steel bars were cut into short pieces about 0,5 cm. The short pieces were weighed on a balance with an accuracy of 0.0001 g and the cross-sectional loss was calculated using Eq. (5.2). The original mass of the short pieces could be calculated from Eq. (5.3).

$$\Delta A_s = \frac{m_0 - m}{m_0} . A_s \quad (5.2)$$

$$m_o = \rho A_s L \quad (5.3)$$

Where: ρ is the density of the steel bar in g/cm^3 (7.85); L is the length of each piece of the steel bars in mm, measured with a vernier caliper; ΔAs is the average cross-section loss of the small piece of bar in mm^2; As is the nominal cross-section of the steel bars in mm^2; m is the residual mass of the small pieces of the corroded bars in g; and m_0 g is the nominal mass of the steel bars in g.

For tensile test, a 500 kN capacity machine (SHIMADZU) was used to carry out the tensile test, with loading rate of 0.5 kN/s as shown in Fig. 5.3. Tensile test was conducted in order to understand the effect of corrosion on the mechanical properties of the steel bars. The tensile bars are steel with 1 cm of diameter. The positions of sample for the tensile test are in middle part of steel bar. The base length of each steel bar was 60 cm. The tensile test was conducted according to the JIS Z 2241-1998 standard at the tensile test machines. Two strain gauge installed in middle of steel bar to measure the strain. The base length L was determined as ten times the diameter of the bar. Further, the effective length L_o was determined as eight times the diameter of the bar. The effective length was detached with two small notches in the steel bar surface, made using nails and a hammer. By using Vernier calipers, the length between the two points indicated by notches was measured. The load and elongation data were recorded using a computerized data acquisition system at pre-determined load intervals up to failure of the specimen. The data obtained were utilized to plot stress-strain diagrams for each of the specimen tested. Using the stress-strain diagrams, yield strength, ultimate strength of the steel bars was compared. The tensile properties of the bar were calculated from the results of the tensile test. The effective length L_o' was measured again to determine the elongation.

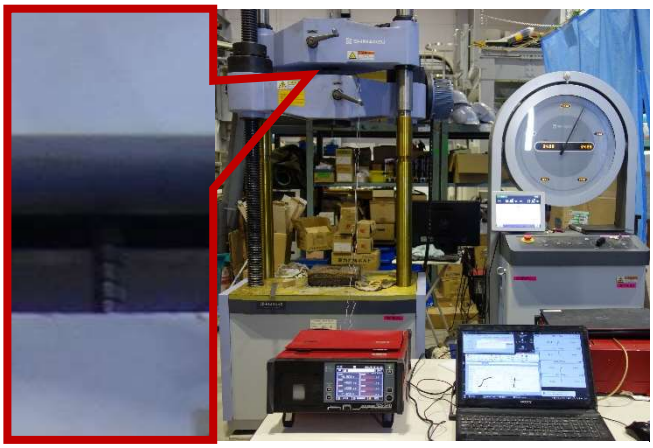

Fig. 5.3—Uniaxial tensile tests of steel bars

5.3 Result and discussion

5.3.1 Visual observation-crack maps

Visual observation enables to describe a global overview of the damage state of the RC beam after long-term exposure. The cracking map of all RC beams after 36-years is shown in Figs. 5.4-5.6. In these figures, some transversal and longitudinal cracks due to corrosion attack beside bending load can be mainly observed on the beams. Visibly, cracks induced corrosion

occurred longitudinally along the steel bar and parallel to steel bar on the end part (point A and B) of beam. As well as transverse cracks from introduced bending load were generated from tension side of the beam. Cracking had generalized along the tensile area and cracks appeared in the end part of the beams. On the contrary, compressive area showed no crack. In addition, the crack depth value already through the concrete cover. According to the appearance of beam, the deterioration degree is determined and presented in Table 5.2. Table 5.2 was constructed based on criteria for the diagnosis of deterioration degree, as presented in Table 2.2 Chapter 2.

Table 5.2—Criteria for the diagnosis of deterioration degree

Specimen	max crack depth (mm)		max crack width (mm)		Evaluation items			Det. degree
	M	A/B	M	A/B	Corrosion (1)	Cracking (2)	Spalling (3)	(1+2+3)
65-L1-SW-T	15	55	0.15	1.50	4	4	3	11
45-L1-SW-T	15	30	0.10	0.50	3	3	2	8
55-L2-SW-T	15	40	0.10	0.40	5	4	2	11
55-L3-SW-T	17	50	0.35	1.20	5	4	3	12
65-L1-SW-S	17	58	0.30	0.45	5	4	2	11
55-L1-SW-S	15	0	0.20	0.00	5	4	2	11
45-L1-SW-S	17	68	0.15	0.40	5	4	2	11
65-L1-TW-T	30	80	0.15	1.50	5	4	3	12
55-L1-TW-T	15	53	0.04	0.35	4	3	3	10
55-L3-TW-T	15	45	0.40	0.55	5	4	3	12

For effect of water mixing, it was observed that tap water mixing (55-L3-TW-T and 65-L1-TW-T) appears much more rough surface due to environmental condition and some spots of rust stains appear at area of corrosion-induced cracks compared to seawater mixing (55-L3-SW-T and 65-L1-SW-T) as shown in Fig. 5.7. The maximum crack width of seawater mixing for 55-L3-SW-T (1.2 mm) was larger than tap water mixing for 55-L3-TW-T (0.5 mm). However, for 65-L1-TW-T and 65-L1-SW-T, the maximum crack width of seawater was same with tap water mixing (1.5 mm). In addition, diagnosis of deterioration degree from visual observation of seawater mixing for 55-L3-SW-T and 65-L1-SW-T (11) was smaller than tap water mixing for 55-L3-TW-T and 65-L1-TW-T (12).

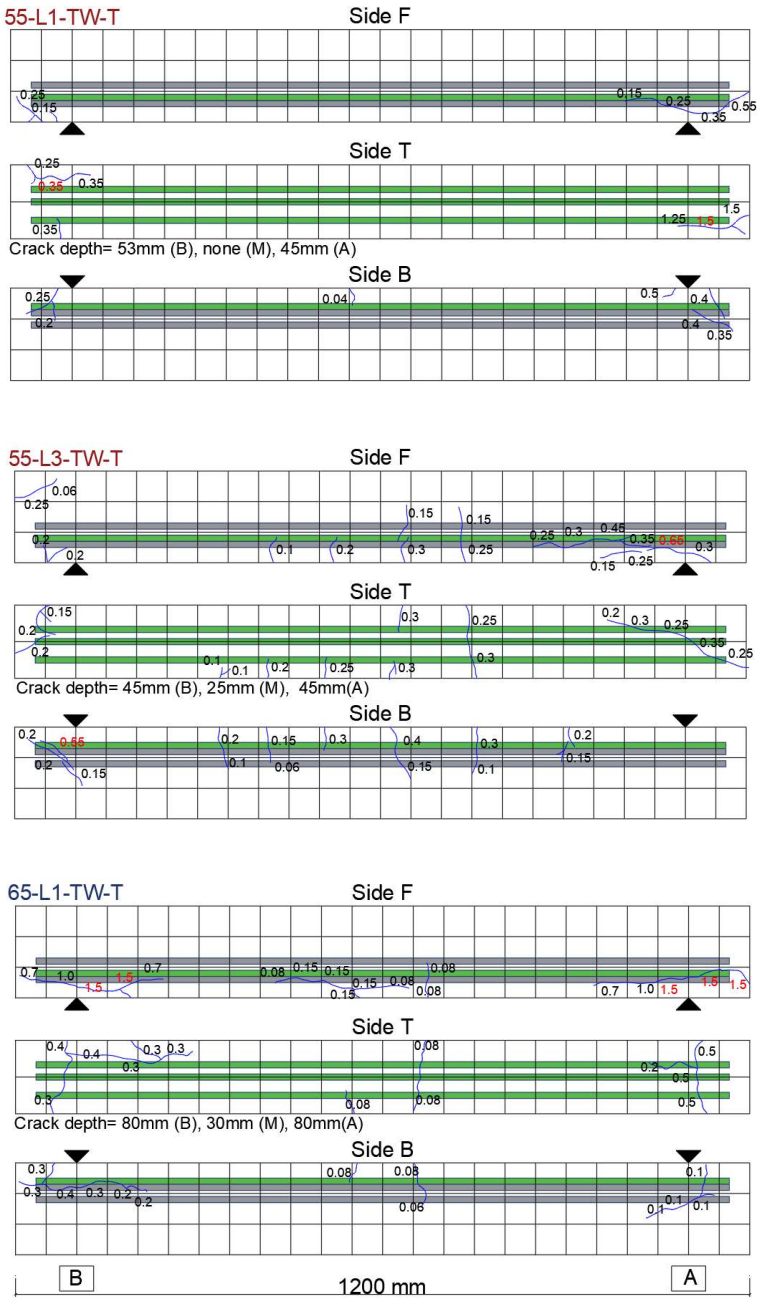

Fig. 5.4—Overview of the three sides of crack maps of 55-L1-TW-T, 55-L3-TW-T, and 65-L1-TW-T

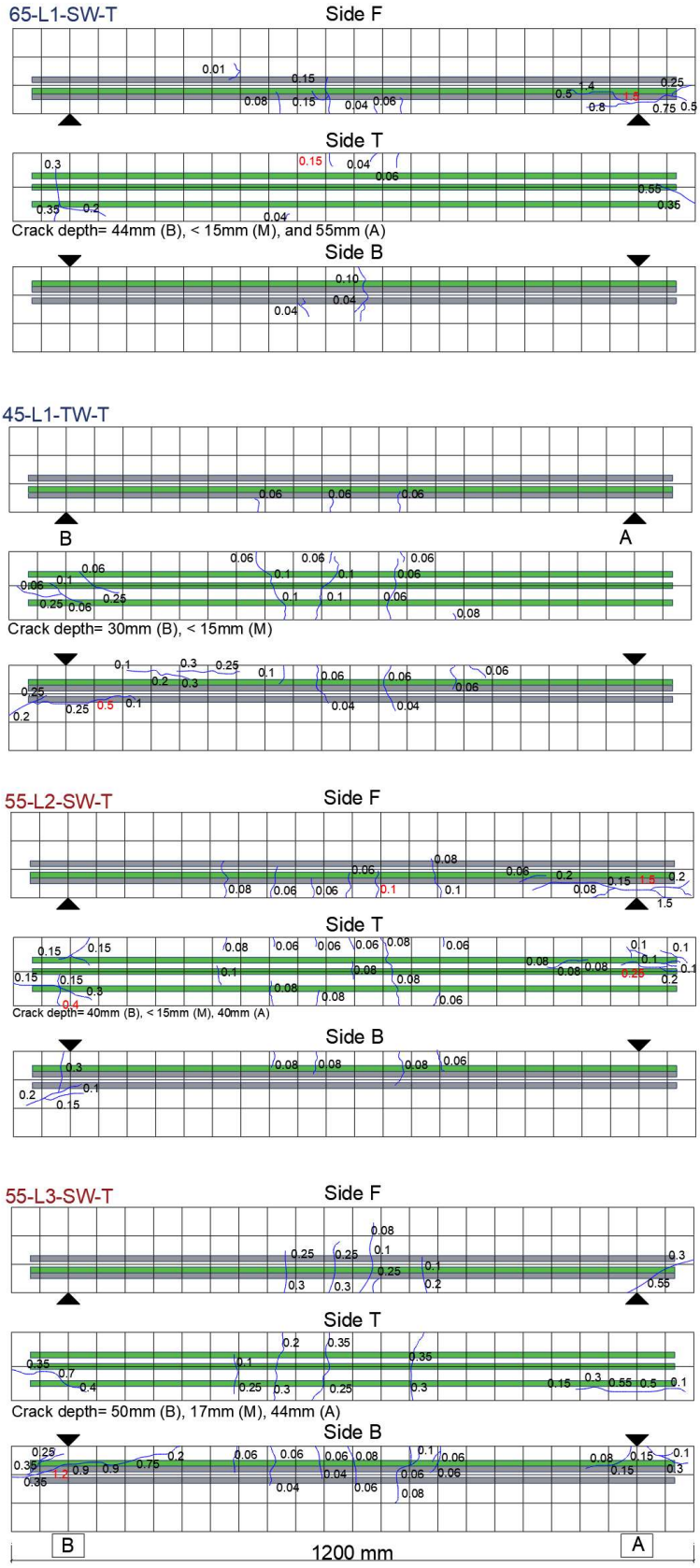

Fig. 5.5—Overview of the three sides of crack maps of 65-L1-SW-T, 45-L1-SW-T, 55-L2-SW-T,55-L3-SW-T

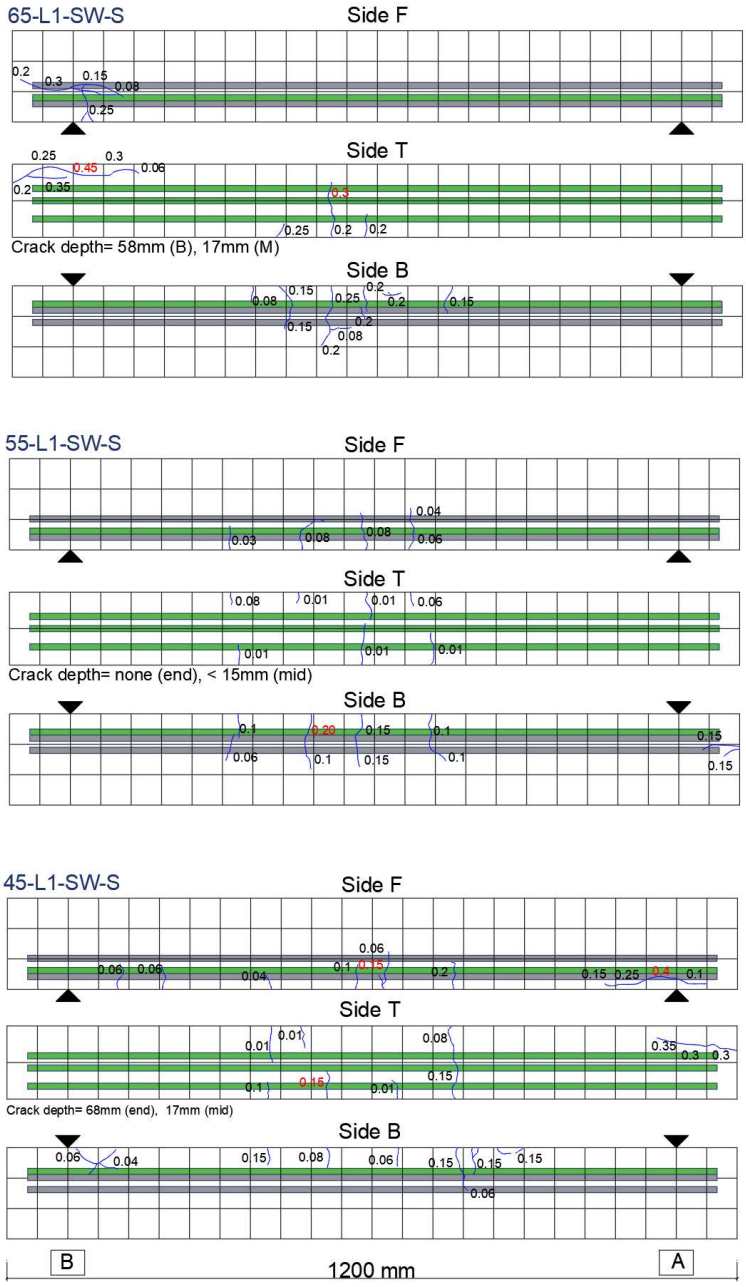

Fig. 5.6—Overview of the three sides of crack maps of 65-L1-SW-S, 55-L1-SW-S, and 45-L1-SW-S

For effect exposure condition, it was observed that both specimens in tidal zone (65-L1-SW-T and 45-L1-SW-T) showed larger crack compared to splash zone (65-L1-SW-S and 45-L1-SW-S). In contrary from diagnosis of deterioration degree, the total deterioration degree for W/C=0.4 in 45-L1-SW-T (8) was small than 45-L1-SW-S (11). While, in W/C=0.6 for 65-L1-SW-T and 65-L1-SW-S the total deterioration degree was same (11). This indicated that effect of W/C has effectiveness for tidal zone, even have larger crack width.

For effect of bending load for seawater group (55-L2-SW-T and 55-L3-SW-T) and tap water group (55-L1-TW-T and 55-L3-TW-T), it was observed general phenomena that as increasing bending load, crack width and the total deterioration degree increase also.

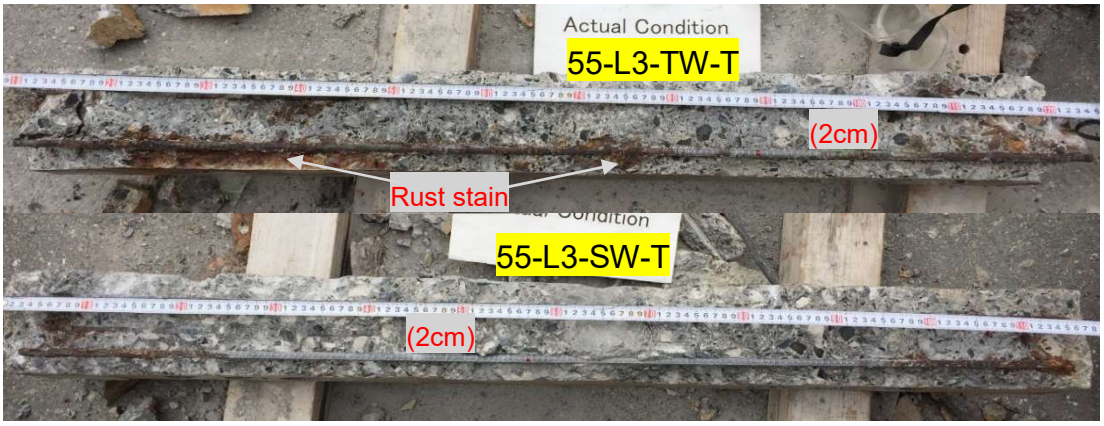

Fig. 5.7—Appearance of RC beam 55-L3-TW-T and 55-L3-SW-T

5.3.2 Electrochemical measurements

(1) Half-cell potential

The HCP of the steel bars embedded at different cover depths are shown in Fig. 5.8. From Fig. 5.8a, negative potentials were observed for tap water mixing in both groups (55-L3-TW-T(2,3,5) and 65-L1-TW-T(2,3,5)) for all cases concrete cover, and the potential value was more negative than -350 mV and categorized 90% corrosion. The same tendencies observed in 55-L3-SW-T(2) and 65-L1-SW-T(2), the potential values of seawater mixing showed very negative value than tap water mixing and categorized 90% corrosion. In contrary, in 55-L3-SW-T(3,5) and 65-L1-SW-T(3,5), the potential of seawater mixing became a positive value and categorized uncertainly in the middle part (Point M), however, in end part (Point A and B) the potential became negative value and categorized 90% corrosion. The possible reason may be due to the number, width, and depth of crack at the end part of beam. Importantly, concrete cover with 2 cm has influences on the HCP value much more than mixing water. However, concrete cover for 3 and 5 cm showed the HCP value for seawater superior or more positive to tap water mixing. Implies that after concrete cover with 3 and 5 cm, mixing water influences much more than concrete cover on HCP value.

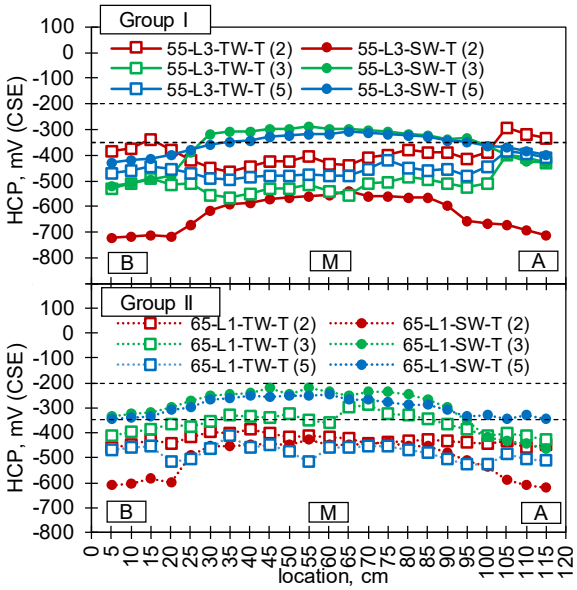

(a) Effect of water mixing

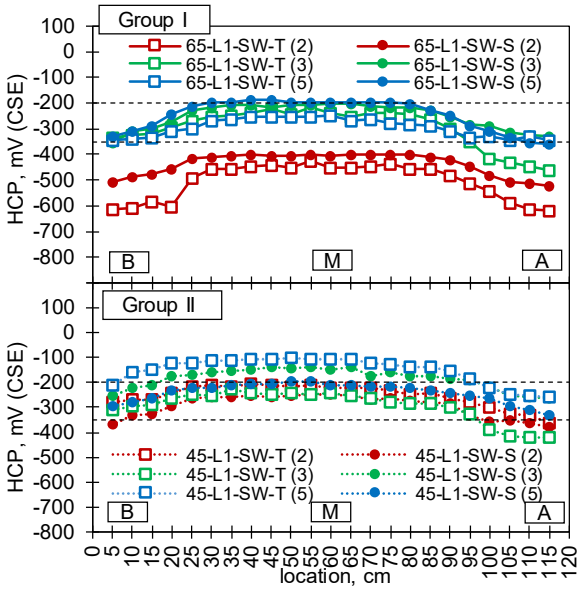

(b) Effect of exposure condition

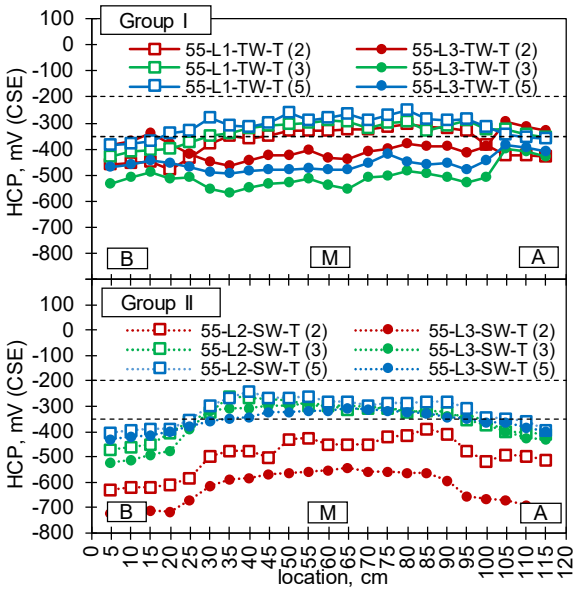

(c) Effect of bending load

Fig. 5.8—Half-cell potential

From Fig. 5.8b, the potential value in Group I for 65-L1-SW-T(3,5) is slightly higher than 65-L1-SW-S(3,5) in all cases of cover depth, but the potential value in Group II for 45-L1-SW-S(2,3,5) is higher than 45-L1-SW-T(2,3,5) in all cases of cover depth and still categorized 90% no corrosion. Only in W/C=0.6 with cover 2 cm (65-L1-SW-T(2) and 65-L1-SW-S(2)), the potential value was less than -350 mV and categorized in 90% corrosion. Further, tidal zone much more affected the HCP value than splash zone. Also, it can be

observed that the thick concrete covers the positive on HCP will be. From Fig. 5.8c, in the tap water group, as increasing bending load, the potential value of steel bar also increases. On the contrary in seawater group, only 55-L2-SW-T(2) and 55-L3-SW-T(2), the potential in more negative value more than -350mV, but for 55-L2-SW-T(3,5) and 55-L3-SW-T(3,5) even bending load increased the potential still more positive than -350mV. Implies, in the existing of premature crack, seawater mixing more reliable than tap water mixing. However, concrete cover with cover depth 3 and 5 cm was required.

(2) Grade of passivity

The polarization curve of all specimen with steel bars embedded at different cover depths is shown in Fig. 5.9. From Fig. 5.9a for APC curve, tap water mixing of 55-L3-TW-T(2,3,5) and 65-L1-TW-T(2,3,5) showed higher current density and indicated higher corrosion activity of the steel bars. In contrast, the ACP of seawater mixing of 55-L3-SW-T(2,3,5) and 65-L1-SW-T(2,3,5) showed lower current density. The passivity grades of all tap water specimen and seawater mixing specimen were categorized in Grade 2 and Grade 3, respectively, for all concrete cover. A similar trend was found from CPC, seawater mixing of both groups showed lower current density, which indicated that oxygen diffusion was smaller. The seawater mixing showed better passivity compared to tap water mixing. A better grade of passivity for the steel bars embedded in seawater mixing indicates less corrosion activity, and this corresponds to HCP value. Corrosion activity broke the passivity film of the steel bar and released much more electron. This mechanism leads to a very negative value of HCP value. From Fig. 5.9b for the effect exposure condition, both Group I (65-L1-SW-T(2,3,5) and 65-L1-TW-T(2,3,5)) and Group II (45-L1-SW-T(2,3,5) and 45-L1-TW-T(2,3,5)) showed same grade passivity which categorized in Grade 3. But even have same passivity, it was found that the maximum current density from 600 mV (APC) of splash zone was higher than tidal zone. Same tendency from CPC showed that splash zone has higher current compared to tidal zone in all cases of concrete cover and both group, which indicated that oxygen diffusion was higher. From Fig. 5.9c for effect bending load, in Group I-tapwater mixing (55-L1-TW-T(2,3,5) and 55-L3-TW-T(2,3,5)), it was found that higher bending load from 2.66 kN-m to 7.97 kN-m showed higher current density which the grade passivity of 55-L3-TW-T(2,3,5) and 55-L3-TW-T(2,3,5) was categorized in Grade 2. In contrary, for Group II-seawater mixing (55-L2-SW-T(2,3,5) and 55-L3-SW-T(2,3,5)), it was found even the bending load increased from 5.32 kN-m to 7.97 kN-m, the grade passivity both specimens were same that categorized into Grade 3. Implies that better performance of seawater mixing was found even the bending load

increased into 7.97 kN-m, and the performance tap water mixing was decreased if the bending load increased into 7.97 kN-m.

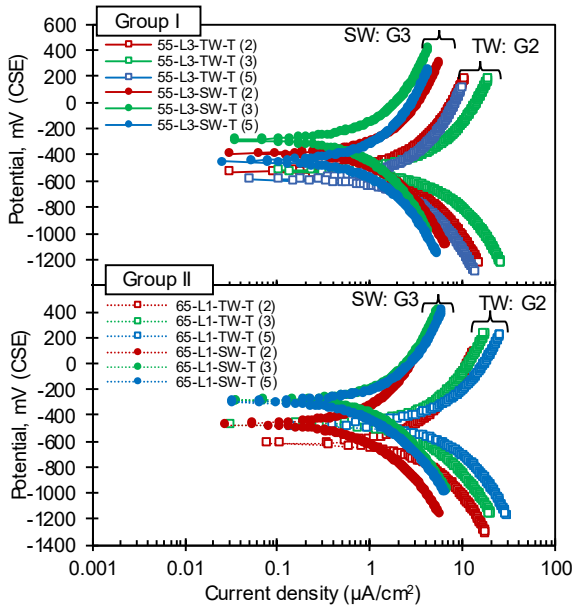

(a)Effect of water mixing

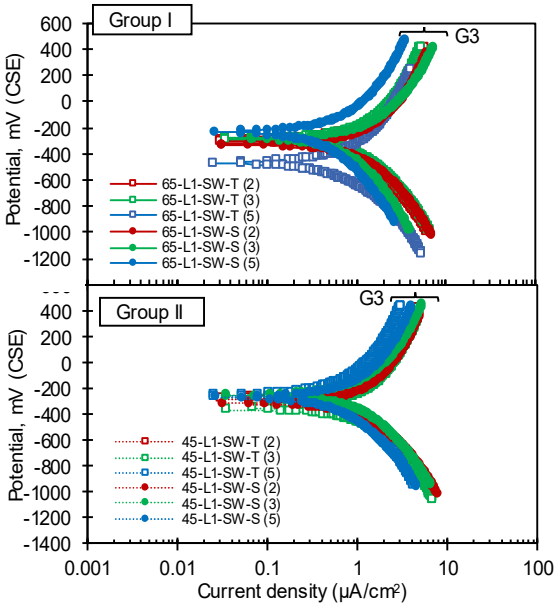

(b)Effect of exposure condition

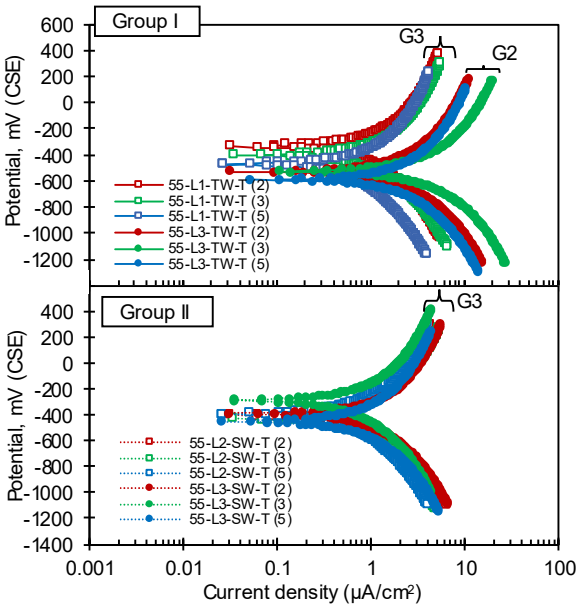

(c)Effect of bending load

Fig. 5.9—Grade of passivity

Table 5.3—Current density of polarization curve

Specimen code	Cover depth,	Anodic current,		Grade passivity	Cathodic current, (maximum)
		(200mV)	(600mV)		
65-L1-SW-T	2	1.38	3.58	3	5.52
	3	1.97	5.19	3	6.30
	5	1.91	4.67	3	6.72
45-L1-SW-T	2	1.59	3.85	3	6.59
	3	1.01	2.68	3	4.32
	5	1.63	4.10	3	6.97
55-L2-SW-T	2	1.59	3.85	3	6.59
	3	1.27	3.58	3	4.14
	5	1.56	4.77	3	5.02
55-L3-SW-T	2	1.97	4.97	3	6.72
	3	1.46	3.79	3	5.41
	5	1.45	3.86	3	4.39
65-L1-SW-S	2	1.94	5.28	3	7.10
	3	1.09	3.02	3	2.76
	5	2.16	6.26	3	4.00
45-L1-SW-S	2	1.78	4.39	3	7.67
	3	1.33	3.45	3	4.62
	5	1.66	4.49	3	6.54
65-L1-TW-T	2	4.08	11.49	2	18.12
	3	7.50	22.14	2	30.24
	5	5.70	15.44	2	20.40
55-L1-TW-T	2	1.97	4.71	2	5.54
	3	1.54	3.79	2	4.06
	5	2.05	4.99	2	6.72
55-L3-TW-T	2	3.50	9.49	2	15.69
	3	3.32	8.97	2	14.22
	5	6.08	17.15	2	27.52

(3) Oxygen permeability

Oxygen permeability at different cover depths for all specimen is estimated from the measured i_{lim}. The results are shown in Fig. 5.10. From these figures, it was clearly seen that the oxygen permeability became low as increasing cover depth. For Fig. 5.10a, oxygen permeability was lower in seawater mixing than tap water mixing in all cover depth (both group). These results support that seawater mixing is effective for controlling the oxygen permeability through the concrete cover, therefore, retarding both anodic and cathodic reactions of steel bars in concrete.

For Fig. 5.10b, the oxygen permeability value of splash zone in 65-L1-SW-T(2,3,5) and 45-L1-SW-S(3,5) was slightly higher than tidal zone in 65-L1-SW-T(2,3,5) and 45-L1-SW-T(3,5). But only in cover depth 2 cm of splash zone (45-L1-SW-S(2), the oxygen permeability of was lower than tidal zone (45-L1-SW-T(2). Probably in the tidal zone, concrete is quite wet, then during drying period the absorbed water contains O_2 more deeper into the concrete particularly in 2 cm of cover depth. This data corresponds from APC and CPC data.

For Fig. 5.10c, it was found higher bending load indicated higher oxygen permeability in all cover depth (both group: 55-L1-TW-T(2,3,5), 55-L3-TW-T(2,3,5), 55-L2-SW-T(2,3,5), 55-L3-SW-T(2,3,5)). Interestingly, when the bending load increased for tap water mixing (55-L1-TW-T(2,3,5) and 55-L3-TW-T(2,3,5)) from 2.22 kN-m to 7.97 kN-m, the oxygen supply also increased until 220%, 138% and 189% in cover depth 2, 3, 5 cm, respectively. But for seawater mixing (55-L1-TW-T(2,3,5) and 55-L3-TW-T(2,3,5)), when bending load increased from 5.23 kN-m to 7.97 kN-m, the oxygen increased slightly lower about 48%, 47% and 8% in cover depth 2, 3, 5 cm, respectively.

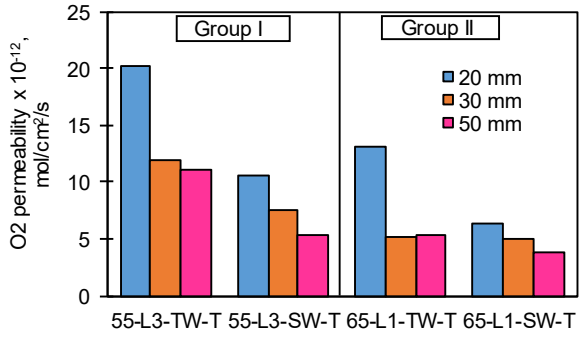

(a)Effect of water mixing

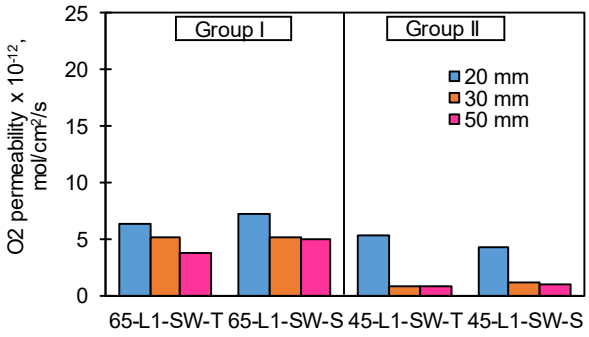

(b)Effect of exposure condition

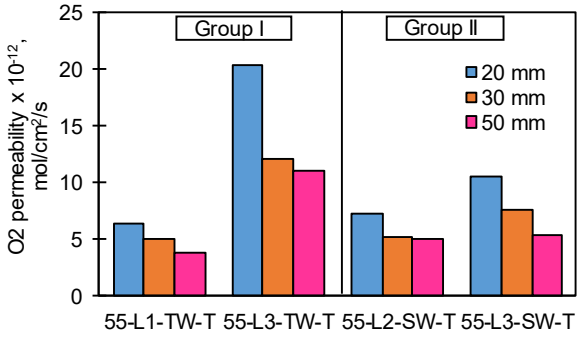

(c)Effect of bending load

Fig. 5.10—Oxygen permeability

5.3.3 Carbonation depth and chloride ingress

The carbonation depth was almost negligible for all RC beams. Only in a few spots, maximum depth is 1-1.5 mm, and it was limited to the surface only. Thus, the steel bars in concrete located at 2, 3, 5 cm of cover depths were free from carbonation-induced corrosion, and corrosion of steel bar must be induced by chloride ingress.

The total chloride, water-soluble chloride, and bond chloride in concrete are summarized in Table 5.4. Chloride ingress pattern for tall specimen from surface to half part was same, which indicate that chloride induces already saturated after long-term exposure. At

the steel bars depth all specimen, the measured values of water-soluble chloride (from minimum value 4.44 kg/m^3 to maximum value 13.01 kg/m^3) exceed the threshold limit of 1.2 kg/m^3 generally pointed out in JSCE. It is generally assumed that for higher chloride content, the corrosion can be initiated at the steel bar surface. These results explain that active corrosion due to chloride ingress can take place at steel bar surface. Also, this is probably due to mechanical damage of the tensile area due to bending load, which leads to a significant increase in the chloride diffusion coefficient.

Table 5.4—Total chloride, water-soluble chloride and bound chloride concentration

Specimen	Cover depth, cm	Total chloride, kg/m^3	Water-soluble chloride, kg/m^3	Bound chloride, kg/m^3
65-L1-SW-T	2	10.31	9.88	0.43
	3	10.70	8.65	2.05
	5	11.32	9.20	2.12
45-L1-SW-T	2	6.46	4.44	2.02
	3	7.32	5.34	1.98
	5	5.75	4.53	1.22
55-L2-SW-T	2	7.09	7.02	0.07
	3	7.48	5.55	1.93
	5	7.22	5.22	2.00
55-L3-SW-T	2	8.42	8.35	0.06
	3	10.01	7.92	2.09
	5	9.00	7.07	1.93
65-L1-SW-S	2	15.41	11.89	3.53
	3	15.18	11.23	3.95
	5	16.20	13.01	3.19
55-L1-SW-S	2	11.52	8.62	2.90
	3	11.74	9.59	2.15
	5	12.67	10.45	2.22
45-L1-SW-S	2	9.53	7.23	2.29
	3	10.64	8.25	2.39
	5	11.29	8.92	2.37
65-L1-TW-T	2	8.06	7.19	0.87
	3	9.02	7.60	1.42
	5	9.65	8.24	1.41
55-L1-TW-T	2	11.10	10.48	0.62
	3	9.57	8.46	1.11
	5	9.81	8.38	1.43
55-L3-TW-T	2	12.67	12.15	0.52
	3	13.10	12.06	1.04
	5	12.40	11.23	1.16

From Table 5.4, for effect mixing water, the amount of water-soluble chloride for 55-L3-SW-T(2,3,5) was lower than 55-L3-TW-T(2,3,5). However, the amount of water-soluble chloride for 65-L1-SW-T(2,3,5) was higher than 65-L1-TW-T(2,3,5), probably due to the initial chloride from seawater. In addition, the bound chloride at cover depth 3 and 5 cm was higher for seawater mixing (55-L3-SW-T and 65-L1-SW-T) compared to tap water mixing (55-L3-TW-T and 65-L1-TW-T), and it was almost 2 kg/m^3 as shown in Table 5.4. Ismail et

al. [5.10] reported that after the chloride ingress, some chlorides could be attached to the pore walls or cement products and react with them, which is called chloride binding. The chloride binding is generally classified as physical and chemical binding. Physical binding occurs when chloride ions transport through the C-S-H type gel surface, and occurs due to electrostatic or Van der Waals forces between chloride and the gel [5.10]. Chemical binding can be defined as chloride ions interact with C-S-H gel by several mechanisms such as chemisorption into the C-S-H layers, in C-S-H spaces, or becoming bound in the lattice or ion exchange sites of C-S-H gel. These bound chloride ions can give rise to an altered matrix microstructure. The chemically bound chlorides in the cementitious materials at the beginning react with the main OPC component, C_3A [5.11].

For effect of exposure condition, the total chloride and water-soluble chloride for splash zone (65-L1-SW-S(2,3,5) and 45-L1-SW-S(2,3,5)) were higher than tidal zone (65-L1-SW-T(2,3,5) and 45-L1-SW-T(2,3,5)). And for effect of bending load (55-L1-TW-T(2,3,5) and 55-L3-TW-T(2,3,5); 55-L2-SW-T(2,3,5) and 55-L3-SW-T(2,3,5)), the amount of total chloride and water-soluble chloride was increased as an increased bending load.

5.3.4 Quality of concrete

Compressive strength, UPV, electrical resistance and total pore volume of concrete are summarized in Table 5.5. For the effect of mixing water after 36-years of exposure, seawater mixing (55-L3-SW-T and 65-L1-SW-T) showed higher strength, denser and higher electrical resistance than tap water mixing (55-L3-TW-T and 65-L1-TW-T). Interestingly, the strength of seawater mixing (55-L3-SW-T and 65-L1-SW-T) showed 10 MPa larger than tap water mixing (55-L3-TW-T and 65-L1-TW-T). The seawater/tap water strength ratio was 1.2 at long-term exposure. This tendency was also reported by Fukute and Hamada [5.7]. Adiwijaya [5.12] reported the compressive strength of seawater was higher than tapwater mixing from at 28-days and 25-years, but the incremental of compressive strength from an early age up to 25-years of tap water (45%) was higher than seawater mixing (37%).

For the effect of exposure condition, tidal zone (65-L1-SW-T and 45-L1-SW-T) showed higher strength, denser and higher electrical resistance than splash zone (65-L1-SW-S and 45-L1-SW-S). Implies that the tidal zone had a good impact on the quality of concrete when specimen exposed to the tidal zone. One possible reason that tidal zone during drying time promotes the concrete absorbed more faster moisture into the concrete. This ensures concrete through the depth hydration process take place. As the longer time exposed, then assist in completing the hydration process. Completed of the hydration process, supported the

improvement of concrete quality. And for effect of bending load, for tap water group (55-L1-TW-T and 55-L3-TW-T) and seawater group (55-L2-SW-T and 55-L3-SW-T), the quality of concrete was decreased as increasing bending load, which much more crack appears on concrete tension surface.

Table 5.5—Summary of quality of concrete

Specimen	Compressive strength, MPa	UPV, km/s	Porosity, g/cm^3	Electrical resistivity, kΩ.cm
65-L1-SW-T	60.09	5.04	0.0390	27.90
45-L1-SW-T	66.62	5.17	0.0243	36.83
55-L2-SW-T	60.81	5.17	0.0406	37.00
55-L3-SW-T	59.10	5.10	0.0360	35.22
65-L1-SW-S	51.50	4.97	0.0426	28.37
55-L1-SW-S	59.63	5.08	0.0331	33.00
45-L1-SW-S	60.87	5.13	0.0327	37.67
65-L1-TW-T	50.21	4.60	0.0589	21.60
55-L1-TW-T	50.62	5.17	0.0499	21.50
55-L3-TW-T	49.36	4.83	0.0380	17.39

Mean cumulative pore volume and incremental pore volume of concrete mixed with tap water and seawater are shown in Fig. 5.11. Interestingly, for effect of mixing water, it was found that pore distribution of seawater mixing (55-L3-SW-T and 65-L1-SW-T) was denser and finer compared than tap water mixing (55-L3-TW-T and 65-L1-TW-T). In addition, tap water mixing 55-L3-TW-T and 65-L1-TW-T) had second peak in incremental pore volume, and for seawater mixing (55-L3-SW-T and 65-L1-SW-T) it was almost smooth. These results are due to higher concrete resistance, higher strength, and chloride in seawater compounds. And same tendencies were found in cement paste at 28-days of porosity, the seawater mixing (cement paste-SW) also showed more denser than tap water mixing (cement paste-TW). Midgley et al. [5.13] reported that for seawater mixing, the transformation of the hydration phase from CAH_{10} to C_3AH_6 had not occurred. By using the NaCl solution as the Cl^- source to study the pore size distribution of cement paste under chloride ingress, it was found that the intrusion of chloride ion leads to more fine pores and less big pores. As soon as the reaction begins, the binding between the chloride ion and cement product can modify the shape of concrete microstructure. Higher concrete resistance of seawater mixing leads to the high resistivity against chloride-induced corrosion. Considerable delay of corrosion reaction which leads to the increase of steel bar volume. Inner pressure as the result of increment steel bar volume is notable on crack appearance. This corrosion activity correlated in Fig. 5.3 which showed seawater mixing (55-L3-SW-T and 65-L1-SW-T) has small number of cracks. For effect of exposure condition, it was found that pore distribution of tidal zone (65-L1-SW-T

and 45-L1-SW-T) and splash zone (65-L1-SW-S and 45-L1-SW-S) had similar tendencies which denser and finer pore. However, splash zone (65-L1-SW-S and 45-L1-SW-S) had slight second peak in incremental pore volume than tidal zone (65-L1-SW-T and 45-L1-SW-T).

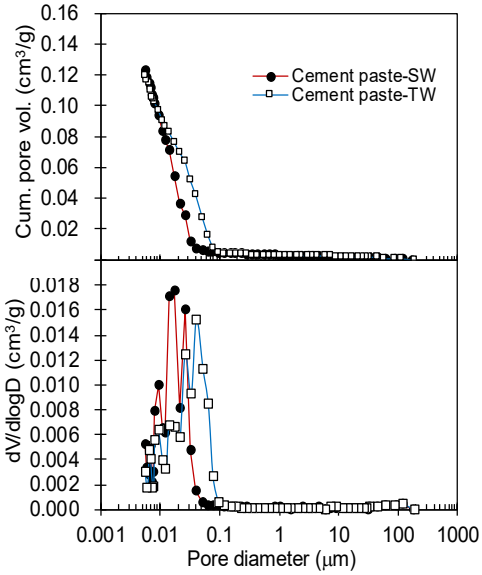

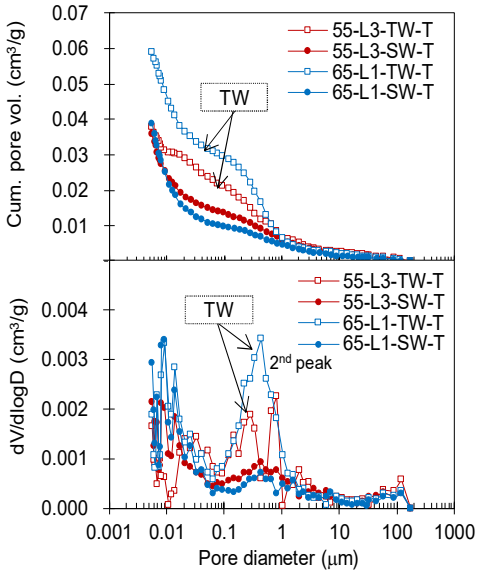

(a)Effect of water mixing

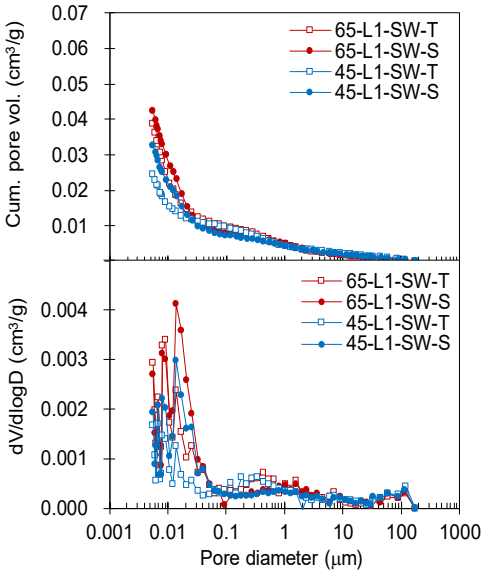

(b)Effect of exposure condition

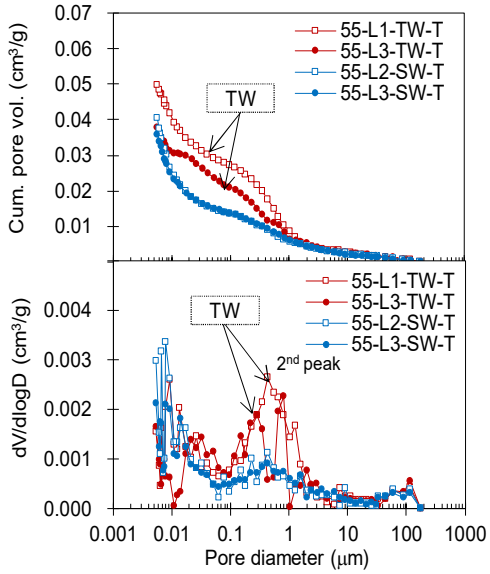

(c)Effect of bending load

Fig. 5.11—Cumulative pore volume and incremental pore volume

For the effect of bending load for tap water group (55-L1-TW-T and 55-L3-TW-T), it was found that as increasing bending load the pore distribution became harmful and both specimens had second peak in incremental pore volume. In contrary, in seawater group (55-L2-SW-T and 55-L3-SW-T), no significant difference was found in pore distribution when the bending load increase and incremental pore volume was almost smooth. Implies that seawater was effect on denser and finer the concrete.

5.3.5 Surface corroded area

Fig. 5.12 illustrates the localized corrosion on a length of steel bar after removing the corrosion products which show the detail of pitting corrosion and general corrosion. The results of the total surface corroded area of each steel bar are shown in Fig. 5.13. In each graph, two groups were determined. From the appearance of steel bar, in general information, the rust of all steel bar was concentrated and dense only in the end part of beam (Point A/B) in all cases of cover depth. The reason for the more corrosion appeared at the end part may be due to that the chloride ingress much more at end part of beam. Therefore, the most damaged zones were close to the position at the maximum cracks width and depth. In addition, the surface corroded area depend on the thickness of cover depths as shown in Fig. 5.13.

a.no corrosion b. pitting c. generates and pitting

Fig. 5.12—View of surface corroded steel bar after removing corrosion products

Interestingly, from data of total corroded area in Fig. 5.13a, it could be noted that the total corroded area for seawater mixing (55-L3-SW-T(2,5) and 65-L1-SW-T(2,3,5)) was almost half of tap water mixing (55-L3-TW-T(2,5) and 65-L1-TW-T(2,3,5)), except for 55-L3-SW-T(3) and 55-L3-TW-T(3), which had almost same total corroded area value. The result indicated that seawater mixing assists for better degree of passivity as discussed previously in electrical measurements. The result leads to understanding that seawater mixing has high resistivity against chloride-induced corrosion. Further, the result showed a strong correlation on crack appearance in Fig. 5.3 and justified by the actual corroded area that seawater mixing had lower corrosion activity. The possible reason why seawater mixing showed smaller corroded area than tap water mixing is the corrosion rate for seawater mixing was controlled due to the lower chloride ingress, as well as lower oxygen permeability, with higher concrete resistance.

From data of total corroded area in Fig. 5.13b, for splash zone in Group I in all cases of cover depth (65-L1-SW-S(2,3,5)) and Group II for 45-L1-SW-S(2) was higher than tidal zone. But in Group II for 45-L1-SW-S(3,5) are slightly higher than splash zone. The result described that in high W/C of 0.65, splash zone more severe. Implies that water to cement ratio affects corrosion much more than exposure condition with necessary certain depth. In

addition, 5 cm cover depth has reliable for the severe environment such tidal and splash zone.

From data of total corroded area in Fig. 5.13c, in Group I for 55-L1-TW-T(2,3) was almost 10% higher than 55-L3-TW-T(2,3). The result was out of the expectation that the increasing of load would increase the corrosion rate. This because in the end part of beam 55-L1-TW-T(2,3) had larger crack width (1.5 mm) and the crack already thought to at 4.5 cm as shown in Fig.5.3. In contrary, in Group I with cover depth 5 cm (55-L1-TW-T(5), 55-L3-TW-T(5)) and Group II in all cases of cover depth (55-L2-SW-T(2,3,5), 55-L3-SW-T(2,3,5)), the tendency is according expectations as usual that as increasing bending load, increase total corroded area. From this data, the effect of seawater to bending load had the effectiveness that even have higher bending load, the total corroded area was lower2 times that tap water mixing.

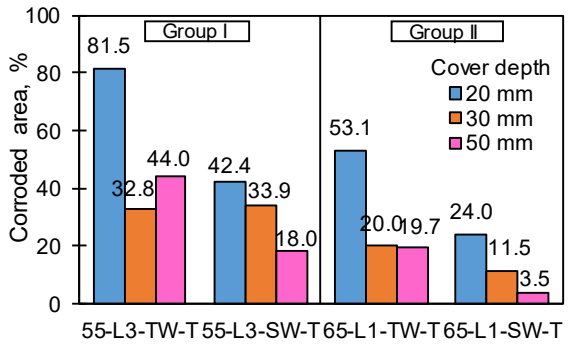

(a) effect of water mixing

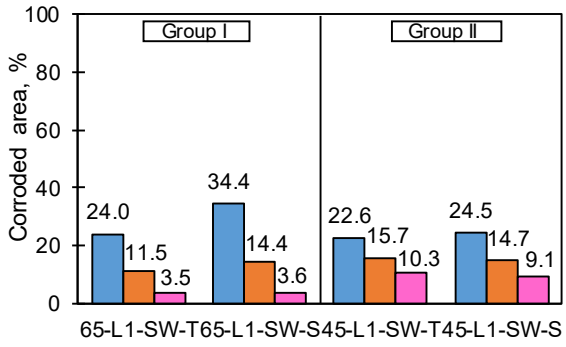

(b) effect of exposure condition

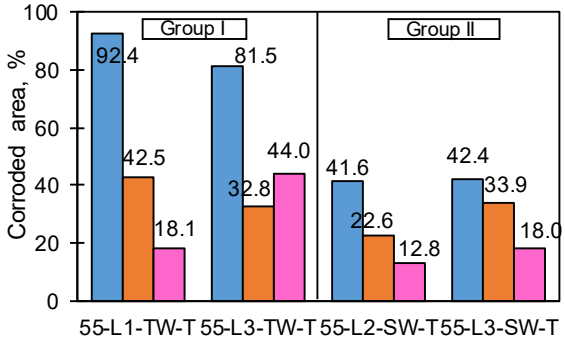

(c) effect of bending load

Fig. 5.13—Corroded area of steel bars

5.3.6 Cross-sectional loss

Corrosion distribution provides information on the corrosion behavior of steel bars, such as the type of corrosion regarding homogeneity. The corrosion behavior of steel is also characterized by the form of corrosion as either general or pit corrosion. The type and form of corrosion are important parameters affecting the mechanical behavior of the corroded RC

beam. Since the forms of corrosion in the steel bars are varied, determining the cross-sectional loss based on diameter loss causes an overestimate. Therefore, cross-sectional loss was determined by cutting the corroded steel bar into short pieces about 5 mm and then measuring the weight loss. The results of the corrosion distributions along the length of the corroded beams for effect of water mixing, exposure condition and bending load are shown in Figs. 5.14–5.16, respectively. From Fig. 5.14, for Group I, 55-L3-TW-T(2,3) and 55-L3-SW-T(2,3) showed that the cross-sectional loss was generated along the beam. Only in 55-L3-TW-T(5) and 55-L3-SW-T(5), no cross-sectional loss could be observed at middle part (Point M) of the beam. It assumes that flexural cracks from sustained load do not reach the steel bar with cover depth 5 cm. The highest cross-sectional loss was found in the end part of beam (Point A/B) for 55-L3-TW-T(2) and 55-L3-SW-T(2), and the value was 28.6 mm^2 and 14.3 mm^2 (with a corrosion degree of approximately 40.1% and 20.1%) respectively.

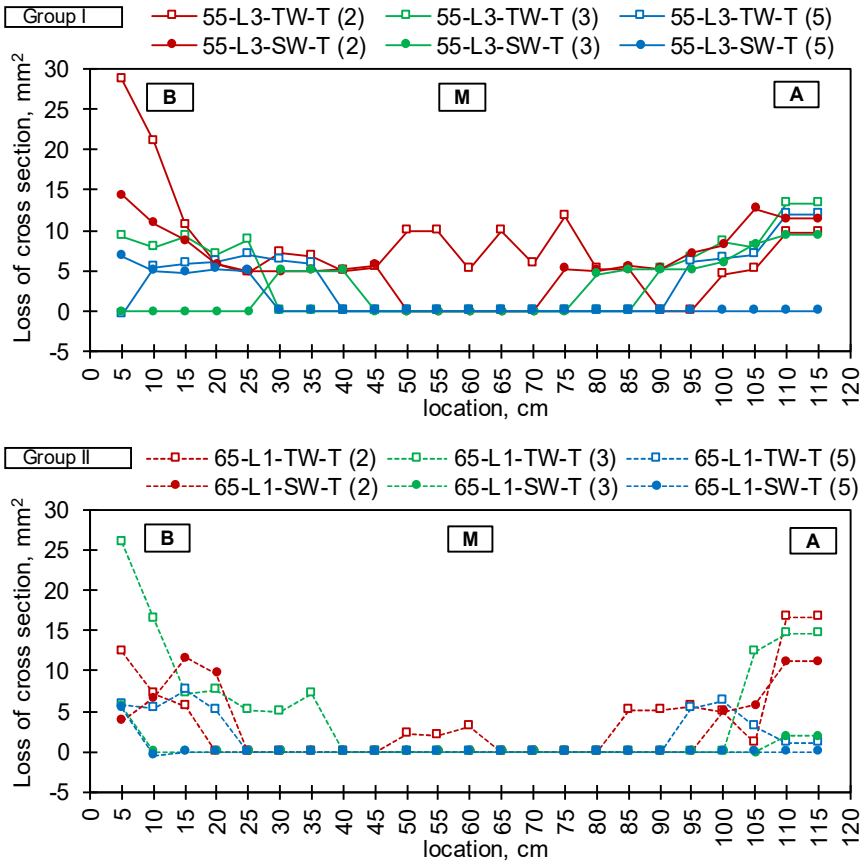

Fig. 5.14—Loss of cross-section of mixing water: tap water and seawater

For Group II of tap water mixing, only in 65-L1-TW-T (2), the cross-sectional loss was almost generated along the beam. In 65-L1-TW-T (3,5), the cross-sectional loss was mainly

concentrated at the end of the beam. For Group II of seawater mixing, the cross-sectional loss of 65-L1-SW-T (2,3) was at the end of the beam, and a slight no cross-sectional loss was found at middle part of the beam. Only 65-L1-SW-T (5) show almost no cross-sectional loss. The highest cross-sectional loss value for tap water mixing and seawater mixing in Group II was found in 65-L1-TW-T(3) and 65-L1-SW-T(3), the value reached 25.8 mm^2 (36.2%) and 11.6 mm^2 (16.2%), respectively. These results correspond to the HCP data explained previously.

From Fig. 5.15 for Group I (65-L1-SW-T(2,3,5) and (65-L1-SW-S(2,3,5)), both exposure showed that the cross-sectional loss was only mainly concentrated in the end part of the beam. And no significant different distribution value of the cross-sectional loss was found for each exposure. Different result on Group II (45-L1-SW-T(2,3,5) and (45-L1-SW-S(2,3,5)), tidal exposure showed more severe compared to splash exposure. It was found that some part of beam concentrated of the cross-sectional loss for all cover depth for tidal exposure.

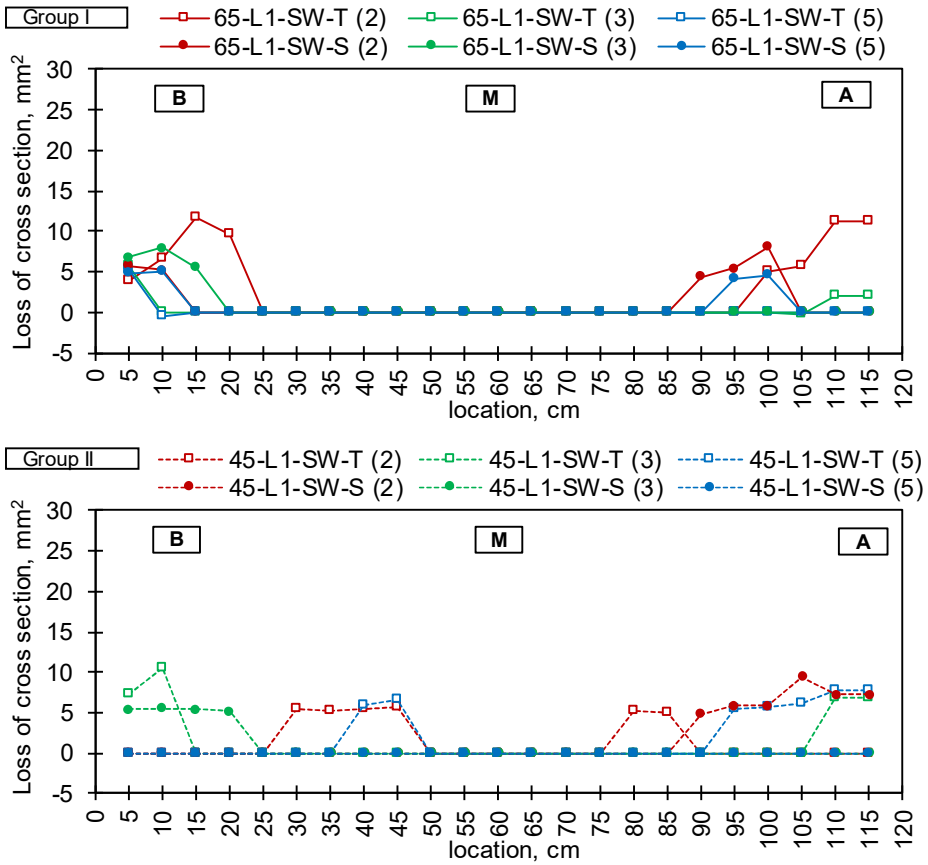

Fig. 5.15—Loss of cross-section of exposure condition: tidal and splash zone

From Fig. 5.16, for Group I in 55-L1-TW-T(2) and 55-L3-TW-T(2) showed the cross-sectional loss was generated along the beam. The cross-sectional along with the beam exhibit

that even in an area without crack corrosion still occurred. Implies that concrete cover 2 cm sensitive to corrosion, particularly in the marine environment. And at 55-L1-TW-T(3,5) and 55-L3-TW-T(3,5), the cross-sectional loss was found only at end part of the beam. The higher cross-sectional loss value of each load reached 27.89 mm^2 (39.1%) and 28.62 mm^2 (40.1%) at 55-L1-TW-T(3) and 55-L3-TW-T(3). It meant no effect of load for tap water mixing after long term exposure less significant. For Group II, no significant different distribution of cross-sectional loss was found for each load and all cover depth and cross-sectional loss was at end part of beam. And at middle part showed no cross-sectional loss was found.

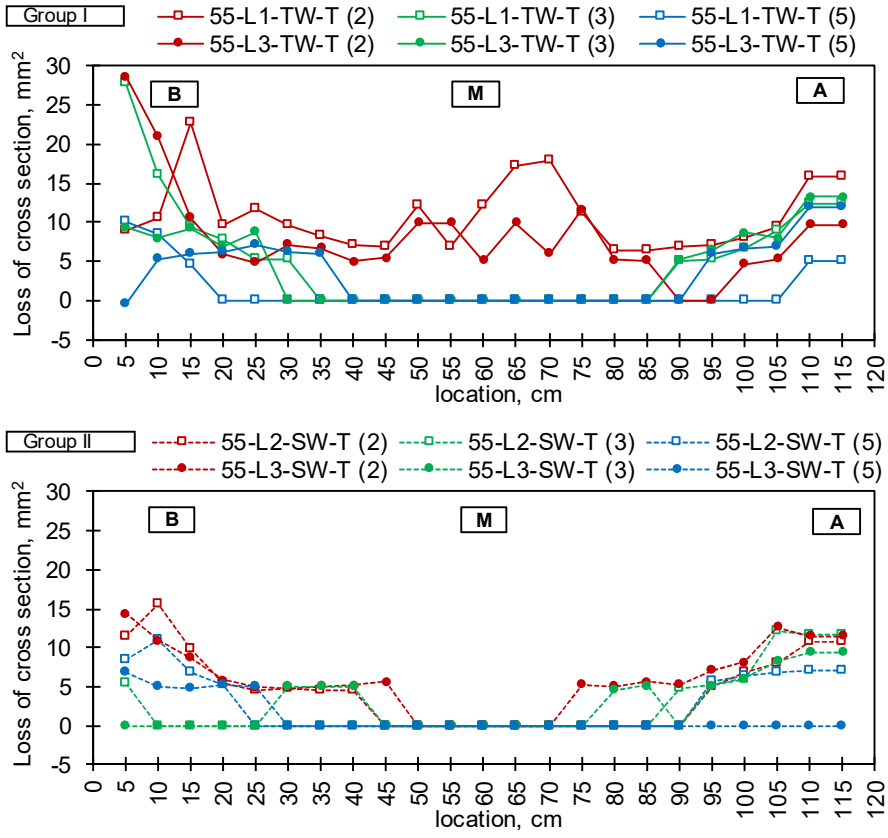

Fig. 5.16—Loss of cross-section of bending load

It should be understanding, if no cross-sectional loss was found, this does not mean that no corrosion occurred in these zones; it is possible that a small amount of corrosion was ignored as the experimental values were small by comparison with the original values of the mass and cross-section. Also, the reason end part of beam much more appears the cross-sectional loss due to the number of crack and width that position and concrete would promote corrosion, as oxygen or water can become entrapped in these features. These results are in accordance with the corrosion rate evaluation: the corrosion degree is more important in tensile area of the beam than in its compressive area because much affect the mechanic of beam.

From visual observation, electrochemical evaluation and confirm by actual condition of all specimen, the result demonstrated that seawater mixing showed better resistant performance against the corrosion of steel bar. Actually, seawater mixing generated 20% of total corroded area, however, passivity grade was more reasonable than tap water mixing. For the seawater mixing in W/C=0.55 with M=5.32 and M=7.97 kN-m, the amount of corroded area was less than 20% with concrete cover 5 cm while tap water mixing the total corroded area reach 44%. Therefore, seawater mixing has reliable for application in a case such as in marine tidal exposure. Further, it is also interesting to observed the result of seawater mixing in W/C=0.65 with M=2.66 kN-m, that is, the amount of corroded area was only 3.47%. It is suggested that the smaller bending load reduced the corroded area. From this result, the maximum bending load should be taken into account. It is also considered that concrete cover is one key factor for reasonable use of seawater as mixing water. Therefore, it is also observed the result of seawater mixing in splash marine environment for W/C ratio of 0.45 and 0.65 with M=2.66 kN-m, that is, the amount of corroded area was lower than 10.3% at concrete cover 5 cm. From these result, seawater mixing may be more also reasonable for application in a case such as in splash marine environment with required W/C ratio of 0.45-0.65, and applied bending load M=2.22 kN-m with design concrete cover 5 cm.

5.3.7 Tensile Test

The mechanical properties standard for steel bar used in Japan based on JIS G 3112 is shown in Table 5.6. The position failure points of each steel bars were variated so that their mechanical properties could be investigated more effectively as shown in Fig. 5.17.

Table 5.6—Mechanical properties of steel bar (JIS G 3112)

Type	F_y, MPa	F_u, MPa	Specimen	Elongation, %
SR 235	> 235	380-520	No. 2	> 20
			No. 14A	> 22

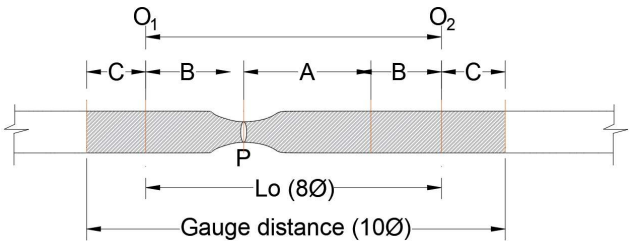

Fig. 5.17—Classification of failure point

All the failure point of the steel bar after the tensile test are shown at Figure 5.18. From Fig. 5.18, the failure points of three steel bar (55-L1-SW-S(3) for seawater mixing; 55-L1-TW-T(2) and 55-L3-TW-T(2) for tap water mixing) occurred at location in pit area, namely corrosion pit bar. For another steel bar without corrosion pit (namely non-corrosion pit bar), the failure point was variated and the location was not always in A and B area, but some of them located in C area. The corrosion pit bars showed elongation very limited at fracture location during the tensile test and exhibited more brittle behavior than the non-corrosion pit bars, which were ductile and showed necking at failure point (as shown in Fig. 5.19). As the corrosion pit bar showed a brittle response, there was almost no necking at the failure point. But, for the non-corrosion pit bar, the necking could not be ignored.

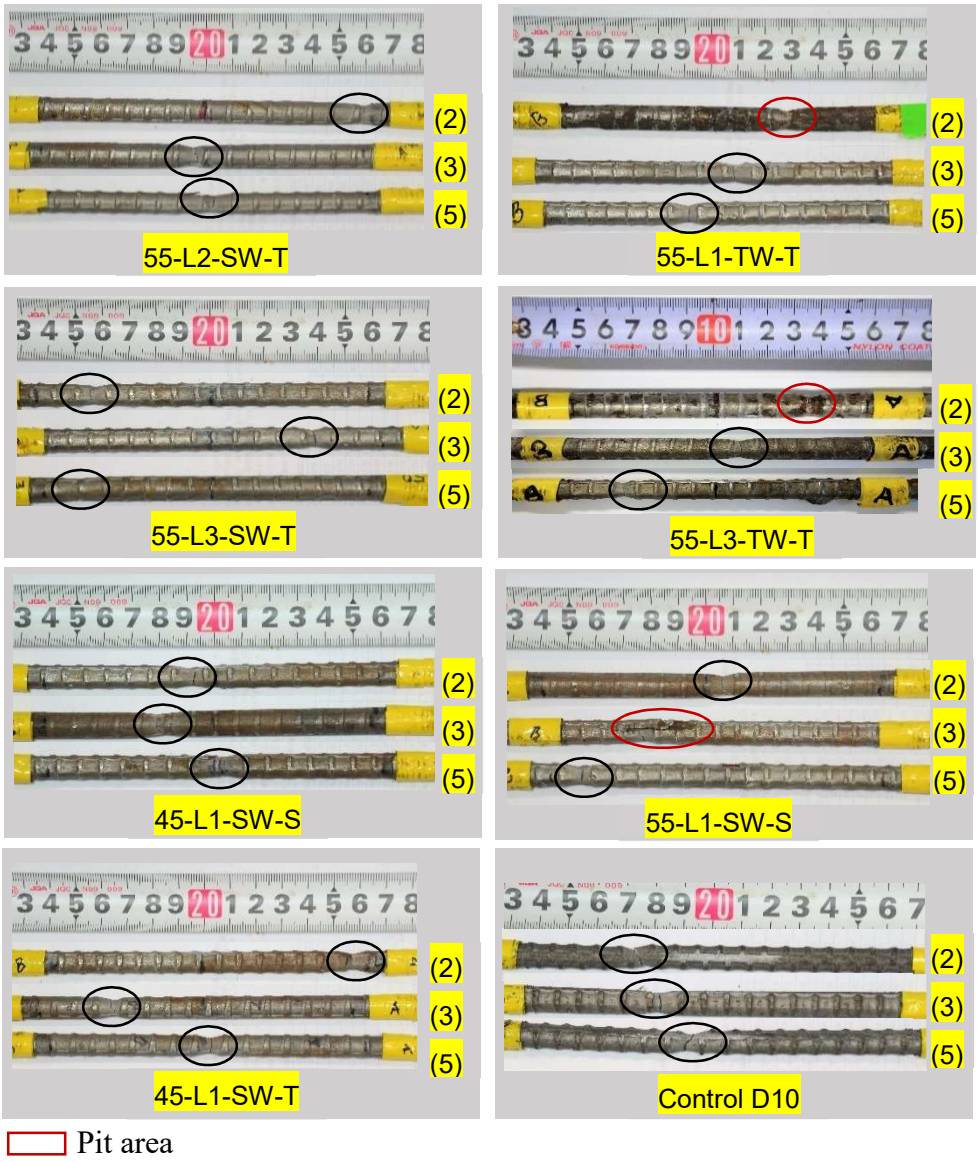

Fig. 5.18—Failure point of the corrosion pit bar, non-corrosion pit bar, and control bar

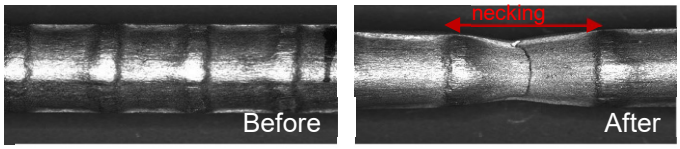

a. non-corrosion pit bar 55-L3-SW-T (3)

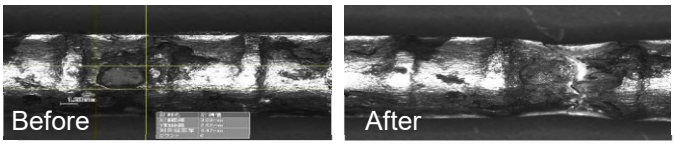

b. corrosion pit bar 55-L3-TW-T (3)

Fig. 5.19—Failure point of non-corrosion pit bar and corrosion pit bar

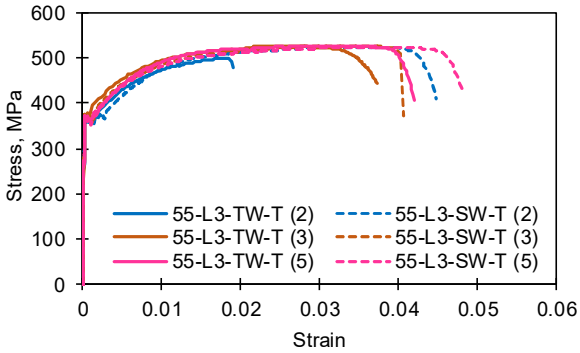

(a)Effect of mixing water

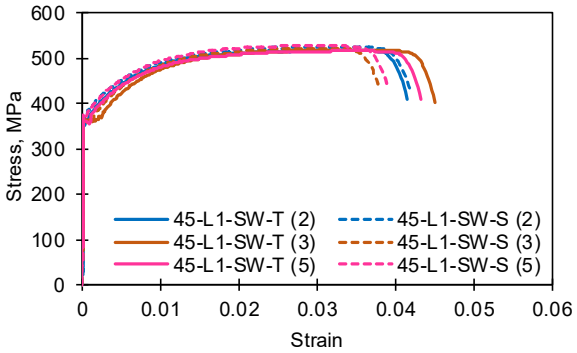

(b)Effect of exposure condition

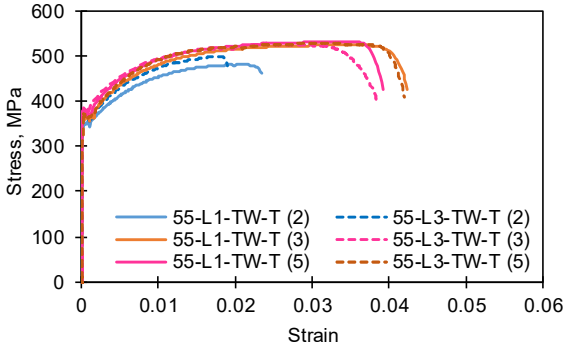

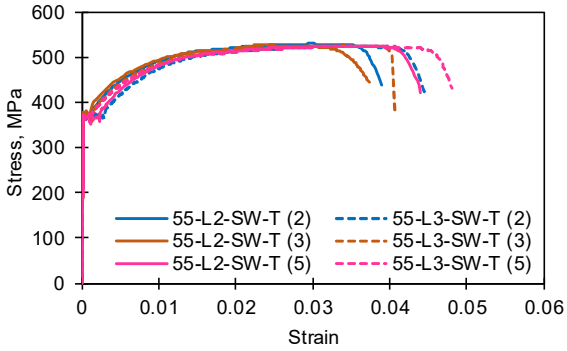

(c)Effect of bending load

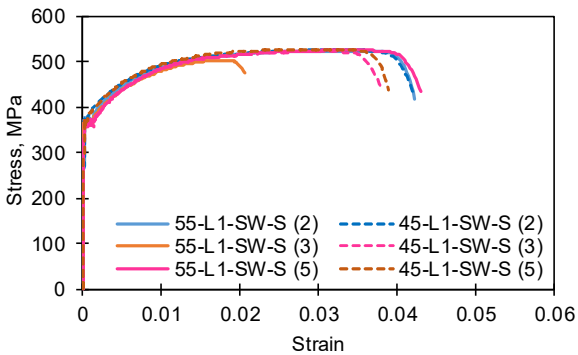

(a)Effect of W/C

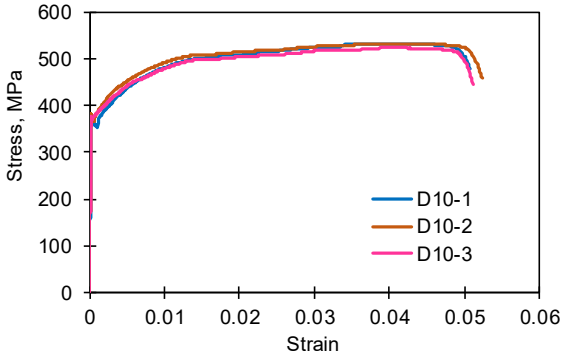

(b) Control bar

Fig. 5.20—Stress-strain curves of the tensile tests

The stress and strain curves for the tensile test of all steel bar are shown in Fig. 5.20. The curves for all steel bar were not identical. In general, the ductility of 36-years old bar (all corrosion pit bar and non-corrosion pit bar) was lower than the control bar. Compared to the control bar, the ductility of non-corrosion pit bar reduced from 8.52% to 20.00% and from 11.45 to 23.91% for seawater bar and tap water bar, respectively. And for corrosion pit bar, the ductility was also reduced about 42.93%, 48.24 and 59.36% for 55-L1-SW-S(3), 55-L1-TW-T(2), and 55-L3-TW-T(2), respectively, from the control bar. It can be observed that ductile behavior of steel bar extracted from beam of seawater mixing slightly better than tap water mixing. However, it still had great loss ductility compared to the control bar. From Fig. 5.20a, the shape of the curve for corrosion pit bar 55-L3-TW-T(2) was not similar to non-corrosion pit bar 55-L3-TW-T(3,5) and 55-L3-SW-T(2,3,5). The ductility of the corrosion pit bar 55-L3-TW-T(2) and non-corrosion pit bar 55-L3-TW-T(3,5) of tap water mixing appears to be strongly reduced, but both the yield stress and the ultimate stress of the non-corrosion pit bars 55-L3-TW-T (3,5) almost similar in comparison with the non-corrosion pit bars of seawater 55-L3-TW-T(3,5). The stress-strain curve leads to understanding that corrosion, particularly pit type not much reduce both f_u and f_y, however, greatly reduce strain. Importantly, the concrete cover seems greatly affects corrosion degree on steel bar. The ductility of steel bar with thin cover would be greatly reduced. Further, it showed the ductility of steel bar from seawater mixing much better than tap water mixing. From Fig. 5.20b, the ductility of the tidal zone bar was slightly higher than the splash zone bar, but both the yield stress and ultimate stress was almost similar. For Fig. 5.20c, Group I-tap water mixing, the ductility of corrosion pit bar (55-L1-TW-T(2) and 55-L3-TW-T(2)) also in same condition that ductility was reduced almost half from control bar and non-corrosion pit bar (55-L1-TW-T(3,5) and 55-L3-TW-T(3,5)). For tap water mixing, as increasing of bending load the ductility of steel bar reduced. But difference phenomena were found for Group II-seawater mixing (55-L2-SW-T(2,3,5) and 55-L3-SW-T(2,3,5)), as increasing bending load the ductility of steel bar also increased.

According to Euro code 2 [5.20] the reinforcement should have adequate ductility as defined by the ratio of the tensile strength to the yield strength, f_u/f_y, and the elongation at maximum force, ε_{uk} (ultimate strain), indicated in Table 5.7. The properties of each steel bars are shown in Table 5.8. In comparison with the non-corrosion pit bars, the properties of the corrosion pit bars had been changed tremendously, including the yield strength, the ultimate strength and the ratio f_u/f_y, the ultimate strain at maximum load ε_u. From Table 5.7, the control bar and all old bar (corrosion pit bar and non-corrosion pit bars) were slightly lower than the nominal value in the 400-600 MPa range defined by Euro code 2 [5.20].

Table 5.7—Properties of reinforcement according to Euro code 2 [5.20]

Product form	Bars and de-coiled rods		
Class	A	B	C
Characteristic yield strength f_y (MPa)	400 to 600		
Minimum value of f_u/f_y	≥1.05	≥1.08	≥1.15 and ≤1.35
Characteristic strain at maximum force, ε_{uk} (%)	≥2.5	≥5.0	≥7.5

Table 5.8— Summary of tensile test results

Specimen	d, cm	f_y, Mpa	f_u, Mpa	f_u/f_y	Strain at max force	Elongation, %	Surface corroded area, %	Cross-sectional loss, %	Remark
Control bar		363.5	532.9	1.466	0.0403	32.79	0.00	0.00	
		368.1	533.2	1.448	0.0397	29.42	0.00	0.00	
		365.4	524.0	1.434	0.0404	33.61	0.00	0.00	
45-L1-SW-T	2	360.0	518.9	1.441	0.0327	*	0.00	0.00	
	3	363.8	518.9	1.426	0.0364	28.10	0.00	0.00	
	5	360.6	516.8	1.433	0.0345	28.67	0.08	0.00	
55-L2-SW-T	2	369.0	529.1	1.434	0.0321	26.53	1.10	0.00	
	3	361.2	523.7	1.450	0.0337	29.22	0.26	0.00	
	5	365.4	523.5	1.432	0.0360	*	2.10	0.00	
55-L3-SW-T	2	368.5	523.1	1.420	0.0353	27.02	0.06	0.00	
	3	367.4	525.6	1.431	0.0348	*	0.00	0.00	
	5	363.5	523.7	1.441	0.0367	28.14	0.00	0.00	
55-L1-SW-S	2	369.4	524.5	1.420	0.0298	28.45	0.67	0.00	
	3	362.0	504.0	1.392	0.0171	18.23	0.45	7.25	corrosion pit bar
	5	363.5	525.4	1.445	0.0342	*	0.15	0.00	
45-S1-SW-S	2	367.4	526.0	1.432	0.0329	27.98	0.34	0.00	
	3	365.1	522.1	1.430	0.0301	25.55	0.24	0.00	
	5	364.1	527.5	1.449	0.0283	27.06	0.65	0.00	
55-L1-TW-T	2	341.8	480.3	1.405	0.0212	16.53	17.30	25.14	corrosion pit bar
	3	365.2	524.6	1.437	0.0343	28.03	0.09	0.00	
	5	372.9	531.1	1.424	0.0341	24.30	0.02	0.00	
55-L3-TW-T	2	357.8	498.0	1.392	0.0179	12.98	16.30	16.36	corrosion pit bar
	3	370.1	526.6	1.423	0.0232	28.28	1.22	0.00	
	5	369.9	526.7	1.424	0.0300	26.93	0.53	0.00	

*Failure point at area B, ** Failure point at area C

The relationship between ultimate strength and yield strength against cross-sectional loss is shown in Fig. 5.21. In this figure, it was found that the ultimate strength for corrosion pit bar was reduced about 4.91% (55-L1-SW-S(3)), 9.38% (55-L1-TW-T(2)) and 6.05% (55-L3-TW-T(2)) from the control bar. For yield strength, only corrosion pit bar was reduced about 6.51% (55-L1-TW-T(2)) and 2.14% (55-L3-TW-T(2)), respectively, from control bar. But in general, it was found that the yield strength and ultimate strength of all non-corrosion pit bar were almost similar to those of the control bar even the age of steel bar was almost 36-years old and corroded area appears in the bar. Some researcher has focused on the effect of

corrosion on the strength of steel bars. Zhu and François [5.14, 5.15] found that the yield strength of corroded steel bars was nearly the same as that of non-corroded bar, and the ultimate strength of corroded bars was greater than that of control bar. Cairns et al. [5.16] reported that increasing reinforcement corrosion increased yield strength and ultimate strength. Du et al. [5.17] and Almusallam [5.20] stated that the yield strength and ultimate strength decreased with increasing corrosion degree. However, all the research mentioned above found that corrosion resulted in a relatively modest change of strength but a significant loss of ductility. For the ultimate strength and the ratio of f_u/f_y, all the values of the corrosion pit bars were over the non-corrosion pit bar. The reason could be due to the different deformation performance of the corrosion pit bars. The type of pit corrosion (e.g., depth and width) also believe as the main factor. In addition, the elongation of corrosion pit bar for 55-L1-TW-T(2), 55-L3-TW-T(2) and 55-L1-SW-S(3) were 16.53 mm, 12.98 mm, and 18.23 mm, respectively. This value was lower than the threshold value (22%) as per JIS G 3112, as shown in Table 5.5. The ductility of the corrosion pit bar was also significantly reduced, the value almost half of that non-corrosion pit bar and control bar.

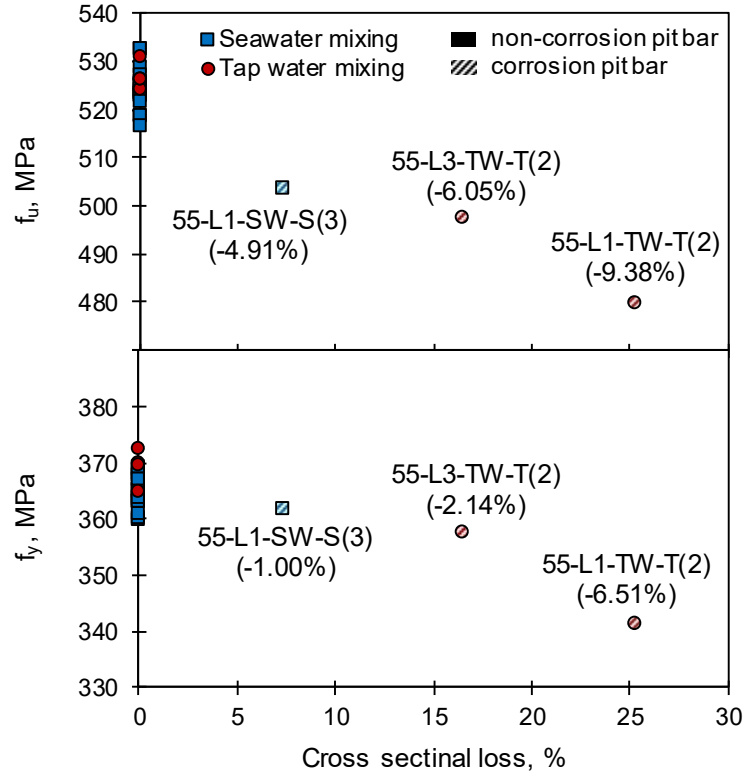

Fig. 5.21—Relationship between f_u and f_y with cross-sectional loss

The residual load-carrying capacity of the beam is greatly affected by corrosion of the reinforcements. The loss of bonding between the steel bar and concrete is caused by cross-

sectional loss. Dasar [5.2] reported cross-sectional loss greatly affects the load-carrying capacity of the RC beam and the tensile bars, in particular, are the most severely affected by the flexural bending moment. Therefore, if the local cross-sectional loss is known, it is possible to estimate the residual load-carrying capacity of the beam. The result indicates that each percentage point of local cross-sectional loss in the tensile bars corresponds to a 1% reduction in the residual load-carrying capacity of the beams, which is similar to the previous findings Malumbela [5.23] and Zhang et al. [5.24].

Fig. 5.22 shows the relationship between the ratio of ultimate tensile strength and yield strength including (f_u/f_y) and the ultimate strain ε_u. All steel bar was set in the graph and divided into seawater mixing and tap water mixing as well as corrosion pit bar and non-corrosion pit bar. All the results of non-corrosion pit bar were in Class A, on the contrary, the corrosion pit bar was out of the range and lower of Class A (2.5%) threshold, which the residual ductility of the corroded bars was not sufficient according to Table 5.6. The nominal ratio (f_u/f_y) of all-steel bar (include corrosion pit bar) mostly over the Class C threshold, which indicated all-steel bar had stronger yield strength and ultimate strength. However, the ultimate strain for corrosion pit bar was too weak to reach the threshold value of 2.5%, which meant that ductility would be the determinant factor for highly corrosion pit bars, and the brittle behavior of steel bars would require special attention to assess the quality of the existence of corroded structures.

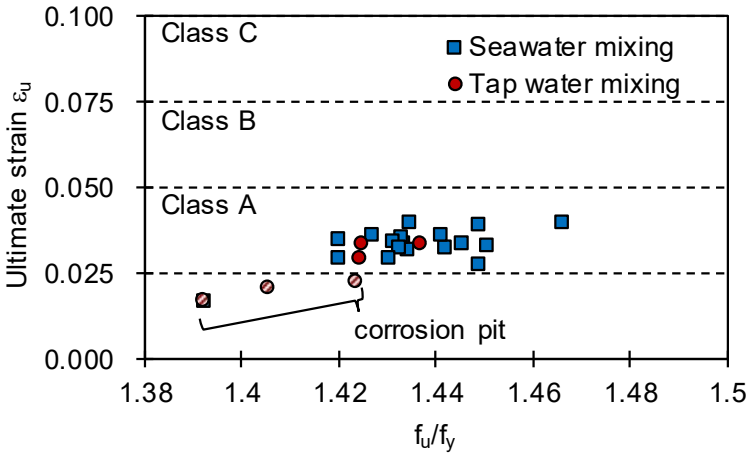

Fig. 5.22—Failure point of the non-corroded bar and corroded bar

Sharper and deeper corrosion pit would lead to more pronounced concentration for the strain and stress and more brittle failure would occur. The stress concentration caused to partial yielding of the cross-section and according to the fracture mechanics theory, when the entire cross-section of steel bar reached to the elastic limit, a large part of yielding reserve had been

consumed, which cause to premature rupture of the bar. However, it should be noted that such asymmetry effect would be less significant for a bar embedded in concrete than those tested in air. As the corrosion products could fill into the corrosion zone, concrete bond and constraint around the bar could make some contribution to mechanical performance [5.16, 5.18, 5.19]. Yield stress of corrosion pit bars increased deeply and the scatter on the measurement of the effective nominal ratio of f_u/f_y was not enough to explain it, because out of the threshold limit. More research was needed to understand these results which could be influenced by the steel bar diameter. Indeed, a 16 mm diameter used in François et al. [5.15] showed the weakest increase in yield stress. Ultimate stress also increased sharply for corroded steel, but the comparison with non-corroded steel was complex due to a strong reduction of necking phenomena for corroded bars. Also the sample position was in the middle area (M) which almost all steel bar does not have corrosion pit in middle area, however, susceptible affected by bending stress.

Corrosion does not reduce the yield or ultimate strength of the steel bars, but their ultimate strain decreased significantly. These results agreed with the model by Castel et al. [5.19] although the model was relatively conservative because it was constructed from results obtained with artificial notches rather than natural pitting corrosion. The pitting corrosion leads to mass loss higher than general corrosion, considering that it occurs in isolated areas, however, pitting corrosion can cause highly detrimental effects on armor because where pitting corrosion occurs there is an amplification of tensile stresses. Furthermore, this occurrence is due to high length/radius of these defects, that affects the resistance of armor fatigue and other side effects [5.22]. Also, the cross-sectional loss and depth of pitting corrosion were found to be less important than the shape of corrosion in the cross-section, which was considered to be main factor for the ductile behavior of corroded bars. When corrosion was distributed uniformly around the cross-section, the steel bar exhibited good ductility. Nevertheless, when the pitting corrosion occurred asymmetrically around the cross-section, the steel bar responded with more brittle behavior. Although both the yield stress and ultimate stress of all the corroded bars were improved, the ductility of most of the corroded bars decreased below the threshold fixed by Euro code 2. These result indicated that the ultimate residual elongation of a corroded steel bar might be most important parameter affecting reliability as far as structural performance of RC structure damaged by corrosion in the chloride environment.

5.4 Conclusions

Based on the results of this study, it was demonstrated that the use of seawater as mixing water contributed to maintaining strong performance throughout a long exposure period of 36 years. The following conclusions could be drawn from this experimental study:

1. The use of seawater as mixing water improved concrete strength, concrete resistance, oxygen permeability resistance and maintained very dense microstructure, in RC beam even after 36-years of marine exposure.
2. The strength of seawater mixing showed 10 MPa larger than tap water mixing, with the ratio of seawater/tap water was 1.2 after long-term exposure.
3. The dense microstructure of seawater mixed concrete maintained a high passivity over the steel bars and retarded the onset of corrosion. It could reduce the total corroded area of steel bar for almost half of the tap water mixing.
4. The results of 36-years exposure test of concrete mixed with seawater with concrete cover 50 mm demonstrated the high possibility of using seawater as an alternative and sustainable material of reinforced concrete, especially in a marine tidal environment.
5. The bound chloride of seawater mixed concrete was higher than tap water mixing.
6. The ductility of seawater mixed concrete better than tap water mixing according to the mechanical properties of the extracted bar.
7. Corrosion does not reduce the yield strength and ultimate tensile strength of the steel bar, but their ultimate strain decreased significantly.

References

[5.1] JGC16, "Standard Specification for Concrete Structures (Materials and Construction)," Japan Society of Civil Engineers, 2007.

[5.2] A. Dasar, A Study on Deterioration and Corrosion Behavior of Rc and Pc Members with Initial Defects Under Environmental Action, Kyushu University, 2017.

[5.3] A. Dasar, A Study on Corrosion Evaluation of Steel in Reinforced Concrete due to Chloride Ion, Kyushu University, 2013.

[5.4] A. Dasar, H. Hamada, Y. Sagawa, R. Irmawaty, Corrosion Evaluation of Reinforcing Bar in Sea Water Mixed Mortar by Electrochemical Method, Proceedings of the Japan Concrete Institute, Japan Concrete Institute, Nagoya, 2013, pp. 889-894.

[5.5] A. Dasar, H. Hamada, Y. Sagawa, D. Yamamoto, Recovery in Mix Potential and Polarization Resistance of Steel Bar in Cement Hardened Matrix During Early Age of 6 Months-Sea-Water Mixed Mortar and Cracked Concrete, Proceedings of the Japan Concrete Institute, Japan Concrete Institute, Fukuoka, 2016, pp. 1203-1208.

[5.6] Mohammed, T. U., T. Yamaji, A. Toshiyuki, and H. Hamada. "Marine durability of 15-year old concrete specimens made with ordinary Portland, slag and fly ash cement," ACI Spec., pp.199-30.
[5.7] Fukute, T., and H. Hamada. "A Study on the Durability of Concrete Exposed in Marine Environment for 20 Years." Report of the Port and Harbour Research Institute 31(5) 1993.
[5.8] ASTM C 876-15, "Standard Test Method for Half-cell Potential of Uncoated Reinforcing Steel in Concrete," American Society for Testing and Materials, 2018.
[5.9] Otsuki, N. "A study of effectiveness of chloride on corrosion of steel bar in concrete." Report of Port and Harbor Research Institute, 1985, pp. 127-134.
[5.10] Ismail, Idawati, et al. "Influence of fly ash on the water and chloride permeability of alkali-activated slag mortars and concretes." Construction and Building Materials, 48, 2013, pp.1187-1201.
[5.11] Kayali, Obada, M. S. H. Khan, and M. Sharfuddin Ahmed. "The role of hydrotalcite in chloride binding and corrosion protection in concretes with ground granulated blast furnace slag." Cement and Concrete Composites, 34, No. 8, 2012, pp. 936-945.
[5.12] Adiwijaya. "Dissertation-A Fundamental Study on Seawater-Mixed Concrete Related to Strength, Carbonation and Alkali-Silica Reaction." Kyushu University, Sept 2015.
[5.13] Midgley, H. G., and J. M. Illston. "Effect of chloride penetration on the properties of hardened cement pastes." 7th international congress on the chemistry of cement, Vol. 3., 1986, pp. 101-103.
[5.14] Zhu, Wenjun, and Raoul François. "Effect of corrosion pattern on the ductility of tensile reinforcement extracted from a 26-year-old corroded beam." Adv Concr Constr 1.2 (2013): 121-37.
[5.15] François, R., Khan, I. and Dang, V.H. (2013), "Impact of corrosion on mechanical properties of steel embedded in 27-year-old corroded reinforced concrete beams", Mater. Struct., 46(6), 899-910.
[5.16] Cairns, J., Plizzari, G.A., Du, Y.G., Law, D.W. and Franzoni, C. (2005), "Mechanical properties of corrosion-damaged reinforcement", ACI Mater. J., 102(4), 256-264.
[5.17] Du, Y. G., L. A. Clark, and A. H. C. Chan. "Residual capacity of corroded reinforcing bars." Magazine of Concrete Research 57.3 (2005): 135-147.
[5.18] Almusallam, A.A. (2001), "Effect of degree of corrosion on the properties of reinforcing steel bars", Construct Build Mater, 15(8), 361-368.
[5.19] Castel, A., François, R. and Arligue, G. (2000), "Mechanical behavior of corroded reinforced concrete beams Part 2: Bond and notch effects", Mater. Struct., 33(9), 545-551.
[5.20] EN, BS. "1-1. Eurocode 2: Design of concrete structures–Part 1-1: General rules and rules for buildings." European Committee for Standardization (CEN) (2004).
[5.21] Fukute, T., et al. (1990). "Study on the durability of concrete mixed with seawater." Rep. of the Port and Harbour Research Institute, Ministry of Transport, 29(3), 57–59
[5.22] Ribeiro, Daniel Véras, et al. "Corrosão em estruturas de concreto armado: Teoria, controle e métodos de análise." Rio de Janeiro: Editora CAMPUS 1 (2014).

[5.23] Malumbela, Goitseone, Mark Alexander, and Pilate Moyo. "Variation of steel loss and its effect on the ultimate flexural capacity of RC beams corroded and repaired under load." Construction and Building Materials 24.6 (2010): 1051-1059.

[5.24] Zhang, Ruijin, Arnaud Castel, and Raoul François. "Concrete cover cracking with reinforcement corrosion of RC beam during chloride-induced corrosion process." Cement and Concrete Research 40.3 (2010): 415-425.

[5.25] A. Dasar, H. Hamada, Y. Sagawa, T. Ikeda, Durability of Marine Concrete with Mineral Admixture and Marine Aquatic Organism Layer, Sustainable Construction Materials and Technologies 2013 (2013) e146.

[5.26] A. Dasar, H. Hamada, Y. Sagawa, D. Yamamoto, Deterioration progress and performance reduction of 40-year-old reinforced concrete beams in natural corrosion environments, Construction and Building Materials 149 (2017) 690-704.

[5.27] A. Dasar, R. Irmawaty, H. Hamada, Y. Sagawa, D. Yamamoto, Prestress loss and bending capacity of pre-cracked 40 year-old PC beams exposed to marine environment, MATEC Web of Conferences, EDP Sciences, 2016, p. 02008

[5.28] Patah, Dahlia, et al. "THE EFFECT OF SEAWATER MIXING ON CORROSION OF STEEL BAR IN 36-YEARS OLD RC BEAMS UNDER MARINE TIDAL ENVIRONMENT." コンクリート工学年次論文集 41.1 (2019): 791-796.

CHAPTER 6. AN ASSESSMENT FOR CORROSION ACTIVITY OF RC STRUCTURES IN NATURAL CORROSION ENVIRONMENTS

6.1 Introduction

Considering marine exposure conditions and use either sea sand/seawater for heavy construction in many countries, chloride-induced corrosion is one of major causes of degradation of RC structures. Damage induced by corrosion of steel usually requires proper repair and followed by maintenance. It is reported that the costs of repair and maintenance of corroded structures exceed billions of dollars per year [6.4]. The costs of repair and maintenance vary depending on RC structure condition, including the degree of damage, cause of damage, and effect of damage on structural behavior [6.5]. Various techniques for diagnosis, detecting and measuring corrosion will provide data on the causes, detection, or rate of corrosion [6.6]. An accurate and reliable assessment method is required at an early stage before steel corrosion caused serious damage of RC structure. The assessment method usually provides the current condition of the RC structures, so that the future performance of RC structure can be predicted. Furthermore, the method of assessment is almost a precondition for the rehabilitation of existing RC structures efficiently and cost-effectively. The assessment should be carried out without damaging the RC structures, both new and old ones. Several techniques have been reported in previous literature that can be used for monitoring and evaluating the corrosion of steel bar in concrete structures for diagnosing the cause and effect of corrosion. Visual inspection, corrosion potential, polarization resistance, and other electrochemical methods are more commonly used for corrosion monitoring in RC structures.

Electrochemical methods could be used to estimate the corrosion rate in concrete structures to show the speed at which reinforcing steels are corroding and, therefore, to identify vulnerable locations. This study presents the importance of reinforcement corrosion monitoring and describes the different methods for evaluating the corrosion activity level of RC structures. The main objective of this study was to analyze the corrosion level of laboratory RC specimens using several corrosion measurement methods. By reviewing the literature, then some corrosion measurement methods were selected to assess the corrosion level after long-

term exposure of RC beam under marine environment. Additionally, a potential correlation between main field corrosion measurement procedures was explored. The data of corrosion level were constructed from Chapter 5 then analysis and categorized into deterioration and degradation stage level. This study proposes a reliable assessment method to estimate and evaluate corrosion activity of steel corrosion which caused severe damage of RC structure and involved parameters on each deterioration stage. Also, some considerations utilization of seawater mixed concrete with OPC and mortar contain mineral admixture was proposed.

6.2 Testing program and calculation method

The investigations of four RC beam specimens were carried out. The RC beam specimens were mixed with tap water and seawater. The cement type was Ordinary Portland Cement (OPC). The detailed information of mix proportions of concrete is unavailable. Water-cement ratios (W/C) were 45%, 55% and 65%. The density of concrete was 2,398 kg/m3. Three levels of stress of bar were applied that were 100, 200, and 300 MPa or if interpreted in bending load they were M=2.66, 5.32, and 7.97 kN-m, respectively. The summary of RC beam is shown in Table 6.1.

Table 6.1—Summary of RC beam specimens

Group	Specimen	W/C, %	M, kN-m	Mixing water	Exposure
Seawater	65-L1-SW-T	65	2.66 (L1)	Seawater (SW)	Tidal (T)
	45-L1-SW-T	45	2.66 (L1)	Seawater (SW)	Tidal (T)
	55-L2-SW-T	55	5.32 (L2)	Seawater (SW)	Tidal (T)
	55-L3-SW-T	55	7.97 (L3)	Seawater (SW)	Tidal (T)
	65-L1-SW-S	65	2.66 (L1)	Seawater (SW)	Splash (S)
	55-L1-SW-S	55	2.66 (L1)	Seawater (SW)	Splash (S)
	45-L1-SW-S	45	2.66 (L1)	Seawater (SW)	Splash (S)
Tap water	65-L1-TW-T	65	2.66 (L1)	Tap water (TW)	Tidal (T)
	55-L1-TW-T	55	2.66 (L1)	Tap water (TW)	Tidal (T)
	55-L3-TW-T	55	7.97 (L3)	Tap water (TW)	Tidal (T)

The layout details of the RC beam were shown in Fig. 6.1. Dimensions of beam were 12x15x120 cm. Three deformed steel bars of diameter 10 mm (D-10) were embedded at 2, 3, and 5 cm of cover depth from the two sides in the beam. The four sides of the RC beam were noted “Side C” as compression side, “Side T” as tension side, “Side F” and “Side B as front and backside respectively. The investigations were carried out after 36 years of exposure. The RC beams were cast and then stored in a tidal pool and natural seawater artificial splash under constant bending load at the Port and Airport Research Institute (PARI) laboratory in Yokosuka-Japan for 32-years. Then they were transferred to exposure site at Kyushu

University followed by four years' exposure under outside natural environment, with bending load release already (Fig. 6.2).

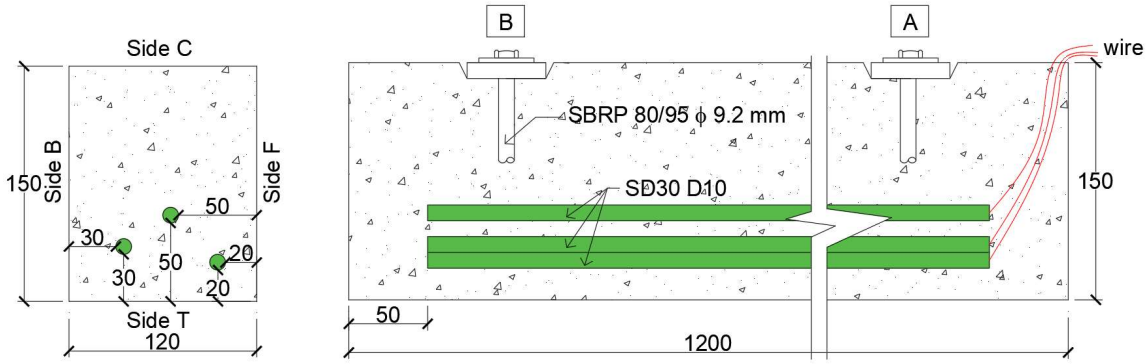

Cross section Longitudinal section (unit in mm)

Fig. 6.1— Layout details of the RC beam

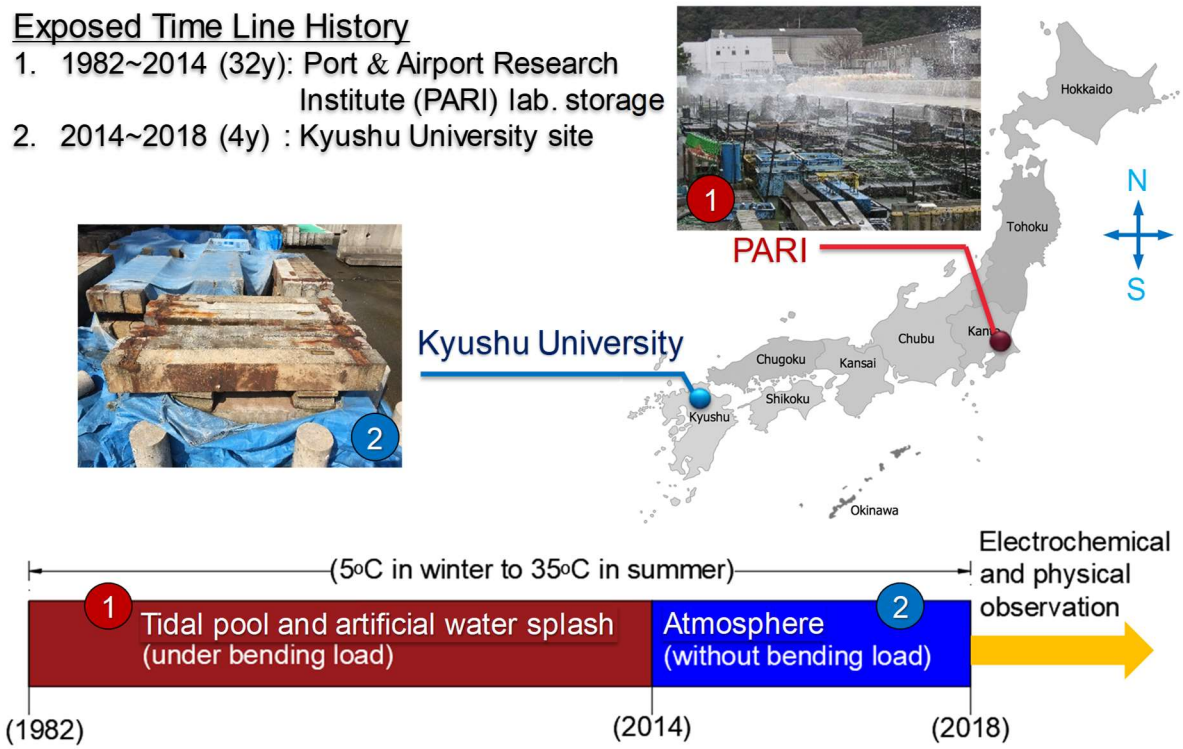

Fig. 6.2—Exposure condition

6.3 Experimental method and establishing corrosion level

The corrosion level of steel bar was estimated based on corrosion testing (electrochemical and physical) results of all RC beams. JSCE, ASTM, CEB standards and several finding from previous researchers have suggested corrosion levels for reinforcing steel in concrete: initiation, propagation, acceleration, and damage that are widely used to select the

suitable repair methods and determine the repair times and for the bridge deck [6.7–6.10]. The various methods have been applied for corrosion monitoring in RC structures. Table 6.2 shows the selected assessment method as a parameter for deterioration degree and performance reduction. And the data of corrosion level were selected from Chapter 5 and summarized in Table 6.3 and Table 6.4, respectively.

Table 6.2—Selected assessment method

Deterioration degree	Variable	Performance reduction	Variable
corrosion potential	x_1	corroded area	x_8
corrosion current density	x_2	cross sectional loss	x_9
chloride content	x_3	ultimate strain at maximum force	x_{10}
grade of passivity	x_4	nominal ratio of f_u/f_y	x_{11}
electrical resistivity	x_5	elongation	y_2
oxygen supply	x_6		
deterioration degree	x_7		
total surface corroded area	y_1		

Table 6.3—Summary result of electrochemical analysis

Mixing water	Specimen code	d, cm	Corrosion measurements							
			x_1	x_2	x_3	x_4	x_5	x_6	x_7	y_1
Seawater	65-L1-SW-T	2	-450	0.11	10.31	3	27.90	2.87	11	24.01
		3	-236	0.09	10.70	3		2.27		11.46
		5	-248	0.05	11.32	3		1.72		3.47
	45-L1-SW-T	2	-224	0.08	6.46	3	36.83	2.39	8	22.60
		3	-244	0.07	7.32	3		0.38		15.70
		5	-108	0.05	5.75	3		0.36		10.29
	55-L2-SW-T	2	-454	0.11	7.09	3	37.00	4.76	10	41.58
		3	-301	0.10	7.48	3		3.41		22.65
		5	-282	0.10	7.22	3		2.55		12.76
	55-L3-SW-T	2	-555	0.03	8.42	3	35.22	4.77	12	42.40
		3	-296	0.11	10.01	3		3.41		33.93
		5	-318	0.10	9.00	3		2.44		18.00
	65-L1-SW-S	2	-394	0.16	15.41	3	28.37	3.23	11	34.36
		3	-193	0.13	15.18	3		2.31		14.43
		5	-187	0.06	16.20	3		2.26		3.57
	55-L1-SW-S	2	-237	0.08	11.52	3	37.00	2.39	11	13.39
		3	-110	0.08	11.74	3		2.13		7.20
		5	-166	0.06	12.67	4		1.23		13.58
	45-L1-SW-S	2	-237	0.08	9.53	3	37.67	1.90	11	24.46
		3	-136	0.08	10.64	3		0.49		14.70
		5	-200	0.06	11.29	4		0.44		9.10

Table 6.3—(continue)

Mixing water	Specimen code	d, cm	Corrosion measurements							
			x_1	x_2	x_3	x_4	x_5	x_6	x_7	y_1
Tap water	65-L1-TW-T	2	-416	0.26	8.06	2	21.6	5.93	12	53.06
		3	-360	0.25	9.02	2		2.31		20.04
		5	-458	0.19	9.65	2		2.45		19.69
	55-L1-TW-T	2	-333	0.05	11.10	3	21.5	7.35	12	92.38
		3	-293	0.05	9.57	3		4.85		42.51
		5	-284	0.04	9.81	3		3.75		18.11
	55-L3-TW-T	2	-432	0.17	12.67	2	17.39	9.16	12	81.46
		3	-539	0.12	13.10	2		5.41		32.84
		5	-481	0.14	12.40	2		4.98		44.04

Where, x_1= corrosion potential, mV; x_2= corrosion current density, $\mu A/cm^2$; x_3=chloride content, kg/m^3; x_4=grade of passivity; x_5=electrical resistivity, kΩ–cm, x_6= oxygen permeability x 10^{-12} $mol/cm^2/s$; x_7=deterioration degree; y_1=total corroded area, %

Table 6.4— Summary result of mechanical properties

Specimen code	d, cm	Mechanical properties				
		x_8	x_9	x_{10}	x_{11}	y_2
Control bar	1	0.00	0.00	0.0403	1.47	32.79
	2	0.00	0.00	0.0397	1.45	29.42
	3	0.00	0.00	0.0404	1.43	33.61
45-L1-SW-T	2	0.00	0.00	0.0327	1.44	*
	3	0.00	0.00	0.0364	1.43	28.10
	5	0.08	0.00	0.0345	1.43	28.67
55-L2-SW-T	2	1.10	0.00	0.0321	1.43	26.53
	3	0.26	0.00	0.0337	1.45	29.22
	5	2.10	0.00	0.0360	1.43	*
55-L3-SW-T	2	0.06	0.00	0.0353	1.42	27.02
	3	0.00	0.00	0.0348	1.43	*
	5	0.00	0.00	0.0367	1.44	28.14
55-L1-SW-S	2	0.67	0.00	0.0298	1.42	28.45
	3	0.45	7.25	0.0171	1.39	18.23
	5	0.15	0.00	0.0342	1.45	*
45-S1-SW-S	2	0.34	0.00	0.0329	1.43	27.98
	3	0.24	0.00	0.0301	1.43	25.55
	5	0.65	0.00	0.0283	1.45	27.06
55-L1-TW-T	2	17.3	25.14	0.0212	1.40	16.53
	3	0.09	0.00	0.0343	1.44	28.03
	5	0.02	0.00	0.0341	1.42	24.30
55-L3-TW-T	2	16.3	16.36	0.0179	1.39	12.98
	3	1.22	0.00	0.0232	1.42	28.28
	5	0.53	0.00	0.0300	1.42	26.93

Where, x_8= corroded area, mm^2, x_9= cross sectional loss, mm^2; x_{10}=maximum ultimate strain, mm/mm; x_{11}= nominal ratio f_u/f_y; y_2=elongation, %

All data from assessment and corrosion testing result would be analyzed and selected to identify the deterioration degree and performance reduction of RC structure after long-term exposure according to the threshold value from JSCE, ASTM, CEB standards and several finding from researchers. The threshold values were defined corresponding to different corrosion levels for estimate corrosion levels based on the result of corrosion testing. There is no consensus among researchers regarding such values. From some literature, certain threshold values were selected to estimate the initiation, propagation, and acceleration and deterioration states of corrosion. This study proposes the corrosion levels as A_1, A_2, B_1, B_2, and C which value means 1, 2, 3, 4, 5, respectively, as shown in Fig. 6.3. The higher number means quality of concrete/steel bar become severe/damage (corrosion risk). The threshold values selected for the corrosion potential (E_{corr}) are values suggested by the ASTM C 867-15[6.11]. For corrosion current intensity (I_{corr}), the value is suggested by CEB Standard [6.12]. The other threshold values of corrosion measurement and their corresponding corrosion levels for deterioration degree and performance reduction are summarized in Table 6.5 and Table 6.6, respectively. However, there is no standardization for the threshold value of cross-sectional loss and total corroded area. Therefore, this study proposed a reliable threshold values of cross-sectional loss and total corroded area for justice the corrosion level based on Cairns and Allussalam. Cairns et al. [6.13] reported that a bar with a maximum reduction in cross-section of 8% lost approximately 20% of its original ductility. In addition, Allussalam [6.14] investigated the mechanical properties of corroded bars and discovered that 12% or more of corrosion could indicate a brittle failure.

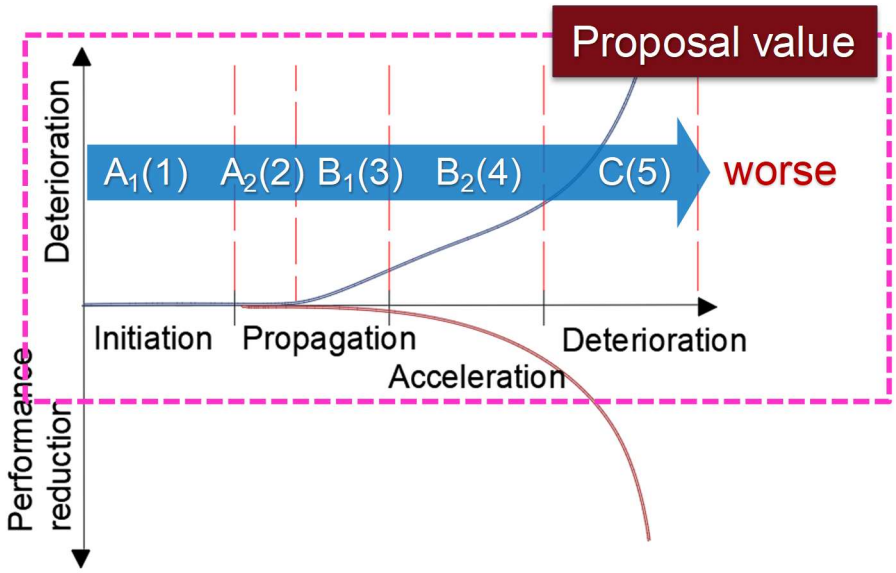

Fig. 6.3— Criteria of deterioration and performance reduction of RC structure

Table 6.5— Interpretation of corrosion level of electrochemical methods

Testing methods	Threshold	Corrosion state/ concrete quality description	Grade of deterioration
Corrosion potential (Ecorr) *ASTM C867-15* [6.11]	E ≥ -200mV	passive corrosion	A1 (1)
	-350mV ≤ E < -200mV	low (<10%) risk of corrosion	A2 (2)
	-450mV ≤ E < -350mV	moderate (50%) risk of corrosion	B1 (3)
	-550mV ≤ E < -450mV	high (>90%) risk of corrosion	B2 (4)
	E > 550mV	Severe corrosion	C (5)
Current density (i_{corr}), *RILEM TC 154-EMC 2004* [6.12]	< 0.1 μA/cm^2	passive corrosion	A1 (1)
	0.1 - 0.5 μA/cm^2	low (<10%) risk of corrosion	A2 (2)
	0.5 - 1 μA/cm^2	moderate (50%) risk of corrosion	B1 (3)
	1- 1.5 μA/cm^2	high (>90%) risk of corrosion	B2 (4)
	> 1.5 μA/cm^2	Severe corrosion	C (5)
Chloride content-total chloride, *JSCE 2004*	Cl^- ≤ 1.2 kg/m^3	passive corrosion	A1 (1)
	1.2 < Cl^- ≤ 5 kg/m^3	low (<10%) risk of corrosion	A2 (2)
	5 < Cl^- ≤ 10 kg/m^3	moderate (50%) risk of corrosion	B1 (3)
	10 < Cl^- ≤ 15 kg/m^3	high (>90%) risk of corrosion	B2 (4)
	Cl^- > 15 kg/m^3	Severe corrosion	C (5)
Grade of passivity, *OTSUKI 1985* [6.17]	I_{corr} <1 μA/cm^2	grade 5	A1 (1)
	≥1 μA/cm^2	grade 4	A1 (1)
	1 - 10 μA/cm^2	grade 3	A2 (2)
	≥ 10 μA/cm^2	grade 2	B1 (3)
	10 - 100 μA/cm^2	grade 1	B2 (4)
	≥ 100 μA/cm^2	grade 0	C (5)
Electrical resisivity (ρ), *Andrade and Alonso 1996* [6.18]	> 100 kΩcm	low corrosion	A1 (1)
	50-100 kΩcm	moderate corrosion	A2 (2)
	10-50 kΩcm	high corrosion	B1 (3) and B2
	< 10 kΩcm	very high corrosion	C (5)
Oxygen permeability	0 - 2 x10^{-12} mol/cm^2/s	passive corrosion	A1 (1)
	2 - 4 x10^{-12} mol/cm^2/s	low (<10%) risk of corrosion	A2 (2)
	4 - 6 x10^{-12} mol/cm^2/s	moderate (50%) risk of corrosion	B1 (3)
	6 - 8 x10^{-12} mol/cm^2/s	high (>90%) risk of corrosion	B2 (4)
	>8 - 10 x10^{-12} mol/cm^2/s	Severe corrosion	C (5)
State of steel-deterioration degree, *JSCE No.4* [6.19]	0 - 3	Passive corrosion	A1 (1)
	4 - 6	Corrosion initiates	A2 (2)
	7 - 9	Cracking occurs and leaching of rust is observed	B1 (3)
	10 - 12	Numerous cracks occur and partial peeling is found	B2 (4)
	13 - 15	a large crack, spalling and displacement are observed	C (5)
Corroded area, *Alussalam* [6.14]	0 – 10 %	Black and red rust not occur, or it is thin and dense	A1 (1)
	11 – 20 %	Partial floating rust, but small spotted	A2 (2)
	21 – 30 %	floating rust occurs around the bar	B1 (3)
	31 – 40 %	Floating rust occurs around the bar, small cross-sectional section defect	B2 (4)
	> 41 %	More cross section defect occurs	C (5)

Table 6.6— Level of mechanical properties

Testing methods	Threshold	Grade of performance
Total corroded area, *Almulsalam* [6.14]	0 – 10 %	A1 (1)
	11 – 20 %	A2 (2)
	21 – 30 %	B1 (3)
	31 – 40 %	B2 (4)
	> 41 %	C (5)
Cross-sectional loss, *Cairns et al.* [6.13]	≤4%	A1 (1)
	4-6%	A2 (2)
	6-8%	B1 (3)
	8-10	B2 (4)
	≥ 10 %	C (5)
Strain at maximum force, ε_{uk} *Euro code 2* [6.20]	≥2.5 %	A1 (1)
	2.3-2.5 %	A2 (2)
	2.0-2.3 %	B1 (3)
	1.7-2.0 %	B2 (4)
	≤1.7 %	C (5)
f_u/f_y, *Euro code 2* [6.20]	≥ 1.05 %	A1 (1)
	1.025-1.05 %	A2 (2)
	1.000-1.025 %	B1 (3)
	0.950-0.975 %	B2 (4)
	≤0.950 %	C (5)
Elongation, JIS G 3112	≥ 22 %	A1 (1)
	20-22 %	A2 (2)
	18-20 %	B1 (3)
	16-18 %	B2 (4)
	≤16 %	C (5)

All assessment method (x_1~x_9 and y_1~y_2) for identified corrosion level was used as input data of multiple regression analysis. The computer program in Microsoft Excel used for this analysis is "Anova". The model with the highest multiple correlation coefficient is treated as the best fit model. This study adopts the analysis model expressed by Eq. (6.1).

$$y_i = a_{i1}.x_1 + a_{i2}.x_2 + a_{i3}.x_3 + b_i + \in \quad 6.1$$

6.4 Result and discussion

6.4.1 Corrosion level

Table 6.7 and 6.8 provide a summary of the testing result and corrosion level of total deterioration degree and performance reduction after long-term exposure. The high number of total evaluation indicates a high corrosion level predicted by each method. From Table 6.7, it was found the total deterioration of seawater mixing was from 17 to 24. For tap water mixing, the total deterioration was from 20 to 26. From this data, tap water mixing considered was severe compared to seawater mixing after long-term exposure.

Marine environment has an intense of chloride ions, therefore reinforced concrete severe to corrosion mainly caused by chloride attack. Severely corrosive environment according to JSCE Standard [6.15] is that the marine structures environment subjected to tides, splash, or

exposed to severe ocean winds. From total deterioration value, the most severe corrosion risk occurred in the splash zone than the tidal zone. This also reported by Revie and Uhlig [6.16] that severest corrosion rate occurred at splash zone. For effect of concrete cover, 5 cm concrete cover is enough to guarantee the performance seawater mixing of 36 years old of RC beam, especially in tidal marine environment. The total deterioration value all of steel bar embedded in 5 cm cover depth was less than 20. It should be underlined, reduced cover is risky even when using high-quality concrete since initial defects such as cracks become more significant than they are with normal cover and may provide a low resistance path to the reinforcing bar.

Table 6.7—Deterioration degree of all RC beams

Mixing water	Specimen code	d, cm	Grade of deterioration								Total deterioration
			x_1	x_2	x_3	x_4	x_5	x_6	x_7	y_1	
Seawater	65-L1-SW-T	2	3	2	4	2	3	2	4	3	23
		3	2	1	4	2	3	2	4	2	20
		5	2	1	4	2	3	1	4	1	18
	45-L1-SW-T	2	2	1	3	2	3	2	3	3	19
		3	2	1	3	2	3	1	3	2	17
		5	1	1	3	2	3	1	3	2	16
	55-L2-SW-T	2	3	2	3	2	3	3	4	5	25
		3	2	2	3	2	3	2	4	3	21
		5	2	1	3	2	3	2	4	2	19
	55-L3-SW-T	2	5	1	3	2	3	3	4	4	25
		3	2	2	4	2	3	2	4	3	22
		5	2	1	3	2	3	2	4	2	19
	65-L1-SW-S	2	3	2	5	2	3	2	4	3	24
		3	1	2	5	2	3	2	4	2	21
		5	1	1	5	2	3	2	4	1	18
	55-L1-SW-S	2	2	1	4	2	3	2	4	2	20
		3	1	1	4	2	3	2	4	1	18
		5	1	1	4	1	3	1	4	2	17
	45-L1-SW-S	2	2	1	3	2	3	1	4	3	19
		3	1	1	4	2	3	1	4	2	18
		5	2	1	4	1	3	1	4	1	17
Tap water	65-L1-TW-T	2	3	2	3	3	4	3	4	4	26
		3	3	2	3	3	4	2	4	3	24
		5	4	2	3	3	4	2	4	2	24
	55-L1-TW-T	2	2	1	4	2	4	4	4	5	26
		3	2	1	3	2	4	3	4	5	24
		5	2	1	3	2	4	2	4	2	20
	55-L3-TW-T	2	3	2	4	3	4	5	4	4	29
		3	4	2	4	3	4	3	4	3	27
		5	4	2	4	3	4	3	4	4	28

Where,

x_1 = corrosion potential, mV;
x_2 = corrosion current density, $\mu A/cm^2$;
x_3 = chloride content, kg/m^3;
x_4 = grade of passivity;
x_5 = electrical resistivity, kΩ–cm
x_6 = oxygen supply x 10^{-12} $mol/cm^2/s$;
x_7 = deterioration degree;
y = total corroded area, %

From Table 6.8, it was shown all-steel bar condition in the same degree (5). Only three steel bar had higher degradation degree which occurred pitting corrosion at the bar. The value was 12, 15 and 17 for 55-L1-SW-S(3), 55-L1-TW-T(2) and 5-L3-TW-T(2), respectively. This higher value indicated the performance of steel bar was reduced. From total degradation degree, compared to steel bar embedded in seawater mixed concrete had good mechanical properties than steel bar embedded in tap water mixed concrete.

Table 6.8— Performance reduction of RC beams

Specimen code	Cover depth, cm	Grade of performance					Total degradation degree
		x_8	x_9	x_{10}	x_{11}	y_2	
Control bar	1	1	1	1	1	1	5
	2	1	1	1	1	1	5
	3	1	1	1	1	1	5
45-L1-SW-T	2	1	1	1	1	1	5
	3	1	1	1	1	1	5
	5	1	1	1	1	1	5
55-L2-SW-T	2	1	1	1	1	1	5
	3	1	1	1	1	1	5
	5	1	1	1	1	1	5
55-L3-SW-T	2	1	1	1	1	1	5
	3	1	1	1	1	1	5
	5	1	1	1	1	1	5
55-L1-SW-S	2	1	1	1	1	1	5
	3	1	3	4	1	3	12
	5	1	1	1	1	1	5
45-S1-SW-S	2	1	1	1	1	1	5
	3	1	1	1	1	1	5
	5	1	1	1	1	1	5
55-L1-TW-T	2	2	5	3	1	4	15
	3	1	1	1	1	1	5
	5	1	1	1	1	1	5
55-L3-TW-T	2	2	5	4	1	5	17
	3	1	1	2	1	1	6
	5	1	1	1	1	1	5

Where,

x_8 = corroded area, mm^2,
x_9 = cross sectional loss, mm^2;
x_{10} = maximum ultimate strain, mm/mm;
x_{11} = nominal ratio f_u/f_y;
y_2 = elongation, %

6.4.2 Multiple regression analysis

Tables 6.7 and 6.8 present the data for input data analysis for multiple regression analysis, then total corroded area and elongation as the criterion variable to judge how far deterioration degree and performance reduction, respectively, of RC structure after long term exposure in the marine environment. In multiple regression analysis, all data obtained at different mixing water and on different cover depth are plotted without any distinction to know

which parameter has more effect for each deterioration and degradation. Multiple correlation coefficient was used as an indicator of the correlation between one parameter to another parameter. And Table 6.9 shows the formula as the result of the relationship between corrosion parameter indicator with deterioration degree and performance reduction. From this table, a high correlation between total evaluation and each parameter methods were found for deterioration degree and performance reduction. The multiple correlation coefficient values (R) was about 0.745 and 0.987 for deterioration degree and performance reduction, respectively. The deterioration degree and performance reduction equation was constructed from higher correlation between y and x, and the lower correlation was not included in this equation. Therefore, it might better to confirm relationship for each variable x (testing method) to variable y_1 and y_2 by each multiple correlation coefficient.

Table 6.9—Equation for deterioration degree and performance reduction

	Coefficients	Standard	t Stat	P-value	Lower 95%	Upper 95%
a. deterioration degree						
Intercept	0.348	1.213	0.287	0.776	-2.150	2.847
X1	0.197	0.195	1.014	0.320	-0.204	0.598
X2	0.129	0.373	0.345	0.733	-0.640	0.898
X5	0.023	0.440	0.052	0.959	-0.884	0.929
X6	0.770	0.226	3.407	0.002	0.304	1.235
Equation: $y_1 = 0.197x_1 + 0.129x_2 + 0.023x_5 + 0.770x_6 + 0.348$ with R = 0.745						
b. Performance reduction						
Intercept	-0.541	0.395	-1.369	0.187	-1.368	0.286
X8	0.689	0.469	1.468	0.158	-0.293	1.670
X9	0.492	0.174	2.821	0.011	0.127	0.857
X10	0.344	0.109	3.159	0.005	0.116	0.572
Equation: $y_2 = 0.689x_8 + 0.492x_9 + 0.344x_{10} - 0.541$ with R = 0.987						

Multiple correlation coefficient with total corroded area and elongation as a criterion variable to each testing method was shown in Table 6.10 and Table 6.11 for deterioration degree and performance reduction, respectively. From Table 6.10, the chloride ion content, grade of passivity, and visual inspection for deterioration degree method showed lower multiple correlation coefficient, while corrosion potential, corrosion current density, electrical resistivity and oxygen supply methods showed higher multiple correlation coefficient. One possible reason the chloride content had less correlation to corrosion risk after long-term exposure of steel bar. These phenomena happen because corrosion already become active and steady. It should be underlined, for visual observation to judge the deterioration degree based

on JSCE standard [6.19] also had a low correlation to corrosion activity due to classification by visual observation which human can make a different sense of judge to classify the degree of damage of the structure. Interestingly, the oxygen permeability evaluation was found as the most important factor to detect deterioration of RC structure after long-term exposure. In addition, from Table 6.11 corroded area, cross-sectional loss and the maximum ultimate strain showed a higher multiple correlation coefficient, while the nominal ratio of f_y/f_u showed no correlation.

Table 6.10— Multiple correlation coefficient with the corroded area as a criterion variable

Variable for deterioration degree	R
Corrosion potential, x_1	0.51
Corrosion current density, x_2	0.39
Chloride ion content, x_3	0.28
Grade of passivity, x_4	0.29
Electrical resistance, x_5	0.48
Oxygen supply, x_6	0.72
Det. degree (visual observation), x_7	0.11

Table 6.11— Multiple correlation coefficient with elongation as criterion variable

Variable for degradation degree	R
Corroded area, x_8	0.832
Cross-sectional loss, x_9	0.978
Maximum ultimate strain at max. force, x_{10}	0.846
Nominal ratio f_u/f_y, x_{11}	0

The established equation for estimation of deterioration degree and performance reduction of RC structure in marine environments is a step forward. The formula presents an engineering approach were total corroded area and elongation of steel bar can be calculated by estimating from the proposed equation in Table 6.9 which formula based on data from the electrochemical and mechanical analysis of steel bar. By establishing some common reliable assessment methods to determine the deterioration degree and performance reduction of RC structure, hopefully, making it simple to assess RC structures.

6.5 Some considerations on utilization of seawater mixed concrete with OPC and mineral admixture

Design for durability has been carried out by selecting concrete mixtures of sufficient strength to resist the maximum design stresses, by adopting a minimum standard for cover for steel bar to meet environmental exposure requirements to match the strength level or mix proportions chosen, and by limiting the width of flexural cracks at the surface. Selection of sufficient strength of concrete mixture using local materials has the possibility, and it can be performed by trial mix. The problem is how to achieve durability through careful design of the cement matrix and its microstructures, and determine the minimum cover depth for reinforcement that meets the requirements of severe environmental exposures. Table 6.12 describes limiting values for composition and properties of concrete subject to general structures for 50-years design life in tidal, splash & spray zones based on code and standard. As can be seen from the table, JSCE [6.25] provides a minimum concrete cover with quite high compressive strength compared to other standards. Swamy et al. [6.21] propose an estimation of corrosion initiation by considering W/C ratio of 30% and concrete cover of 6 cm. However, overall, the values in this table justify the use of large cover (5-7 cm) and lower W/B ratio (30-55) in the marine environment. Reducing concrete cover is very risky even when using high-quality concrete since defects such as cracks and voids become more significant compared to normal covers and may provide low resistance path to the reinforcement.

Table 6.12—Limiting values for composition and properties of concrete subject to general structures for 50 years design life in tidal, splash & spray zones

Corrosion-induced		Carbonation	Chlorides							
Code		EN 206-1 [6.22]		AS 3600 [6.23]		BS 6349-1 [6.24]			JSCE [6.25]		Swamy [6.21]
Max. W/C, %		50	45	35	35	45	50	55	30	40	30
Min. f'c, MPa		30	35	50	40	40	30	25	60	50	-
Min. cement content, kg/m^3		300	340	-	-	400	360	360	-	-	-
Min. concrete cover, cm		4.5	5	5	7	6	5	4	6	7	6
Permitted additions proportion, % by mass	GGBFS PFA					≤ 35 ≤ 20	35-80 20-55	50-80 35-55			

This study aims to provide information regarding durability and performance on utilization of seawater mixed concrete with OPC and mineral admixture. Based on information on actual situation (marine environment) related to chloride penetration on mortar contain mineral admixture in Chapter 3-4 and RC beam in Chapter 5, then connections between field

and laboratory were constructed. Table 6.13 shows summary of the result of composition and properties regarding performance mortar contain mineral admixture (short-term) and RC beam (long-term) during initiation and propagation stage of service life concrete structure.

Table 6.13 Summary of composition and properties of RC-beam and contain mineral admixture mortar

Exposure condition	Tidal	Tidal, splash	Atmosphere			
Cement/ Mineral admixture	OPC Concrete		FA	SA	BB	BBMKP
Max. W/C, %	55	65	50	40	50	40
Min. f'c, MPa	60	60	50	55	50	55
Min. cement content, kg/m^3	Undefined	Undefined	255	232	255	232
Min. concrete cover, cm	5	5	5	5	5	>6
Allowable bending load, MPa	300	100	Undefined			
Permitted additions proportion, % by mass			20	5	45	BB80, MKP20

Where, FA: Fly ash type B; SA: Silica fume type A; BB: BFS type B; and MKP: Metakaolin

By considering use seawater as mixing water, and facing a potentially high risk of corrosion of steel in the chloride-rich environment, so it needs to be careful to determine the requirement of maximum W/C and a minimum of concrete cover. By referring to the Standard and codes in Table 6.12 to use seawater as material in RC structure, this study provides as a proposal and reasonable value of maximum W/C and minimum of concrete cover to use in long-lasting performance of RC structures as shown in Table 6.14. The evaluation result is expected to provide the necessary information and reference for the future design and construction of long-lasting RC structures mixed with seawater, particularly exposure in marine environments. From the result of long-term (field) RC beam even with W/C ratio of 45% (OPC) but concrete cover 2 cm and 3 cm were not enough for concrete subjected into chloride environment particularly tidal and splash zone under sustained load. Further, by considering result and highly durable of OPC concrete of long-term (field case) RC beam, 65% of W/C ratio was not satisfied the requirements to be used in seawater mixing. However, from the result for W/C ratio of 55% with cover depth 5 cm, it showed reliable data and higher resistance to corrosion. Nevertheless, 5 cm of cover depth indicated corrosion practically still occurred. Therefore, if we consider to highly durable concrete and resistant to corrosion especially exposed in marine tidal environment based on the standard from Table 6.12, the W/C ratio should be decreased until 45% and concrete cover should be increased. In addition, in viewpoint of mechanical properties, the compressive strength of RC beam use seawater mixing after long-term exposed was around 60 MPa. The compressive strength data at early age was not available in this study, therefore, if referring to Adiwijaya [6.27] findings that

incremental strength of seawater mixing from 28-days until 25-years old was 37%. From this consideration and standard of BS 6349-1 [6.24], then the minimum required compressive strength for concrete mixed with seawater more than 30 MPa based on this study.

Costa [6.26] found that a cover of 4 cm is enough to guarantee a service life of 50 years except in the atmospheric exposure conditions and for good concrete quality. On contrary result from short-term (laboratory) OPC did not resistance to corrosion if mixed with seawater and subjected to chloride environment, particularly in the atmospheric exposure. Based on measurements of chloride ingress within structures it can be demonstrated that levels of chloride of OPC mortar required to cause activation can be achieved at rebar depth in relatively short periods than mortar contain mineral admixture. The performance mineral admixture against corrosion was effective if concrete exposed to atmosphere condition (carbonation and chloride attack). The results and performance of BFS and fly ash mortar against corrosion on short-term (lab case) showed that for W/C ratio of 40% and 50% had high resistance to seawater (chloride induced corrosion). However, if we consider the performance to achieve highly durable concrete and resistant to corrosion exposed to atmosphere zone, the W/C ratio should be limited with maximum of 40%.

Table 6.14 Proposal utilization of seawater mixing in tidal and atmosphere exposure

Corrosion-induced	Chloride	Chloride and carbonation	
Exposure condition	Tidal	Atmosphere	
Cement/ Mineral admixture	OPC Concrete	FB	BB
Max. W/C, %	45	40	40
Permitted additions proportion, % by mass		20	45

Where, FA: Fly ash type B and BB: BFS type B.

Many studies have revealed that concrete with very low W/B ratios are extremely hard to place, compact and maintain, and highly easy to crack. With a new generation of chemical admixtures, it is certainly possible to overcome some of these difficulties. The data showed in Table 6.14 will use to propose some limitation to use in the applicability of seawater mixing for design life (initiation and propagation) in tidal and atmosphere exposure. Now, there is conclusive evidence that even when specific code requirements for durability in terms of concrete quality and concrete cover are achieved in practice, concrete made with only Portland cement as currently manufactured, are not resistant to deterioration when exposed to aggressive salt-laden environments [6.21]. In addition, it is well-established that one of the key ways of enhancing the durable quality of Portland cement concrete in its fresh and

hardened states is to ensure that pozzolanic and/or cementitious industrial by-product form vital and essential constituents of the concrete.

6.6 Conclusion

Ten RC beam of long-term exposure specimens were tested with several common corrosion testing techniques to estimate the corrosion level of each specimen. Some conclusions from this experiment are summarized below:

1. Propose equation for estimation deterioration and performance reduction of RC structure after long-term exposure as following equation:
   a. deterioration degree:
      Total corroded area = (0.197 x E_{corr}) + (0.129 x I_{corr}) + (0.023 x electrical resistivity) + (0.769 x oxygen supply) + 0.348
   b. performance reduction:
      Elongation = (0.689 x total corroded area) + (0.492 x cross-sectional loss) + (0.344 x maximum ultimate strain) – 0.541
2. The oxygen permeability evaluation was found as the most important factor to detect deterioration of RC structure after long-term exposure.
3. Some consideration seawater mixing of concrete for OPC with requirement of max. W/C ratio of 45% in marine tidal environment; for fly ash and BFS mortar with requirement of max. W/C ratio of 50% in atmosphere exposure.

References

[6.1] Badawi, M.; Soudki, K. Control of corrosion-induced damage in reinforced concrete beams using carbon fiber-reinforced polymer laminates. J. Compos. Constr. 2005, 9, 195–201.

[6.2] Ahmad, S. Reinforcement corrosion in concrete structures, its monitoring and service life prediction—A review. Cem. Concr. Compos. 2003, 25, 459–471.

[6.3] Yuan, Y.; Ji, Y.; Shah, S.P. Comparison of two accelerated corrosion techniques for concrete structures. ACI Struct. J. 2007, 104, 344–347.

[6.4] Song, G.; Shayan, A. Corrosion of Steel in Concrete: Causes, Detection and Prediction; Australian Road Research Board: Vermont South, Australia, 1999.

[6.5] Almusallam, A.A. Effect of degree of corrosion on the properties of reinforcing steel bars. Constr. Build. Mater. 2001, 15, 361–368.

[6.6] Dean Jr, S. W. "Electrochemical Methods of Corrosion Testing, Electrochemical Techniques for Corrosion." 1976 symposium. Edited by R. Baboian. National Association of Corrosion Engineers. Houston. Tex. 1977.

[6.7] Vassie, P. R. "Measurement techniques for the diagnosis detection and rate estimation of corrosion in concrete structures." Controlling Concrete Degradation. Thomas Telford Publishing, 1999. 215-229.
[6.8] Broomfield, J. P., et al. "Corrosion rate measurement and life prediction for reinforced concrete structures." Proc. Structural Faults and Repair-93, University of Edinburgh, Scotland 2 (1993): 155-164.
[6.9] Broomfield, J. P. "Corrosion rate measurements in reinforced concrete structures by a linear polarization device." Special Publication 151 (1994): 163-182.
[6.10] Stratfull, Richard F. "Criteria for the cathodic protection of bridge decks." Society of Chemical Industry, (1983): 287-331.
[6.11] ASTM C876-09. "Standard test method for half-cell potentials of uncoated reinforcing steel in concrete." West Conshohocken, PA, American Society for Testing and Materials (2009).
[6.12] CEB. "Strategies for Testing and Assessment of Concrete Structure" Bulletin n.243, 183 pp., 1998.
[6.13] Cairns, John, et al. "Mechanical properties of corrosion-damaged reinforcement." ACI Materials Journal 102.4 (2005): 256.
[6.14] Almusallam, Abdullah A. "Effect of degree of corrosion on the properties of reinforcing steel bars." Construction and Building Materials 15.8 (2001): 361-368.
[6.15] JSCE Guidelines for Concrete No. 15, “Standard Specifications for Concrete Structures-JSCE (Part: Design)”, 2007.
[6.16] R. W. Revie, H. H. Uhlig, Uhlig's corrosion handbook, John Wiley & Sons.2011.
[6.17] Otsuki, N. "A study of effectiveness of chloride on corrosion of steel bar in concrete." Report of Port and Harbor Research Institute (1985): 127-134.
[6.18] Andrade, C., and Cruz Alonso. "Corrosion rate monitoring in the laboratory and on-site." Construction and Building Materials 10.5 (1996): 315-328.
[6.19] JSCE, Standard Specification for Concrete Structures (Part: Maintenance), Japan Society of Civil Engineers, Japan, 2007.
[6.20] ENV 1992-1-1: Euro code 2. Design of concrete structures. Part I-General rules and rules for buildings.
[6.21] Swamy, R. Narayan. "Sustainable Concrete for the 21st Century Concept of Strength through Durability." Japan Society of Civil Engineers Concrete Committee Newsletter 13 (2008).
[6.22] EN 206-1, “Concrete-Part 1: Specification, Performance, Production and Conformity”, European Standard, 2000.
[6.23] AS 3600, “Concrete Structures”, Australian Standard, 2001.
[6.24] BS 6349-1:2000, “Maritime Structures, Part 1: Code of practice for general criteria”, British Standard.
[6.25] JSCE Guidelines for Concrete No. 15, “Standard Specifications for Concrete Structures-JSCE (Part: Design)”, 2007.
[6.26] Costa, A., and J. Appleton. "Chloride penetration into concrete in marine Environment-Part II: Prediction of long term chloride penetration." Materials and Structures 32.5 (1999): 354-359.
[6.27] Adiwijaya. "Dissertation-A Fundamental Study on Seawater-Mixed Concrete Related to Strength, Carbonation and Alkali-Silica Reaction." Kyushu University, Sept 2015.

CHAPTER 7. CONCLUSIONS AND FUTURE WORKS

7.1 Summary

Deterioration of RC structures due to harsh environmental conditions lead to performance degradation of RC structures, and premature deterioration before completing expected service life is a major concern for engineers and researchers, maintainers, and infrastructure owners. Considering marine exposure conditions and use either sea sand/seawater for heavy construction in many countries, chloride-induced corrosion is one of major causes of deterioration of RC structures. In the literature, reliable chloride threshold for both new structures design and condition assessment of existing structures is important as the remaining service life is often considered as the time required to reach the chloride threshold value at a depth of steel bar. Several critical disasters due to steel corrosion have been reported, including the collapse of building and bridge. The total estimated direct cost for repairing or preventing corrosion is reported to be expensive. For these reasons needs to be increasing consideration of optimum durability design. Different mineral admixtures are often added in concrete to improve the durability, rheology of fresh concrete, and mechanical properties of hardened concrete. Optimal design necessary advances in the knowledge base relevant to the durability evaluation of RC structure in marine environments, including the role of mineral admixture for durability, the methods of measuring, and design for long-lasting of RC structures in marine environments.

Therefore, this study aims 1) to propose a reliable detection method to determine the chloride threshold value to corrosion initiation of steel bars in various mineral admixtures such as fly ash, silica fume, metakaolin, and BFS; 2) to determine the performance of OPC mortar with difference chloride contaminated from moderate to high corrosion rate under certain period of exposure; 3) to determine the better performance of concrete mixed with seawater after 36-years exposure; 4) to propose a reliable assessment method to predict corrosion activity in RC structure; and 5) to determine some consideration regarding durability of seawater in RC structures. Further, this study expected to contribute for necessary information

and may guide engineers in the development of longer-lasting RC structures, because it provides a demonstration of the long-term behavior of a commonly used construction material, permitting the prediction of the behaviors of existing structures and the more informed design and study of structures to be built.

7.2 Overview of contributions and conclusions

Chapter 1 describes the background of this study, research objective, research contribution and dissertation outline. The objective of this study are to investigate the chloride threshold value (CTV) to corrosion initiation of steel reinforcement for different replacement cement using mineral admixture, as the baseline and compare with OPC mortar, and to investigate the performance of seawater-mixed concrete after long-term exposure regarding corrosion behavior and deterioration progress of RC structure in marine environment under sustained load. Further, long-term exposure by field case (i.e., natural corrosion environments) and laboratory case (i.e., artificial corrosion environments) regarding of corrosion behavior and deterioration progress of RC beam and mortar contain mineral admixture is the advantage from this study. The expected result of this study is to propose chloride threshold value to corrosion initiation of steel bar in various mineral admixtures such as fly ash, silica fume, metakaolin, and blast furnace slag; and determine some consideration regarding durability of seawater in RC structure.

Chapter 2 describes the previous study related to durability issues at the current situation (e.g., characteristics of durability, deterioration of concrete due to either carbonation or chloride ingress, and environmental impact), provide literature regarding role chlorides for the corrosion of reinforcements, and the amount chloride for breakdown or initiate corrosion. This such literature or evaluation became necessary information in order to provide an appropriate assessment regarding durability of concrete member. The evaluation result will provide necessary information and reference for the future design and construction of long-lasting reinforcements for concrete structures, particularly in marine environments.

Chapter 3 describes the OPC mortar contaminated chloride was tested during the propagation period of corrosion from moderate to high corrosion rate. The main objective of this study is to identify and determine corrosion behavior and the extent of corrosion of OPC mortar during the early period of the propagation stage by using several corrosion measurement methods. From the present test results, the factors influence of corrosion behavior of OPC mortar with difference chloride contaminated from moderate to high corrosion rate is proposed. The sensitivity of the corrosion potential against chloride content

tends to be decreased after a certain period of exposure. The value is 13~15% of corrosion area can be defined as high corrosion degree and categorized into propagation stage. Therefore, from moderate to high corrosion rate, after 8-years exposure of OPC mortar has increased the probability from pitting to generate corrosion. In addition, the electrochemical method has reliable to evaluate corrosion during entering initiation and propagation stage.

Chapter 4 describes the chloride threshold value to corrosion initiation by using mineral admixtures such as fly ash, silica fume, metakaolin, and BFS. Corrosion potential and corrosion current density were conducted to examine the threshold chloride concentration. The amount of chloride was determined according to the added amount of chlorides, type of mineral admixtures and W/B ratios. The specimens were stored in the laboratory atmosphere condition room and after one year, specimens were exposed in accelerated carbonation chamber until the sign of corrosion initiating. From the present test results, corrosion current density has reliable to evaluate and determine chloride threshold value. The passivity limit to corrosion initiation of I_{corr} for replacement cement with FB, SA, BBMKP and BB being value at range 0.178 $\mu A/cm^2$, 0.149 $\mu A/cm^2$, 0.149 $\mu A/cm^2$, 0.185 $\mu A/cm^2$ respectively to the 0.2 $\mu A/cm^2$. In addition, the reliable ranges of threshold chloride concentration causing active corrosion of steel bar are proposed. The type of water to binder ratio seems to influence the threshold value significantly after depassivation. In performance-based design determined by chloride attack and carbonation, it is possible to use seawater and if mortar mixed with BFS and fly ash with max. W/B ratio of 0.5. BBMKP is also efficient to mix with seawater with a max 0.4 of W/B ratio and cover depth of concrete should not be increased.

Chapter 5 introduces several investigations on concrete mixed with seawater and tap water. Ten number of RC beams have been evaluated. The specimens were exposed to a tidal pool utilizing seawater directly from the sea. The major test variables include mixing water, various of cover depth, water to cement ratios, various bending load and exposure condition. The study aims to evaluate the effect of seawater mixing and exposure condition (tidal and splash) on deterioration and steel corrosion of RC beam under service load after 36-years of exposure. Visual observation, some electrochemical and physical evaluation were evaluated. From the present test results, the strength of seawater mixing showed 10 MPa larger than tap water mixing, with the ratio of seawater/tap water was 1.2 after long-term exposure. The ductility of seawater mixed concrete better than tap water mixing according mechanical properties of extracted bar. The results of 36-years exposure test of concrete mixed with seawater with concrete cover 50 mm demonstrated high possibility of using seawater as an alternative and sustainable material of reinforced concrete, especially in marine tidal

environment. In addition, according to tensile test corrosion does not reduce the yield strength and ultimate tensile strength of the steel bar, but their ultimate strain decreased significantly.

Chapter 6 presents the importance reinforcement corrosion monitoring and describes the different methods for evaluating the corrosion state of RC structures. The main objective of this study was to compare the corrosion level of long-term exposure of RC beam using several corrosion measurement methods and discuss an overview of utilization of seawater in concrete structures. The data of corrosion level were taken from Chapter 5 then analysis and categorized into deterioration and degradation stage level. This study proposes a reliable assessment method to predict corrosion activity of steel corrosion caused severe damage of RC structure. Additionally, a potential correlation of actual corrosion and corrosion measurement was explored. From the present test results, proposal equation for estimation deterioration and performance reduction of RC structure after long-term exposure were included. Some consideration seawater mixing of concrete for OPC with requirement of maximum W/C ratio of 45% in marine tidal environment and for fly ash and BFS mortar with requirement of maximum W/C ratio of 40% in atmosphere exposure. In addition, the corrosion current density was observed as important parameter to detect corrosion initiation of steel bar at short-term exposure. Moreover, the oxygen permeability evaluation was suggested as the most important factor in order to detect deterioration of RC structure after long-term exposure.

Chapter 7 conveys summary, conclusion, and recommendation for research works in the future.

7.3 Future works

Based on research conducted in **Chapter 3, 4, 5** and **6**, this study endeavors to provide information regarding durability and evaluation of RC beam performance under marine environment and utilization of mineral admixture against corrosion. The evaluation result will provide the necessary information and reference for the future design and construction of durable reinforcements for RC structures, particularly in marine environments. To develop necessary information regarding durability evaluation of the long-lasting performance of RC structure, the following aspects are expected in further research:

1. Future study is necessary to clarify corrosion behavior for mineral admixture during initiation and former propagation stage based on the best corrosion monitoring to predict corrosion area without visible crack. And also it is necessary to check-in actual structures with and without crack, as a reference to confirm the research results carried out in the laboratory.

2. Due to an accelerated environmental condition in the CO_2 chamber to check CTV of mineral admixture, it is necessary to check CTV of mineral admixture exposed in the air and dry-wet cycle condition to compared the CTV by the different environmental condition.
3. The CTV in cover depth 5 cm found already. Future study is necessary to check the effect of cover depth applied on utilization mineral admixture mixed with seawater.
4. The oxygen permeability evaluation was found as the most important factor to detect deterioration of RC structure after long-term exposure. Further study is suggested to conduct an oxygen permeability evaluation in real RC structure.

Because each case is unique, in which environmental factors contribute to the deterioration of RC structure, further investigation is necessary on the actual structure, as a reference to confirm the research results carried out in the laboratory and to determine the parameters for analysis.